



University
of Glasgow

Mughal, Waqas (2017) *High dynamic range image sensor using tone mapping operation*. PhD thesis.

<http://theses.gla.ac.uk/8151/>

Copyright and moral rights for this work are retained by the author

A copy can be downloaded for personal non-commercial research or study, without prior permission or charge

This work cannot be reproduced or quoted extensively from without first obtaining permission in writing from the author

The content must not be changed in any way or sold commercially in any format or medium without the formal permission of the author

When referring to this work, full bibliographic details including the author, title, awarding institution and date of the thesis must be given

Enlighten:Theses

<http://theses.gla.ac.uk/>

theses@gla.ac.uk

High Dynamic Range Image Sensor Using Tone Mapping Operation

Waqas Mughal

A thesis presented for the degree of
Doctor of Philosophy



SCHOOL OF ENGINEERING
UNIVERSITY OF GLASGOW

UK

January 2017

Abstract

In nature, the dynamic range of a scene can be on the order of 10^6 to 10^0 from bright to dark areas. The human eye is capable of capturing images over a wide dynamic range of illumination while CMOS image sensors have limited ability to capture dynamic range available in nature. A Wide dynamic range (WDR) image is captured and displayed on low dynamic range (LDR) conventional media by a technique called tone mapping (TM). It is reported that most of the tone mapping operators have a monotonically increasing transduction function. A new CMOS pixel is proposed that aims to capture and display the wide dynamic range of illuminations by using the tone mapping monotonically increasing reference function. Different tone mapping functions like Reinhard photographic operator, Drago operator, etc. reference function are proposed and discussed. The tone mapping monotonically increasing function enables new pixel to capture WDR up to 6 decades of intensity.

A pixel model of different tone mapping operators is developed with parameters that characterise the pixel response. It is proposed that the pixel model of certain tone mapping operators exists. In addition, the parameters extraction routine is also discussed. The pixel model response is compared with the simulated response to check its validity. The model error is presented and suggests that the developed model fits well with the simulation data. Fixed pattern noise (FPN) limits the performance of image sensors, and it is mainly due the variations between the responses of individual pixels within an array of pixels. A simple procedure has been adapted to reduce FPN in which parametric response of the pixel is used, with FPN modeled as variations in the individual parameters. The parameters of each pixel are measured, recorded and then used to correct their response.

Acknowledgements

First of all, I wish to thank Almighty Allah for all the wisdom and strength he granted to me during my Ph.D study time. Nothing would have been achieved without his mercy.

I would like to thank my supervisor, Dr. Bhaskar Choubey for his continuous support, help and motivation throughout the duration of this work. Although he moved to the University of Oxford during my Ph.D time, his continuous guidance helped me in all the time of research and writing of this thesis. I would like to thank him for all the time that he has invested in me over the past 4 years. I would also like to thank Dr. Edward Wasige for his time and valuable feedback. I would say many thanks to Dr. Luiz Gouveia for his kind advice and help on my research work and proofreading my papers.

In addition, I would like to thank all of my family members for their continuous emotional support. Special thanks to my dear parents for their endless love, prayers, support and encouragement. I would also like to thank my wife, Hameera, for her constant encouragement and support throughout the course of my Ph.D. Thank you for cheering me up whenever I have had a hard day. A special thanks and love to my son Azaan for cheering my life up.

Lastly, I would like to thank Engineering and Physical Sciences Research Council (EPSRC) for a doctoral training scholarship.

Publications

- [1] L. C. Gouveia, W. Mughal, and B. Choubey, "A reconfigurable cmos pixel for applying tone mapping on high dynamic range images," IEEE Instrumentation and Measurement Technology Conference (I2MTC) Proceedings, pp. 1098–1101, 2014.
- [2] W. Mughal, L. C. Gouveia, and B. Choubey, "On Threshold Comparing Biomorphic Image Sensors," Procedia Computer Science, vol. 41, pp. 140–145, 2014.
- [3] B. Choubey, W. Mughal, and L. Gouveia. "Circuits for high performance complementary metal-oxide-semiconductor (CMOS) image sensors," High Performance Silicon Imaging: Fundamentals and Applications of CMOS and CCD sensors , pp. 124-164, 2014.
- [4] W. Mughal, and B. Choubey, "Fixed pattern noise correction for wide dynamic range CMOS image sensor with Reinhard tone mapping operator." IEEE Nordic Circuits and Systems Conference (NORCAS): NORCHIP & International Symposium on System-on-Chip (SoC), pp. 1-4, 2015.
- [5] W. Mughal, and B. Choubey. "On High Dynamic Range Tone Mapping CMOS Image Sensor," IEEE Sensors Journal, March 2017 (Submitted and under review).

Table of Contents

Abstract

Acknowledgments

1	Introduction	1
1.1	Background	1
1.2	Image Sensor Designs	3
1.2.1	Charge Couple Devices	3
1.2.2	CMOS Devices	5
1.3	Wide Dynamic Range Image Sensor	5
1.3.1	Well Capacity Adjustment Sensors	7
1.3.2	Logarithmic Sensors	8
1.3.3	Threshold Comparing Sensors	9
1.3.4	Integration Time Control Sensors	9
1.3.5	Threshold Comparing and Integration Time Control Pixels	10

1.4	A New Wide Dynamic Range Pixel Design	11
1.4.1	Tone mapping	12
1.4.2	Tone mapping on an integrating CMOS pixel	13
1.5	Fixed Pattern Noise	14
1.6	Thesis Objectives	17
1.7	Thesis Organisation	18
2	Tone Mapping	20
2.1	Introduction	20
2.2	Background	21
2.3	Tone Mapping	24
2.3.1	Global Operators	26
2.3.2	Local Operators	27
2.3.3	Frequency Domain Operators	27
2.3.4	Segmentation Operators	27
2.4	Global Operators	28
2.4.1	Linear Scaling	28
2.4.2	Logarithmic Mapping	29
2.4.3	Exponential Mapping	29
2.4.4	Drago Mapping Operator	29
2.4.5	Schlick Operator	30

2.4.6	Tumblin and Rushmeier Operator	31
2.4.7	Miller Brightness Operator	32
2.4.8	Reinhard Mapping Operator	33
2.4.9	Ward Histogram Adjustment	34
2.5	Comparison Results	36
2.6	Conclusion	43
3	Wide Dynamic Range CMOS Image Sensor	45
3.1	Introduction	45
3.2	Active Pixel Sensor	46
3.3	Wide Dynamic Range Pixel	48
3.3.1	Pixel Operation and Schematic	48
3.3.2	Tone Mapping Reference Function	51
3.4	WDR Pixel Simulation	64
3.5	Conclusion	67
4	Pixel Modeling and Fixed Pattern Noise	68
4.1	Introduction	68
4.2	Pixel Modeling	69
4.3	Parameter Extraction	74
4.3.1	Reinhard Simple	74
4.3.2	Reinhard Complex	76

4.4	Model Error	77
4.5	Fixed Pattern Noise	78
4.5.1	Transistor Mismatch	79
4.6	Fixed Pattern Noise Measurement	80
4.7	FPN Correction	84
4.8	FPN Effects on a Test Image	89
4.9	Conclusion	92
5	Pixel Modeling for Different Mapping Operators	93
5.1	Introduction	93
5.2	Drago Pixel Model	94
5.3	Exponential Pixel Model	97
5.4	Schlick Pixel Model	100
5.5	Miller Pixel Model	102
5.6	Tumblin and Rush Pixel Model	104
5.7	Log Pixel Model	105
5.8	Conclusion	107
6	Conclusion and Future Work	109
6.1	Summary	110
6.1.1	Tone Mapping	111
6.1.2	A Wide Dynamic Range Pixel	112

6.1.3	Pixel Modeling and Fixed Pattern Noise Correction	113
6.1.4	Pixel Modeling of Different Mapping Operators	114
6.2	Future Work	115
6.2.1	Image Sensor Chip Design	115
6.2.2	Local Tone Mapping	115
6.2.3	Video Tone Mapping	118
6.2.4	3D Stacked CMOS Image Sensor	119
6.3	Conclusion	121
7	A Appendix	122
7.1	Tone Mapping Operators	122
7.2	Reference Function Extraction	133
7.3	Model Error	137
7.4	Fixed Pattern Noise	139
	Bibliography	141

List of Figures

1.1	CMOS image sensors yearly growth [Data is taken from IC insights]. . .	3
1.2	(a) The typical CCD pixel structure. (b) The basic structure of interline CCD sensor.	4
1.3	(a) Schematic of a typical CMOS linear pixel. (b) CMOS pixel array. . .	6
1.4	A steeped reset signal and corresponding charge for dynamic range en- hancement for well capacity adjustment sensors.	7
1.5	A schematic of typical logarithmic pixel.	8
1.6	Signal flow diagram in an integration pixel.	10
1.7	(a) High dynamic range pixel schematic with adjustable reference func- tion. (b) Operation of the wide dynamic range pixel.	12
1.8	(a) A wide dynamic range image. (b) Same image after tone mapping operation.	14
1.9	(a) Drago operator reference function. (b) Exponential operator refer- ence function.	15
1.10	(a) Image without fixed pattern noise. (b) Image with fixed pattern noise. .	17

2.1	(a) Image perceived by the camera. (b) Image perceived by the human visual system.	23
2.2	Tone Mapping problem: Faithful representation of HDR content on LDR display device.	25
2.3	Input images used for Matlab simulation.	38
2.4	Results of standard dynamic range image after tone mapping operation.	41
2.5	Results of high dynamic range image after tone mapping operation. . .	42
3.1	Active pixel sensor schematic and signal flow diagram.	48
3.2	Wide dynamic range pixel schematic and signal flow diagram.	50
3.3	Monotonically increasing reference function for Reinhard simple and complex mapping operator with two different values of I_w	55
3.4	Drago reference function.	57
3.5	Exponential reference function.	58
3.6	Schlick reference function.	60
3.7	Miller reference function.	61
3.8	Tumblin and Rushmeier reference function.	62
3.9	Logarithmic reference function.	63
3.10	WDR pixel response at different monotonous reference functions. . . .	66
4.1	A WDR pixel with a typical column circuitry.	70
4.2	Comparison of parameter model and simulated pixel response.	78
4.3	Model error between pixel simulated and model response.	79

4.4	Reinhard simple FPN expressed as contrast error before correction. . . .	83
4.5	Reinhard complex FPN expressed as contrast error before correction. . .	84
4.6	Reinhard simple FPN expressed as contrast error after one parameter a correction.	86
4.7	Reinhard simple FPN expressed as contrast error after two parameters a and b correction.	86
4.8	Reinhard simple FPN expressed as contrast error after three parameters a, b, c correction.	87
4.9	Reinhard simple FPN expressed as contrast error after all parameters correction.	87
4.10	Reinhard complex FPN expressed as contrast error after one parameter P correction.	88
4.11	Reinhard complex FPN expressed as contrast error after two parameters P, Q correction.	89
4.12	Reinhard complex FPN expressed as contrast error after three param- eters P, Q, R correction.	89
4.13	Reinhard complex FPN expressed as contrast error after four parameters correction.	90
4.14	Test image.	91
4.15	Test image with fixed pattern noise.	91
4.16	(a) Test image after FPN correction of Reinhard simple. (b) Test image after FPN correction of Reinhard complex.	91

5.1	Comparison of model and simulated Drago response.	96
5.2	Model error between simulated and model response.	97
5.3	Comparison of model and simulated exponential response.	99
5.4	Error between simulated and model response.	99
6.1	Block diagram of image sensor chip.	116
6.2	Chiu local tone mapping operator.	118
6.3	Structure of conventional and 3D stacked CMOS image sensor.	120
7.1	Input and output image after logarithmic tone mapping operation.	124
7.2	Image before tone mapping operation.	125
7.3	Image after Exponential tone mapping operation.	126
7.4	Input and output image after Drago tone mapping operation.	127
7.5	Input and output image after Reinhard tone mapping operation.	130
7.6	Input images used for Matlab simulation.	132

List of Tables

2.1	Luminance levels for some common scenes	21
2.2	Different mapping operator image quality simulation result for standard and high dynamic range image. Our comparison results are in a good agreement with other studies presented by different authors	39
4.1	Extracted parameters using different calibration currents over 9 decades of photocurrent.	75
4.2	Reinhard complex extracted parameters using different calibration currents over 9 decades of photocurrent.	77
4.3	Mean and standard deviations of 1000 extracted parameters for Reinhard simple pixel.	82
4.4	Mean and standard deviations of 1000 extracted parameters for Reinhard complex pixel.	82
4.5	Summary Table.	89
5.1	Schlick extracted parameters using different calibration current.	101
5.2	Summary Table.	106

Chapter 1

Introduction

1.1 Background

Electronic imaging devices have experienced rapid growth in their usage in the last decade, and these electronic devices replace traditional imaging techniques of film-based cameras. Traditional imaging techniques of film-based are rarely used in these times. Although electronic imaging devices have replaced film-based cameras, the human eye remains the ultimate standard of comparison, and it vastly outperforms the best cameras in many respects [1].

Electronic imaging devices may be divided into two categories: charge coupled device (CCD) sensor and complimentary metal-oxide semiconductor (CMOS) sensor. These imaging devices are mostly used in mobile phones, still and video cameras, automobiles, security, and biometrics. The earlier digital cameras were mostly made from CCD sensor technology. Charged coupled devices, having benefited from longer development and maturation, yield superior quality color images, higher signal to noise ratios, high

photosensitive area, and low readout noise [2]. However, microelectronic manufacturing of CCD sensor is expensive and hence the cost of these image sensors was typically high. Besides, these also suffered from high power consumption with no functional integration to other devices.

On the other hand, CMOS image sensors were first introduced in the low-end application like toys and mobile phones. Also, CMOS image devices benefit from low power consumption, lower fabrication costs, ability to integrate with other circuits blocks on a single chip and faster readout time. These days, CMOS sensors have replaced CCD in the most low end as well as professional cameras. According to IC Insights 2015 O-S-D Report, a market analysis and forecast for optoelectronics, Sensors/Actuators, and Discretes, CMOS image sensor sales are climbing 15% in 2015 to reach an all-time high of \$10.1 billion after a strong 19% increase in 2014, and 4% growth in 2013 that primarily resulted from steep price erosion and inventory corrections in camera phones. CMOS image sensor unit shipments are now projected to grow 19% in 2015 to a record-high \$3.7 billion after rising 20% in 2014 and 2013. Overall, total CMOS image sensor sales are projected to grow by 11.1% in the five-year forecast period to reach \$15 billion in 2019 as shown in Figure¹ 1.1.

Figure 1.1 shows the strong growth in the usage of CMOS image sensors. CMOS image sensors sales were mainly driven by the camera integration inside a mobile phone. Besides, global shutter and BSI (Back Side Illumination) technology have enabled CMOS image sensors to compete with CCD sensors on high-end devices like DSLR (Digital Single Lens Reflex) and video cameras while keeping its traditional advantages like low power consumption, high resolution, and high integration [3].

¹image is taken from IC Insights 2015 O-S-D Report, A Market Analysis and Forecast for Optoelectronic, Sensors/Actuators, and Discrete.



Figure 1.1: CMOS image sensors yearly growth [Data is taken from IC insights].

1.2 Image Sensor Designs

Electronics image sensors can be divided into two main categories: charge coupled device (CCD) sensor and complimentary metal-oxide semiconductor (CMOS) sensor. The common element in these image sensors are photoreceptors like photodiode and phototransistor that interacts with the light energy reflected from an object in a scene. The basic function of the photoreceptor are charge capture generated from capture of photons and later, this charge is transferred and converted into a desirable quantity such as a voltage or current for further processing.

1.2.1 Charge Couple Devices

Figure 1.2(a) illustrates the basic structure of interline transfer CCD pixel. The CCD sensor has three basic functions: a) charge collection, b) charge transfer and c) charge conversion into a measurable voltage. During the first stage, incoming light strikes the

photosensitive area of each pixel. These photons generate electron-hole pairs in the depletion region of the CCD structure. After some time, during readout process, every pixel charge is transferred through vertical shift registers to an amplifier where it is converted to a voltage, buffered, and sent off-chip as an analog signal. The typical CCD sensor is composed of a pixel arranged in vertical and horizontal shift registers as shown in Figure 1.2(b).

The main disadvantages of CCD sensors are that their fabrication is quite complex, they require more electronics circuit outside sensor, and also suffer from high power consumption that leads to heat issues in the camera. The overheating issue impacts the image quality.

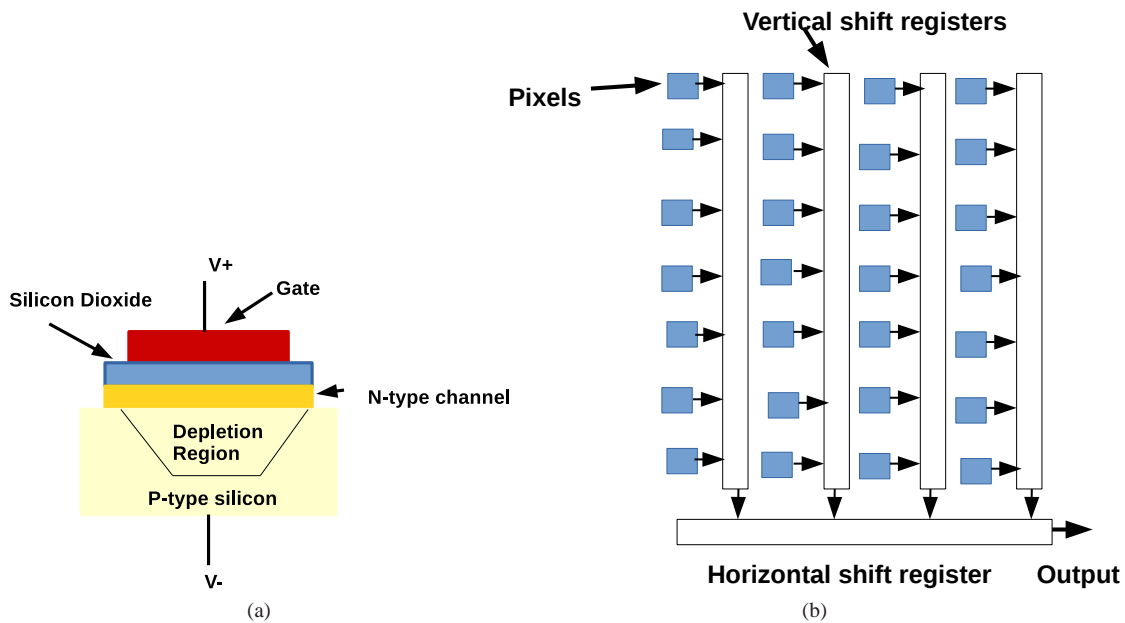


Figure 1.2: (a) The typical CCD pixel structure. (b) The basic structure of interline CCD sensor.

1.2.2 CMOS Devices

A typical CMOS image sensor pixel consists of a photodetector, usually photodiode and a couple of transistors and capacitors. When light falls on the photodiode, charge carriers are produced which are used to produce the output voltage or current signal. A typical CMOS 3 transistor linear pixel is shown in Figure 1.3. $M1$, $M2$ and $M3$ are all NMOS devices. Transistor $M1$, $M2$ and $M3$ are reset, source follower and row select switch respectively. PD is a photodiode which converts input light into charge. Pixel operation starts with the high reset voltage at the gate of transistor $M1$. Due to high voltage at $M1$, the $V_{dd} - V_t$ will be transferred to node N . Light falling on the photodiode then generates charge at node N , which acts to reduce the voltage being held on the diode capacitance. The voltage at node N is readout using the source follower $M2$ and select switch $M3$.

Figure 1.3(b) shows the typical CMOS image sensor array. In the array, charge voltage signals are read out one row at a time in a manner similar to a random access memory using row and column select circuits [4]. The random access readout provides the high-speed readout at low power consumption. However, readout path comprises of several devices that introduce temporal and fixed pattern noise that degrades the image quality of CMOS image sensor.

1.3 Wide Dynamic Range Image Sensor

Nature have a dynamic range of light intensities up to 6 decades. Typical CMOS APS (active pixel sensor) and CCD have limited ability to capture the light available in nature. The dynamic range of CMOS sensor is the ratio between the maximum and minimum

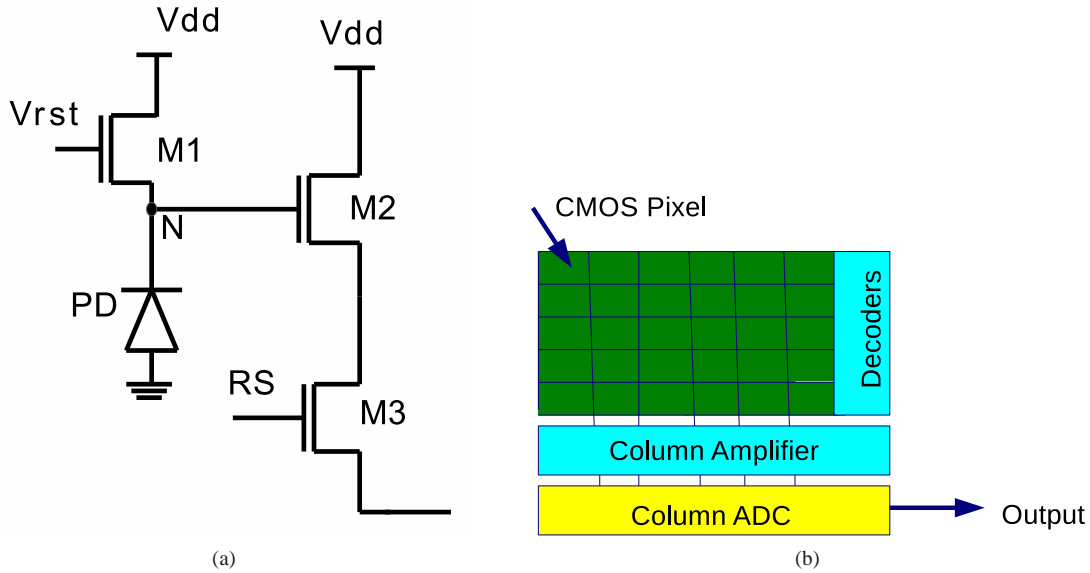


Figure 1.3: (a) Schematic of a typical CMOS linear pixel. (b) CMOS pixel array.

luminance in a scene and is limited by the semiconductor device used to capture the image [5]. This semiconductor device converts input light into a charge that is read out and digitised to store the image. High input light generates a large amount of charge which saturates the pixel. On the other hand, very low input light generates a low charge that is very difficult to read out faithfully. Typical CMOS sensors using the basic APS have a dynamic range between $40dB$ to $60dB$.

Several different approaches and CMOS circuits have been proposed to extend the dynamic range of CMOS pixels. These include logarithmic sensors using the weak inversion region of operation of a MOS transistor [6], well capacity adjustment [7], threshold comparison, integration time control [8], neuromorphic approaches [9] and linear-logarithmic pixel [10]. More detailed discussion about these techniques and circuits to enhance the wide dynamic range of CMOS sensors are presented in the next section.

1.3.1 Well Capacity Adjustment Sensors

One way to increase the dynamic range of image sensor is to enhance the well capacity by changing the reset signal during the integration period. Decker and co-workers have proposed the similar technique to change the reset signal at a rate increasing with time [7]. This change in reset voltage changes the pixel charge as shown in Figure 1.4.

By increasing the pixel operating voltage, one can also adjust the well capacity. However, this will lead to increasing power consumption. It has been noted that with the power supply constant, any charge generated in the pixel after its saturation often spills. Controlling this spilling charge operation can be used to enhance the dynamic range of the pixel. One can also use the pinned photodiode in APS to integrate the spilled charge and photodiode charge to extract the input light on the pixel [11].

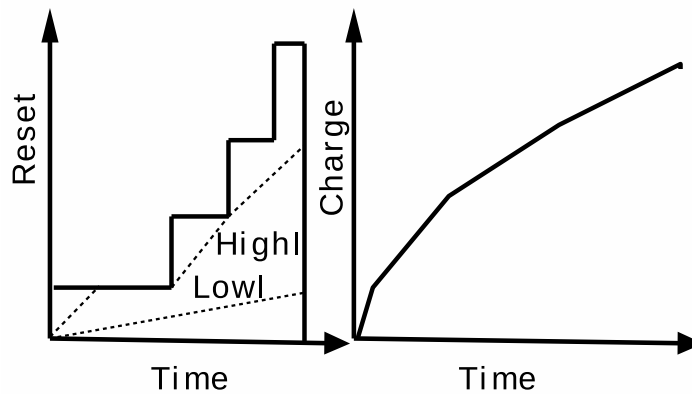


Figure 1.4: A stepped reset signal and corresponding charge for dynamic range enhancement for well capacity adjustment sensors.

1.3.2 Logarithmic Sensors

Logarithmic pixel is another technique to capture wide dynamic range. Logarithmic pixel is similar to active pixel sensor except NMOS reset transistor operating in a weak inversion region with its gate shortened to the drain as shown in Figure 1.5. Reset NMOS transistor in weak inversion region act as a logarithmic amplifier, which compresses the input photocurrent and converts into logarithmic voltage.

A logarithmic pixel can capture wide dynamic range more than 6 decades of light intensity. The main disadvantage of logarithmic pixels is high fixed pattern noise. They are highly susceptible to fixed pattern noise, as any double sampling operation is difficult to undertake.

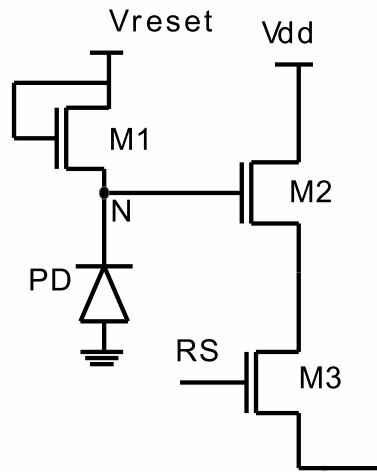


Figure 1.5: A schematic of typical logarithmic pixel.

1.3.3 Threshold Comparing Sensors

Wide dynamic range can be enhanced by using threshold comparing pixels. Threshold pixels integrate the photocurrent till the output reaches a known threshold value [12]. For example, Hyneceks pixel provides a provision for resetting the pixel only when the accumulated charge exceeds a certain threshold voltage and ignoring the reset at all other instances [12]. Later, the number of resets can be stored in local memory inside each pixel. Due to a large number of compactors and memories inside each pixel reduce the pixel fill factor and effect its quantum efficiency.

In an another approach, Anaxagoras and Allinson have proposed an active pixel which resets every time it saturates [13]. The number of saturations is measured on a counter. This count in combination with the final pixel output is used to extend the dynamic range of the pixel. The main drawback of threshold comparing pixels is low light sensitivity due to a large pixel size and a small area reserved for light capture.

1.3.4 Integration Time Control Sensors

Integration time control technique can be used to capture wide dynamic range information. The integration time can be controlled by locally adapting the integration time for each pixel or group of pixels [14, 15]. This may be achieved by continuously comparing the pixel output to one or many references and using the output of comparison to generate reset pulses or a few bits of flags to be stored in a memory [15]. Integration time control sensors have high fixed pattern noise due to the mismatch of a circuit element as well as integration time mismatch between pixels.

1.3.5 Threshold Comparing and Integration Time Control Pixels

By combining the two approaches of threshold comparing and integration time control, provides another design to capture the dynamic range information [10]. Figure 1.6 shows the signal flow diagram of an integration pixel. In a typical linear pixel, high photocurrent I_1 shown by dashed lines saturates the pixel that leads to incomplete wide dynamic range capture. However, in an integration pixel, a continuously increasing reference signal is compared to the integrated signal shown as I_1, I_2, I_3 in Figure 1.6, and the integration is stopped when the two signals are equal. The voltage at which these two signals are equal is recorded and used as pixel output. Hence, pixel output depends on the increasing reference voltage V_{ref} .

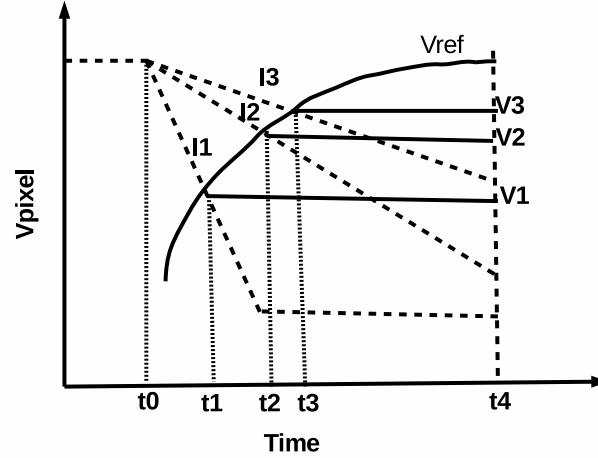


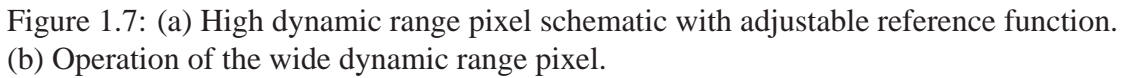
Figure 1.6: Signal flow diagram in an integration pixel.

1.4 A New Wide Dynamic Range Pixel Design

A new wide dynamic range integration pixel which uses NMOS transistors as shown in Figure 1.7 is proposed which aims to capture the wide dynamic range of intensities available in nature otherwise lost in active pixel sensor. WDR capture can be performed by introducing a monotonically increasing reference signal V_{ref} . It is possible to capture high intensity information by comparing the integrated voltage at node N to a reference voltage V_{ref} . The pixel output follows a known reference signal, which is sampled and held at a value when the photo-generated signal on the diode becomes lower than the reference voltage. The potential at which these two signals are equal is recorded and is used as the pixel's response [16]. In the pixel, $M1$, $M2$, $M3$ and $M4$ are reset device, reference voltage switch, source follower and row select switch.

The pixel operation starts by resetting the transistor $M1$, by applying the high reset signal V_{rst} at the gate of transistor $M1$. Due to the high voltage at the gate of $M1$, voltage $V_{dd} - V_{th}$ is transferred to device $M1$ source node N . The high voltage placed on the capacitance of node N is discharged by the photo-generated charge when transistor $M1$ is off, by lowering its gate voltage. A monotonically increasing reference function V_{ref} is applied to transistor $M2$ drain. At the start of integration, the voltage V_{ref} is lower than node voltage N and hence transistor $M2$ is on. However, discharging node voltage at N and monotonically increasing V_{ref} leads to transistor $M2$ being switched off. After this time, the gate voltage of $M3$ is held by its gate capacitance until its readout and a pixel is reset. The output voltage of the pixel depends on the signal V_{ref} and I_{ph} .

Hence, a novel NMOS pixel with reference switch can capture wide range of light intensities by using the monotonically increasing reference function. In this thesis, we proposed different reference functions extracted from tone mapping operators.



In a real world, the dynamic range of a scene can be on the order of 10^6 to 10^0 from light to dark areas. However, display devices available to us are unable to produce such wide dynamic range that nature has. In order to obtain realistic images on display devices, it is necessary for the images to be a faithful representation of the scene they depict. In addition, for good and realistic image reproduction on display devices, it is also necessary to take into account the way HVS (Human Vision System) operates. To solve the problem of displaying wide dynamic range content on low dynamic range displays, computational algorithms known as tone mapping operators have been proposed. Tone mapping is a technique that aims to match the dynamic range of WDR content with the display device dynamic range. Tone mapping compresses or expands the luminance to fit WDR content on LDR (Low Dynamic Range) display. The goal of tone mapping can be different and depends on the particular application. In some cases producing

just 'nice looking' image is the main goal while other applications might emphasize reproducing as much detail as possible, or might maximize the image contrast [17]. Figure 1.8 shows the wide dynamic range image and processed image after tone mapping. It can be noted that tone mapping operation enhanced the overall image quality and contrast. In addition, image detail in dark areas is more visible after tone mapping.

Tone mapping operators can be divided into four groups called

- Global operators
- Local operators
- Frequency operators
- Segmentation operators

The detail discussion about these operators will be presented in next chapter. Global tone mapping operators are used for wide dynamic range capture and display because they are computationally efficient and can be executed in real time [17], faster than other operators.

1.4.2 Tone mapping on an integrating CMOS pixel

As discussed earlier, a CMOS image sensor can capture a wide dynamic range using the monotonically increasing reference voltage. Most of the tone mapping operators have monotonically increasing transduction function. Hence, tone mapping transfer function for CMOS pixel has been proposed which aims to perform tone mapping at the image acquisition stage, thereby enabling direct display of HDR images. Figure 1.9 presents



Figure 1.8: (a) A wide dynamic range image. (b) Same image after tone mapping operation.

the two reference function extracted from Drago and Exponential tone mapping operators for CMOS image sensor. Tone mapping operation using a CMOS pixel in practice performs two operations; one is to capture wide dynamic range using a reference voltage and second is to enable direct display of an image on LDR display devices. This reduces the two step process of typical cameras, where the image is captured in one stage and tone mapping is then applied to make this image displayable on display devices.

Different global tone mapping reference functions will be presented in the chapter 3 with an aim to capture and display wide dynamic range scenes. Also, WDR pixel simulation with different reference functions in Cadence using the AMS (Austria Micro Systems) process technology is also presented in chapter 3.

1.5 Fixed Pattern Noise

A WDR CMOS image sensor has different kinds of noise which includes model error, fixed pattern noise (FPN), and temporal noise. Model error originates due to the differ-

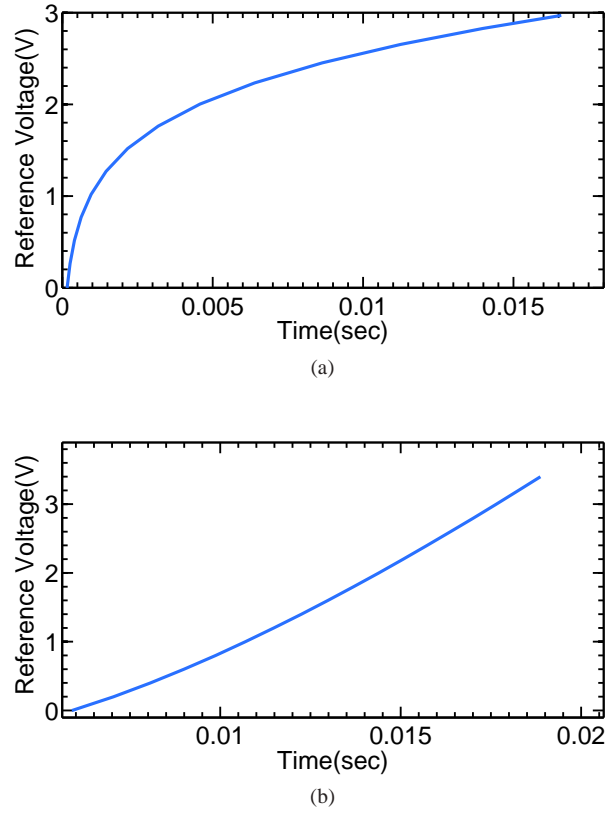


Figure 1.9: (a) Drago operator reference function. (b) Exponential operator reference function.

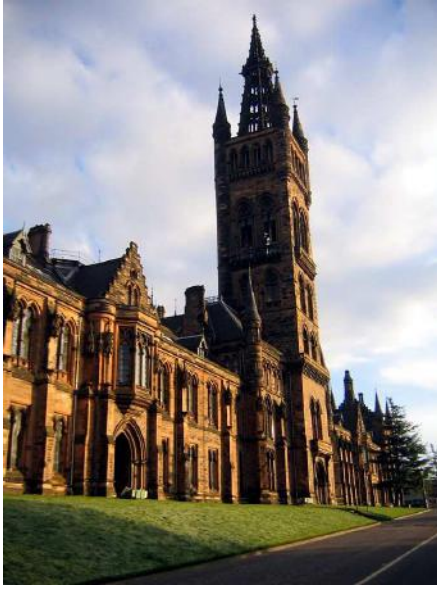
ence between pixel simulated and pixel model response. FPN generates due to the pixel mismatch in an array of image sensor. There is a need to develop a pixel model with different parameters that characterize the pixel response before analysing model error. A new wide dynamic range pixel parameter model for Reinhard simple and complex operators is developed [17]. The model response for Reinhard simple pixel is given as

$$y = a - \frac{b(x+d)}{1+c(x+d)} \quad (1.1)$$

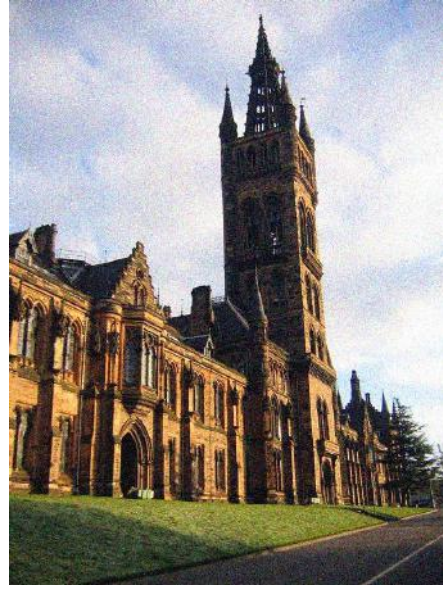
where y is pixel output, x is input photocurrent, a is pixel offset voltage, b and c represents the pixel gain and d is the dark current. Similarly, other mapping operators pixel model is also developed and presented in later chapters. Parameters need to be extracted to find the model response and model error. After finding the required parameters, Reinhard model response can be calculated by inserting the extracted parameters into equation 1.1.

FPN severely degrades the quality of an image taken by an image sensor. Figure 1.10 shows the image with and without fixed pattern noise. The image with FPN exhibits the salt and pepper pattern that distorts the image quality. The variations between responses of individual pixels generate FPN. These variations are caused by the device and interconnect parameter mismatches in an individual pixel. FPN can be quantified by making the human visual system as a standard. Fixed pattern noise can be described as a contrast threshold error, and 1% error value becomes the best attempt at matching FPN error to the sensitivity of the human visual system.

In this thesis, we present the new FPN correction technique in which parametric response of the pixel is used, with FPN modeled as variations in the individual parameters. The parameters of each pixel are measured, recorded and then used to correct their response. We simulated the Reinhard pixel using Monte Carlo simulation and extracted the parameters for 1000 pixels. Pixel parameters could be extracted using function minimization or curve fit technique. However, this is too complex to be applied in real time and will require several measurements from the pixel. The typical approach of double sampling to correct fixed pattern noise is difficult to implement in this kind of pixel. Hence, parameters are used to correct fixed pattern noise. The detail discussion about FPN correction is presented in later chapters.



(a)



(b)

Figure 1.10: (a) Image without fixed pattern noise. (b) Image with fixed pattern noise.

1.6 Thesis Objectives

This thesis is mainly concerned with the capture and display of wide dynamic range scenes available in nature. CMOS based typical sensor are unable to capture the wide dynamic range. Tone mapping technique is used to enable the capture and direct display of wide dynamic range scenes simultaneously. The image is algorithmically transformed by tone mapping operators to fit the limited dynamic range. In this thesis, a new pixel is proposed which aims to capture wide dynamic range scenes. The detail literature review on different tone mapping operators is presented with the Matlab simulations. In addition, the comparison between different mapping operators through Matlab simulations are also presented. Reference voltages are extracted from different tone mapping operators and applied on a pixel for wide dynamic range capture. The

derivation of 6 tone mapping operator reference functions is proposed. To verify the performance of these tone mapping reference function, a typical pixel is simulated using a $0.35\mu m$ CMOS process from Austria Microsystems. Simulation results show that the pixel response can capture 6 decades of light intensity.

This thesis also deals with the WDR pixel model. A pixel model with different parameters that characterizes the pixel response is presented. In addition, a model error between pixel simulation and model response is also considered. Fixed pattern noise arises due to variations in characteristics of individual pixels within an array of a pixel. This thesis presents the simple technique to correct FPN in which parametric response of the pixel is used, with FPN modeled as variations in the individual parameters. The parameters of each pixel are measured, recorded and then used to correct their response.

1.7 Thesis Organisation

The rest of thesis organisation is given as follows. Chapter 2 describes the introduction and background of the tone mapping technique. A detailed discussion about different global operators is also presented in this chapter. A comparison of results for different mapping operators using Matlab routine are discussed. A Matlab routine simulates each mapping operator transfer function to check the quality and faithfulness of output image after the tone mapping operation. Two input images with different background illumination conditions are selected for Matlab simulation. A qualitative criteria are used to assess the image quality that is simple and straightforward to implement.

Chapter 3 presents the wide dynamic range capture and display using tone mapping operation on a pixel. A new pixel is presented which, aims to capture wide dynamic

available in nature. Different reference functions are extracted from global tone mapping operators and applied on a CMOS pixel to obtain wide dynamic range information. Tone mapping operation on a CMOS pixel in practice performs two operations; one is to capture wide dynamic range using reference voltage and second is to enable direct display of an image on low dynamic range display devices. WDR pixel simulation results are presented by applying a reference function. The results show the pixel ability to capture more than 6 decades of dynamic range.

In chapter 4, a pixel model of the Reinhard operator is developed with different parameters that characterise the pixel response. In addition, parameter extraction routine is also discussed. Pixel model response is compared with the simulated response to check its validity. Model error is presented and suggests that developed model fits well with the simulation data. This chapter also presents the fixed pattern noise investigation and correction technique. The variations between individual pixel response within an array of pixels cause FPN generation. A simple procedure is adapted to reduce FPN in which parametric response of pixel is used, with FPN modeled as variations in the individual parameters. The response of 1000 pixel is obtained using Monte Carlo simulations in Cadence circuit simulator. Parameters values are measured using the response of 1000 pixels and then used to correct the fixed pattern noise.

Chapter 5 presents the pixel model and model error of rest of the global operators. These includes Drago operator, Exponential, Schlick, Miller, Tumblin and Rushmeier, and logarithmic pixel. Chapter 6 discusses the conclusion and future work. Chapter 7 presents an appendix.

Chapter 2

Tone Mapping

2.1 Introduction

A number of industries including defence, night vision imaging, games and computer graphics are demanding for more realistic images displayed on a computer that matches the real scene as seen by the human visual system (HVS). However, in a natural world, there are a wide range of colors and intensities. In addition, the appearance of a scene depends upon the level of illumination. For example, scenes appear more bright on a sunny day, whereas the same scene appears dull during night. Luminance is the amount of light that passes through or is emitted from a particular surface. The standard unit of luminance is candela per square meter (cd/m^2). The dynamic range is the ratio between the maximum and minimum luminance in a scene. The real world can produce such a wide dynamic range of illumination, for example, the sun at noon may be 100 million times brighter than starlight [18].

However, display devices available in the market are unable to produce the image detail

Condition	Illumination
Starlight	10^{-3}
Moonlight	10^{-1}
Roomlight	10^2
Sunlight	10^5
CRT monitors	10^2

Table 2.1: Luminance levels for some common scenes

as seen by human eye. Tone mapping is the operation that matches the dynamic range of high dynamic range (HDR) content with the display device dynamic range. When the dynamic range of the captured scene is smaller or larger than that of the display device, tone mapping expands or compresses the luminance respectively [19].

Section 2.2 presents the background of a wide dynamic range of intensities available in nature and how the human eye perceives the light. Section 2.3 discusses the tone mapping basic theory and operation. Section 2.4 presents the different global tone mapping operators. Section 2.5 presents the Matlab simulation result to check the quality of different mapping operators and with a conclusion being presented in section 2.6.

2.2 Background

The human eye can capture the light intensity of about five orders of magnitude simultaneously available in the real world as can be seen in Table 2.1. It gathers light onto photoreceptors which then convert light into signals. These signals are then passed through the optical nerve to the brain that processes these signals producing the perceived image or percept [20]. The human eye has two types of photoreceptors, cones and rods. The cones are more sensitive at luminance between $10^{-2}cd/m^2$ and $10^8cd/m^2$ (daylight vi-

sion). They are also responsible for the perception of high frequency pattern and colors. The rods are more sensitive at luminance between $10^{-6}cd/m^2$ and $10^0cd/m^2$ (night vision). The rods and cones also compress the incoming light signal and reduce dynamic range by following sigmoid function [21],

$$\frac{R}{R_{max}} = \frac{I^n}{I^n + \sigma^n} \quad (2.1)$$

where R is the photoreceptor response, R_{max} is the maximum photoreceptor response and I is the light intensity. The variables σ and n are the semi saturation constant and the sensitivity control exponent [20] respectively.

The human visual system uses non-linear processing in the form of sigmoid function to compress the dynamic range of an image. After compression, HVS forms an image that we call percept. Figure 2.1 shows an image¹ which is perceived by the human visual system and the same image capture by the camera. It can be seen that human eye is able to capture wide dynamic range of intensities available in nature. If the scene dynamic range is greater than the dynamic range of display device, then it is called high dynamic range scene. Some information will be lost in a scene if this high dynamic range scene is displayed on a low dynamic range scene. A scene is said to be a low dynamic range (LDR) when its dynamic range is lower than that of the output medium. In this case, scene dynamic range has to be expanded to fit the output medium dynamic range. If the scene dynamic range and display device dynamic range is same then it is called standard dynamic range scene [19].

There are a number of ways to capture HDR content including software and hardware techniques. However, HDR capture using hardware have some limitations until recently.

¹image is taken from <http://www.morguefile.com/>



(b)

Figure 2.1: (a) Image perceived by the camera. (b) Image perceived by the human visual system.

The most commonly used method to capture HDR image is taking a multiple exposure images of the same scene from the darkest to brightest areas using a standard camera [20]. Each pixel in an image will be properly exposed or underexposed. HDR image can be obtained by combining images with different exposure time. Some camera manufactures like Canon, Nikon and Sony have launched DSLR cameras with HDR capturing features such as multiexposure capturing and automatic exposure merging.

There are group of 360 degree panoramic cameras, which claim to capture full HDR like SpheronCam HDR, Panoscan Mk-3 and Civetta 360 by Weiss AG. HDR image can also be generated using computer graphics.

If one can capture the HDR content somehow, however to display this HDR content faithfully, HDR display device is needed. Typical display devices like liquid crystal displays have a standard dynamic range and can reproduce about two orders of magnitude of intensity variations. To overcome the limitations of these Low Dynamic Range (LDR) displays, some research, and industrial interest have been drawn to develop High Dynamic Range (HDR) displays; however these have proven to be either insufficient or costly [22].

2.3 Tone Mapping

In order to obtain realistic images on display devices, it is necessary for the images to be a faithful representation of the scene they depict. In addition, for good and realistic image reproduction on display devices, it is also necessary to take into account the way HVS operates. The rods and cones compress the incoming light and reduce the dynamic range of the scene using the sigmoid function. Nature has a wide dynamic range of illumination on the order of 100,000 to 1 sunlight to shadow. However, display devices available to us are unable to produce such wide dynamic range that nature has. Typical display devices can only produce an image of dynamic range of less than 100 to 1 [18] as an example of CRT monitors given in Table 2.1. Hence, it is a problem to reproduce high dynamic range scenes using media with very limited dynamic range like CRT/LCD displays, hard-copy prints, and projectors. In order to solve the problem

of displaying HDR images on LDR displays, computational algorithms known as tone mapping operators have been proposed.

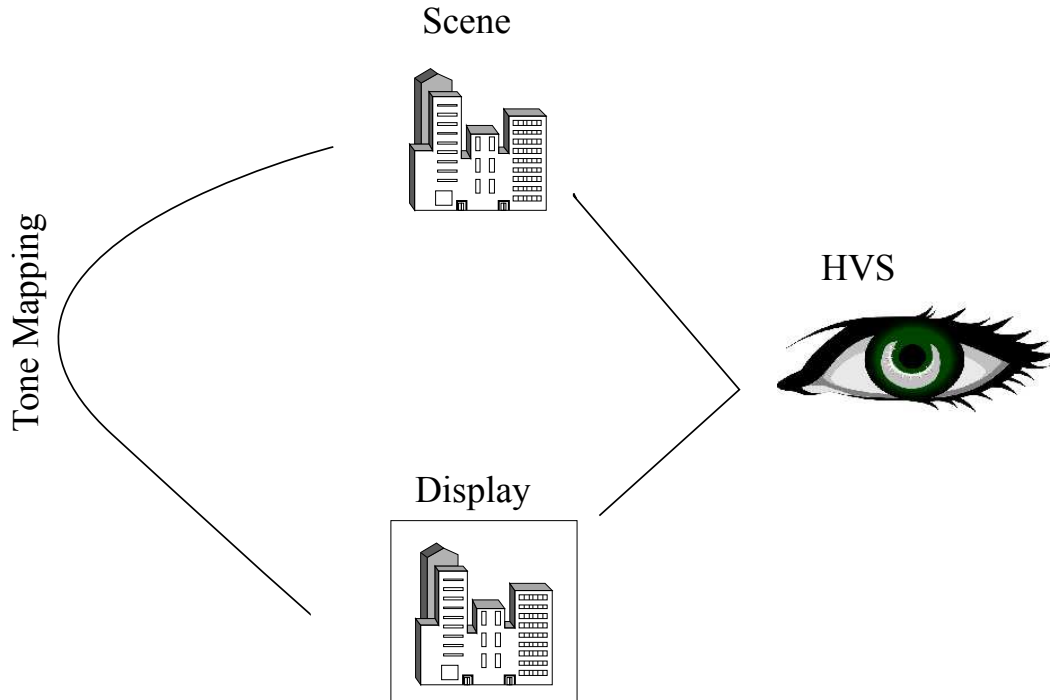


Figure 2.2: Tone Mapping problem: Faithful representation of HDR content on LDR display device.

Tone mapping is the operation that matches the dynamic range of HDR content with the display device dynamic range. When the dynamic range of the captured scene is smaller or larger than that of the display device, tone mapping expands or compresses the luminance, respectively [19]. On the display device, the image should be a faithful representation of the real image with some characteristics of the real image such as contrast and details should be kept same or improved on the display.

The purpose of applying tone mapping on an image can be different and depends on the particular application. In some cases producing just 'nice looking' image is the main

goal, while other applications might emphasize reproducing as many details as possible, or might maximize the image contrast [23]. However, the ultimate goal of tone mapping is to match the perception of tone mapped image with the real world perception seen by human visual system as can be seen in Figure 2.2. The tone mapping operator (TMO) f is used for tone mapping operation can be defined as [20]

$$f(I) : R^{w \times h \times c} \rightarrow D^{w \times h \times c} \quad (2.2)$$

Here I is an image, f is operator, w is width, h is height and c is number of color bands which is 3 in RGB color space. The selection of a suitable tone mapping operator depends on a particular application and a type of display device (LCD, Plasma, CRT) and its characteristics.

Tone mapping operators mainly classified into four groups given as

2.3.1 Global Operators

The same mapping function is applied to all pixels of the image. Mapping function treats each pixel of the image independently. Global operators take each pixel value and a globally derived quantity such as maximum luminance, minimum luminance and the arithmetic average for the compression. Global operators are computationally efficient, easy to implement and can be executed in real time. The main drawback of global operators is that they may not always preserve visibility if the dynamic range of an image is extremely high. In addition, since they make use of global image statistics, they are unable to maintain local contrast too [20].

2.3.2 Local Operators

A local mapping operator function compress each pixel value according to its luminance values and set of neighboring pixels luminance values. Hence, for each pixel the computation is adjusted according to an average over a local neighborhood of pixels [18]. However, halos around edges can appear if neighbors were not chosen carefully. Halos are sometimes desired when attention needs to be given to a particular area but if the phenomenon is uncontrolled it can produce unpleasant images [20].

2.3.3 Frequency Domain Operators

Frequency based operators have the same goal of preserving edges and local contrast as local operators. However, this is achieved by computing in the frequency domain instead of spatial [20]. Frequency Mapping operator is applied only to the low frequencies while high frequencies are kept same as they preserve fine details.

2.3.4 Segmentation Operators

The image is divided into different uniform regions, a global mapping operator is applied on each region and finally these are merged.

Global operators will be discussed in the next sections in detail. Global tone mapping is selected for further research. Local, frequency and segmentation operators are out of the scope of the thesis.

2.4 Global Operators

Global operators compress each pixel with the same function or a compression curve within an image. In addition, the tone mapping function treats each pixel of the image independently. These operators often use globally derived image statistics to reduce the dynamic range of the image. Some common statistics are maximum luminance, minimum luminance, and geometric or arithmetic average values [20]. The goal of the global operator is to mimic the performance of HVS non-linearity in order to get a visually more appealing image.

Global operators are computationally efficient and can be executed in real time, faster than other operators. On the other hand, local tone mapping operators are computationally more expensive. In order to get local contrast improved, local operators need to be used along with global operators. Different global tone mapping operators will be discussed in detail next.

2.4.1 Linear Scaling

A simple linear scaling is a straightforward mapping operator. Input or world luminance $L_w(x,y)$ is multiplied by a constant e and output or display luminance $L_d(x,y)$ is given as,

$$L_d(x,y) = eL_w(x,y) \quad (2.3)$$

where e is user controllable value. When $e = \frac{1}{L_{wmax}}$, the scaling is called normalization. A simple linear scaling is not an efficient tone mapping operator and is unable to compress the dynamic range of the scene.

2.4.2 Logarithmic Mapping

Logarithmic mapping compress the HDR using a logarithm function and given as [24]

$$L_d(x, y) = \frac{\log_{10}(1 + L_w(x, y))}{\log_{10}(1 + L_{max})} \quad (2.4)$$

where L_{max} is maximum world luminance. For medium dynamic range images, logarithmic mapping produce good results and in fact be competitive with more complex operators [18].

2.4.3 Exponential Mapping

Exponential function compress the HDR luminance using the exponential function [25], and the operator is given as,

$$L_d(x, y) = 1 - \exp\left(\frac{-L_w(x, y)}{L_{av}}\right) \quad (2.5)$$

where L_{av} is the average world luminance. For medium dynamic range images, logarithmic and exponential mapping produce very good results. However, both operators struggles when compressing full HDR content [18]. For HDR content compression, other approaches may be suitable.

2.4.4 Drago Mapping Operator

Drago [26] presented a tone mapping operator that applies a logarithmic mapping to the input luminance. However, the base of the logarithm is adjusted according to each pixel's value. It was noted that logarithm with base 10 compress the maximum high

luminance values while logarithm with base 2 gives good contrast and preserve details in dark and medium luminance regions. By combining the two different logarithmic bases, Drago presented a tone mapping operator given as,

$$L_d(x, y) = \frac{L_{dmax} \log_{10}(1 + L_w(x, y))}{100 \log_{10}(1 + L_{wmax}) \log_{10}[2 + 8(\frac{L_w(x, y)}{L_{wmax}})^{\frac{\log_{10}(p)}{\log_{10}(0.5)}}]} \quad (2.6)$$

L_{dmax} is maximum display luminance with a value of $100cd/m^2$. p is user controllable value and has a value between 0.7 to 0.9 produces good result. A higher value of p result in less contrast and better compression, whereas smaller values increase the available contrast [18].

2.4.5 Schlick Operator

Schlick operator based on rational functions provides straight forward approach to tone mapping as given as [27],

$$L_d(x, y) = \frac{p L_w(x, y)}{(p - 1)L_w(x, y) + L_{max}} \quad (2.7)$$

where $p \in [1, \infty)$ value of p can be calculated as,

$$p = \frac{L_0 L_{wmax}}{2^N L_{wmin}} \quad (2.8)$$

N is the number of different luminance levels of display device and L_0 is the lowest luminance value of a monitor that can be perceived by the HVS. The value of p given in Equation 2.8 corresponds a uniform quantization process as the same function is applied to all pixels. A non uniform quantization process can be applied by using spatially

varying p' given as,

$$p' = p(1 - k + k \frac{L_{wavg}(x,y)}{\sqrt{L_{wmax} L_{wmin}}}) \quad (2.9)$$

where $k \in [0, 1]$. Schlick operator produces reasonable good result. However, in order to find the values of two parameters some experimentation needed to be done.

2.4.6 Tumblin and Rushmeier Operator

The operator is inspired by the HVS and adopts Stevens work on brightness [28, 29].

The operator is defined as ,

$$L_d(x,y) = mL_{da}(\frac{L_w(x,y)}{L_{wa}})^\alpha \quad (2.10)$$

where $\alpha = \frac{\gamma(L_{wa})}{\gamma(L_{da})}$

L_{da} and L_{wa} are display and image adaptation luminance values respectively. The typical value of display luminance is between 30 and 100cd/m² for standard display device.

The gamma function $\gamma(L)$ is human contrast sensitivity and given as,

$$\gamma(L) = \begin{cases} 2.665 & \text{for } L > 100\text{cd/m}^2 \\ 1.855 + 0.4\log_{10}(L + 2.3 \times 10^{-5}) & \text{otherwise} \end{cases}$$

The term m is the world adaptation dependent term and its value is given as

$$m = C_{max}^{\frac{\gamma_{wd}-1}{2}}$$

$$\gamma_{wd} = \frac{\gamma_w}{1.855 + 0.4 \log(L_{da})} \quad (2.11)$$

where C_{max} is the maximum display contrast. This tone mapping operator compresses HDR images, preserving brightness and producing plausible results when calibrated luminance values are available.

2.4.7 Miller Brightness Operator

Miller and colleagues [30] have presented a tone mapping operator that improves the brightness of the image before and after dynamic range reduction. The mapping operator is given as,

$$Q = k L_v^b \quad (2.12)$$

where Q is the brightness and L_v is the luminance. Miller experimented with three different formulations for determining brightness values from luminance and found that the one presented by Stevens [28] produces the most plausible results. By fitting data from Stevens work, Miller produced the values of k and b as follows,

$$\begin{aligned} b &= 0.338 L_v^{0.034} \\ k &= -1.5 \log_{10} L_v + 6.1 \end{aligned} \quad (2.13)$$

Hence, the final relationship between brightness Q and luminance L_v is given as,

$$Q = (-1.5 \log_{10} L_v + 6.1) L_v^{0.338 L_v^{0.034}} \quad (2.14)$$

The operator is fast and simple to implement and produced plausible results.

2.4.8 Reinhard Mapping Operator

Photographers were often faced with the tone mapping problem. Their main goal is to produce realistic 'renderings' of captured scene in order to get a quality print on photographic papers. Ansel Adams [31] presented the Zone system approach as a solution of photographic problems. It is the system of practical sensitometry, where the photographer uses measured information in the field to improve the chances of producing a good final print [17]. There are eleven print zones from pure black (Zone 0) to pure white (Zone X). The key is the scene indicative of light, normal and dark areas in the scene. In order to choose the correct zone, the photographer first takes a luminance reading he/she perceives as a middle grey. In a typical situation, this will be mapped to zone V, which corresponds to the 18% reflectance of the print. For high-key scenes the middle-grey will be one of the darker regions, whereas in low-key scenes this will be one of the lighter regions [17].

The procedure discussed above was used to develop a tone mapping operator by Reinhard [17]. Log average luminance L_w is taken as useful approximation of scene's key and given as,

$$L_{av} = \exp\left(\frac{1}{N} \sum_{x,y} \log(L_w(x,y))\right) \quad (2.15)$$

where $L_w(x,y)$ is a pixel luminance and N is the total number of pixels in the image. If the scene has normal-key we would like to map this to middle grey of the displayed image, or 0.18 on a scale from zero to one. This suggests the equation,

$$L(x,y) = \frac{a}{L_{av}} L_w(x,y) \quad (2.16)$$

where $L(x,y)$ is scaled luminance and $a = 0.18$. The value of a can be varied from 0.045

to 0.72. Modern photography uses a transfer function that compress high luminance. A simple mapping operator with that compress high luminance is given as,

$$L_d(x,y) = \frac{L(x,y)}{1 + L(x,y)} \quad (2.17)$$

It is clear from equation 2.17 that high luminance are scaled by approximately by $\frac{1}{L}$ and low luminance are scaled by 1. In some cases it is desirable to let bright areas burn out in a controllable fashion. Hence, in order to burn out bright areas above equation can be rewritten as,

$$L_d(x,y) = \frac{L(x,y)}{1 + L(x,y)} \left(1 + \frac{L(x,y)}{L_{white}^2}\right) \quad (2.18)$$

where L_{white}^2 is the smallest luminance that will be mapped to white . By default, this parameter is set to the maximum luminance value in the scene. For many high dynamic range images, this operator produced sufficient compression to preserve detail in low contrast areas, while compressing high luminance to a displayable range. However, for very high dynamic range images, this operator loses important details in the image. Hence, for a very HDR images a local tone mapping operator that applies dodging and burning effect has been presented by Reinhard [17].

2.4.9 Ward Histogram Adjustment

Ward applied the classic technique of histogram enhancement to reproduce HDR images simulating both visibility and contrast [32]. The operator first calculates the image histogram I of \log_2 space, using a number of bins n_{bin} . 100 bins are sufficient for

accurate results. The cumulative histogram $P(x)$ is given as,

$$\begin{aligned} P(x) &= \sum_{i=1}^x \frac{I(i)}{T} \\ T &= \sum_{i=1}^{n_{bin}} I(i) \end{aligned} \quad (2.19)$$

Histogram is itself the derivate of the cumulative histogram and given as,

$$\begin{aligned} \frac{d P(b)}{dx} &= \frac{I(x)}{T \Delta x} \\ \Delta x &= \frac{\log(\frac{L_{wmax}}{L_{wmin}})}{n_{bin}} \end{aligned} \quad (2.20)$$

The contrast equalization is given as,

$$\log(L_d(x,y)) = \log(L_{dmin}) + P(\log L_w(x,y)) \log(\frac{L_{dmax}}{L_{dmin}}) \quad (2.21)$$

Exaggeration of contrast is highly undesirable and can be dealt through following refinement,

$$\frac{d L_d}{d L_w} \leq \frac{L_d}{L_w} \quad (2.22)$$

$$L_d \frac{f(\log(L_w))}{T \Delta x} \frac{\log(\frac{L_{wmax}}{L_{wmin}})}{L_w} \leq \frac{L_d}{L_w} \quad (2.23)$$

which is reduced to a condition on $f(x)$,

$$\begin{aligned} f(x) &\leq c \\ c &= \frac{T \Delta x}{\log(\frac{L_{wmax}}{L_{wmin}})} \end{aligned} \quad (2.24)$$

This means that exaggeration may occur when Equation 2.24 is not satisfied. A solution is to truncate $f(x)$ which has to be done iteratively to avoid changes in T . Overall, the operator used modified histogram method in order to have good compression and overall contrast while simulating some aspects of the HVS [20].

2.5 Comparison Results

Tone mapping operators as discussed in earlier section were simulated with two images, standard dynamic range and high dynamic range as shown in Figure 2.3 in Matlab to understand the effects of tone mapping compression on HDR images. A number of other authors work [33–36] has been presented in literature to evaluate the different tone mapping operators. The attributes used for tone mapping operator evaluation in their work are overall image quality, brightness, contrast, reproduction of colors and reproduction of details in very dark and very bright areas. According to M.Cadick and co-worker [33], overall image quality can be presented in terms of other attributes given as,

$$IQ = 0.327Bri + 0.267Con + 0.102Det + 0.230 Col \quad (2.25)$$

where IQ is image quality in the interval of $[0, 1]$, Bri is image brightness, Con is image contrast, Det is detail and Col is color. Matlab code presented in appendix 7.1 was written and simulated for each operator in order to check image quality after tone mapping compression.

It should be noted that to assess the quality of images after tone mapping operation, a qualitative criteria is adapted. It means that we assessed the image quality by visually looking at it. A quantitative measure of image quality to check how good or bad the

result was not taken into consideration. The qualitative criteria used to assess the image quality is simple and straightforward to implement. On the other hand, the quantitative technique is time consuming and needs a number of resources; this includes the set of observers, high-end HDR cameras and display devices. Hence, qualitative criteria were chosen to evaluate different tone mapping operators.

Two different input images are used for simulations as shown in Figure 2.3. Image shown in Figure 2.3(a) is standard dynamic range image, whereas Figure 2.3(b) presents a high dynamic range image. Matlab HDR toolbox² is used for simulations. A simple Matlab code for logarithmic tone mapping operators is presented on next page as an example. This code takes the input image in the form of 'jpg' or 'hdr' picture format and checks that input image is a gray or three color. The next step is a change of input image values into luminance values. These input luminance values are used for tone mapping operation and the final output luminance values are displayed back as an output image.

Different tone mapping operators are applied to both images to check their performance. Logarithmic, Exponential, Drago and Reinhard operator performed better than others in terms of overall image quality when standard dynamic range image was used as can be seen in Figure 2.4(a)-(d). It can be noted from the figures that overall brightness, contrast and image detail in the dark are enhanced in Logarithmic and Drago operators when standard dynamic range image was used. Also, brightness and contrast is enhanced in the case of Exponential and Reinhard operator. Schlick, Tumblin, and Ward histogram operator are unable to produce good results in terms of brightness, contrast and details in dark.

²Toolbox is taken from 'Advanced High Dynamic Range Imaging' by Francesco Banterle and co-authors.



(a) Standard dynamic range image.



(b) High dynamic range image.

Figure 2.3: Input images used for Matlab simulation.

On the other hand, Exponential, Reinhard and Tumblin operator performed better than others when high dynamic range image was used as seen in Figure 2.5(b),(d) and (f). These three operators reproduced details in dark areas very well with improved image contrast and overall brightness. Logarithmic, Drago, Schlick and ward histogram oper-

Mapping Operator	Standard dynamic Range Image	High Dynamic Range Image
Logarithmic	Good	Bad
Exponential	Good	Good
Drago	Good	Bad
Reinhard	Good	Good
Schlick	Average	Bad
Tumblin	Bad	Good
Ward Histogram	Bad	Average

Table 2.2: Different mapping operator image quality simulation result for standard and high dynamic range image. Our comparison results are in a good agreement with other studies presented by different authors

ators seen in Figure 2.5(a),(c),(e) and (g) are unable to generate great results in terms of brightness, contrast and details in the dark.

Overall, Exponential and Reinhard operator produced good results for standard and high dynamic range images. Because, as mentioned earlier that Exponential operator is capable of producing very good result due to the exponential compression for standard dynamic range image. In addition, Reinhard operator uses photographic technique of dodging and burning that enhance the dynamic range and overall quality of an image. Hence, we can say that in terms of overall image quality and other attributes, both operators are best for HDR compression. Our comparison results are in a good agreement with other studies presented by different authors [33–36]. It should be noted that overall image quality after tone mapping operator can be different if we change the input image. In brief, overall output image quality depends on input image and mapping operator. According to them, Reinhard photographic, Exponential and Drago operators were performed better than others. Table 2.2 summarizes the different mapping operator overall image quality simulation results for standard and high dynamic range image.

Logarithmic Matlab code

```

function imgOut = LogarithmicTMO(img,qlogarithmic,klogarithmic)
img = hdrimread('image.jpg');    %input image read
check3Color(img);    %3 color check
L = lum(img);    %Luminance extraction from image
if( exist('qlogarithmic')|| exist('klogarithmic'))
qlogarithmic = 20;
klogarithmic = 15;
end
if(qlogarithmic < 1)    %check for qlogarithmic >= 1
qlogarithmic = 1;
endif(klogarithmic < 1)    %check for klogarithmic >= 1
klogarithmic = 1;end
LMax = max(max(L));    %computing maximum luminance value
Ld    =    log10(1    +    L    *    qlogarithmic)/log10(1    +    LMax    *
klogarithmic); %dynamic Range Reduction
imgOut = zeros(size(img));
fori = 1 : 3
imgOut(:, :, i) = img(:, :, i). * Ld./L;
end
imgOut = RemoveSpecials(imgOut);
figure();
imshow(imgOut);    %out put image display
end

```



(a) Logarithmic Operator.



(b) Exponential Operator.



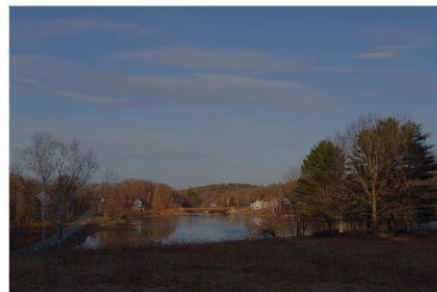
(c) Drago Operator.



(d) Reinhard Operator.



(e) Schlick Operator.



(f) Tumblin Operator.



(g) Ward Histogram Operator.

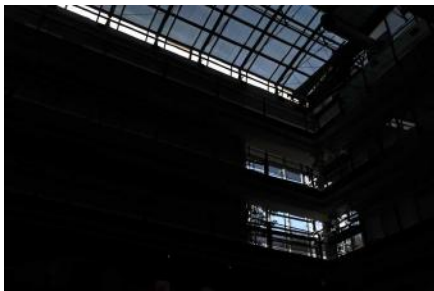
Figure 2.4: Results of standard dynamic range image after tone mapping operation.



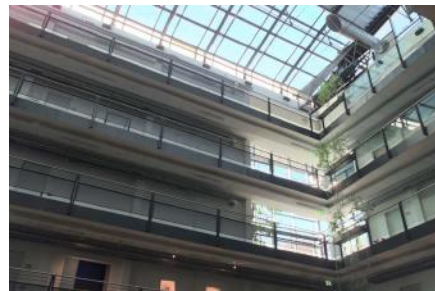
(a) Logarithmic Operator.



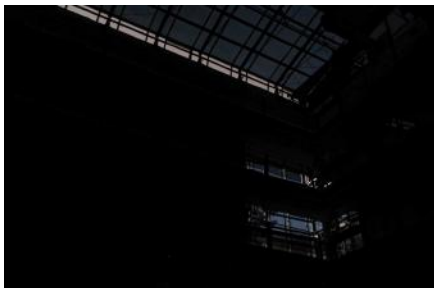
(b) Exponential Operator.



(c) Drago Operator.



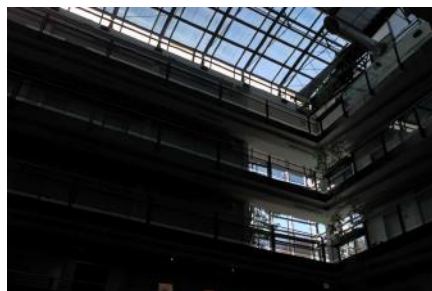
(d) Reinhard Operator.



(e) Schlick Operator.



(f) Tumblin Operator.



(g) Ward Histogram Operator

Figure 2.5: Results of high dynamic range image after tone mapping operation.

2.6 Conclusion

In a real world, the dynamic range of the scene can be of the order of 10^6 to 1 from light to dark areas. Most of display devices available in the market are unable to display high dynamic range images and can only display images of dynamic range on the order of 200:1 which is not sufficient. In order to obtain realistic images on display devices, it is necessary that images should be a faithful representation of the scene they depict. Hence, it is a problem to reproduce such scenes using media with very limited dynamic range like CRT/LCD displays, hard-copy prints, and projectors. In order to solve the problem of displaying HDR images on LDR displays, the tone mapping operators have been proposed.

Tone mapping is the operation that matches the dynamic range of HDR content with the display device dynamic range. When the dynamic range of the captured scene is smaller or larger than that of the display device, tone mapping expands or compresses the luminance respectively [19]. On the display device, the image should be a faithful representation of the the real image with some characteristics of real image such as contrast, details etc. should be kept same or improved on the display.

In this chapter, different global tone mapping operators were discussed in detail. In addition, Matlab simulation was performed in order to check the quality and faithfulness of the image after tone mapping operation. It should be noted that in order to assess the quality of images after tone mapping operation a qualitative criteria is adapted. It means that we assess the image quality by visually looking at it. A quantitative measure of image quality to check how good or bad the result was not taken into consideration. Two operators, Reinhard and Exponential performed better than others on two different dynamic range images. Exponential and Reinhard operator have produced good results

for both standard and high dynamic range images. Hence, we can say that in terms of overall image quality and other attributes, both operators are best for HDR compression. Our comparison results are in a good agreement with other studies presented by different authors [33–36].

Chapter 3

Wide Dynamic Range CMOS Image Sensor

3.1 Introduction

Image sensors are widely used in many industrial applications like mobile phones, automobiles, security, and biometrics. CMOS (Complementary Metal Oxide Semiconductor) image sensors have been experiencing rapid growth in their usage in recent years and now shares the market with CCD (Charge Coupled Device) image sensors [37]. They have also replaced CCD in most low end as well as professional cameras. The ability to integrate with other circuit blocks make CMOS sensors ideal to use as compared to CCD. Thus, any post processing required to increase the dynamic range in CMOS can be performed easily. On the other hand, CCD dynamic range is limited by the well capacity and hence can not be improved upon, without post-processing using multiple frame capture [5]. Hence, CMOS sensors will be the ideal choice for those

applications where the main emphasis is to capture wide dynamic range. However, with all these advancements and popularity, the CMOS camera still suffers from many limitations including that of limited dynamic range and inability to reproduce a scene as would be visible by the human eye. Nature has dynamic range of upto 6 decades i.e $150dB$, whereas CMOS image sensor dynamic range are limited from 2 to 4 decades i.e $40db$ to $80db$. Hence, there is need to increase the dynamic range of CMOS sensor so it can capture the dynamic range available in nature.

In this chapter, a new pixel sensor is introduced with an ability to capture a wide dynamic range scenes using tone mapping operation. Section 3.2 presents the basic building block of CMOS active pixel sensor. Section 3.3 presents the new CMOS pixel with an ability to capture the wide dynamic range of intensities and produce them faithfully using tone mapping operation. In addition, this section also discusses the different global tone mapping operator monotonically increasing reference functions. Section 3.4 presents the pixel simulation results and with a conclusion being presented in section 3.5.

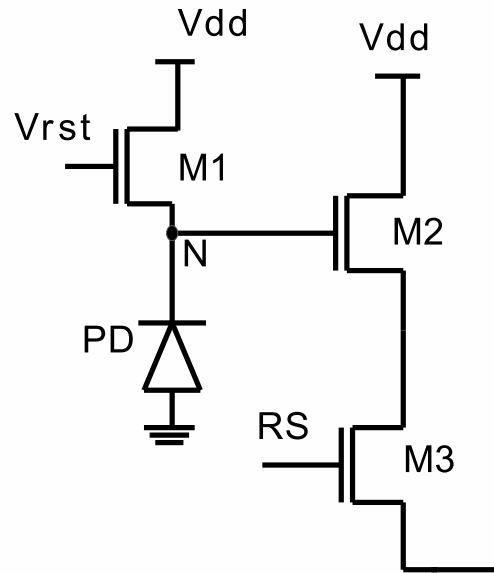
3.2 Active Pixel Sensor

The basic building block of CMOS sensor is APS (Active pixel sensor). A typical APS schematic and signal flow diagram are shown in Figure 3.1. The dynamic range of APS is limited. The photodiode converts input light into a charge, which is readout and digitized to store the image. High input light generates a large amount of charge which saturates the pixel. On the other hand, very low input light generates low charge which is very difficult to readout faithfully. Typical CMOS sensors using the basic APS have

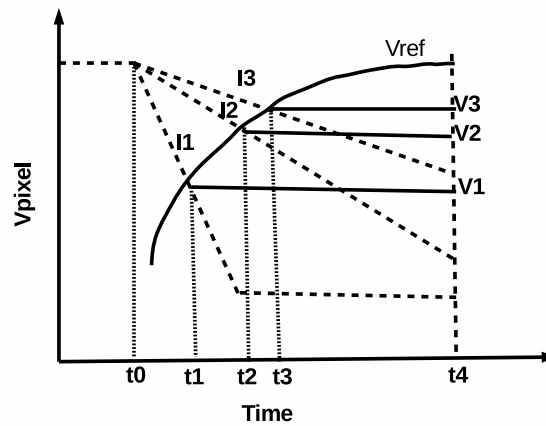
a dynamic range between $40db$ to $60db$ due to light saturation. In Figure 3.1, transistor $M1$, $M2$ and $M3$ are reset, source follower and row select switch respectively. PD is photodiode which converts input light into charge. At time $t1$, high voltage is applied at the gate of device $M1$, then the voltage $V_{dd} - V_t$ is transferred to node N . At time $t2$, the gate of device $M1$ is pulled low due to this V_{reset} is not connected to the pixel circuit anymore. The photo-diode then generates charge at node N which acts to reduce the voltage being held on the diode capacitance. This discharge will take place until integration time t_{int} and then voltage at node N is readout using the source follower $M2$ and select switch $M3$. A time $t3$, this cycle begin again and a new frame is started. The integrated voltage at the node N is given as,

$$V_N = V_{dd} - V_t - t_{int} \frac{I_p}{C_{pd}} \quad (3.1)$$

t_{int} is the integration time, I_p is photogenerated current and C_{pd} is the capacitance at node N . For low and medium currents I_1 and I_2 , the pixel faithfully produces a unique output voltage corresponding to the photocurrent. However, for higher current I_3 , the pixel saturates and is unable to readout faithfully. The information at higher photocurrent is therefore lost, which limits the dynamic range of the pixel. The dynamic range of pixel can be increased if the integration inside the pixel is stopped at a certain time determined to produce a known response. The output during integration is compared to another signal V_{ref} and stopped when these two signals are the same. Hence, the output of a pixel will depend on signal V_{ref} .



(a) Active pixel sensor schematic.



(b) Signal flow diagram.

Figure 3.1: Active pixel sensor schematic and signal flow diagram.

3.3 Wide Dynamic Range Pixel

3.3.1 Pixel Operation and Schematic

It is possible to capture wide dynamic range information by combining the threshold and integration time control approaches. A WDR pixel is presented which aims to capture

the wide range of light intensities available in nature. A pixel schematic and signal flow diagram is shown in Figure 3.2. $M1$, $M2$, $M3$ and $M4$ are reset device, reference voltage switch, source follower and row select switch respectively. In a typical linear pixel as discussed earlier, high photocurrent I_1 saturate the pixel due to which linear pixel is not able to capture the WDR information. However, in the new pixel approach, the integrated signal at node N is compared to a constantly increasing reference signal V_{ref} and the integration is stopped when the two are equal. This means for the high current, I_1 , the integration will stop at lower voltage V_1 than the voltages for lower currents I_2 and I_3 . The pixel output after the integration time will follow the V_{ref} signal.

The pixel operation starts by resetting the transistor $M1$, by applying the high reset signal V_{rst} at the gate of transistor $M1$. Due to the high voltage at the gate of $M1$, voltage $V_{dd} - V_{th}$ is transferred to device $M1$ source node N . The high voltage placed on the capacitance of node N is discharged by the photo-generated charge when transistor $M1$ is off, by lowering its gate voltage. A monotonically increasing reference function V_{ref} is applied to transistor $M2$ drain. At the start of integration, the voltage V_{ref} is lower than node voltage N and hence transistor $M2$ is on. However, discharging V_N and monotonically increasing V_{ref} leads to transistor $M2$ being switched off. After this time, the gate voltage of $M3$ is held by its gate capacitance until it's read out and the pixel is reset. The output voltage of the pixel depends on the signal V_{ref} and I_{ph} .

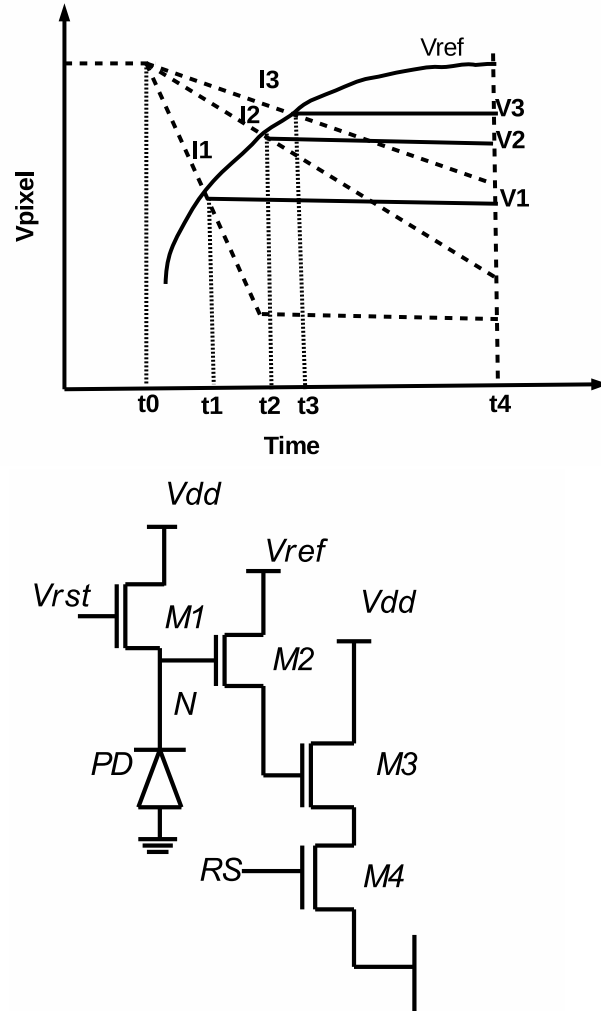


Figure 3.2: Wide dynamic range pixel schematic and signal flow diagram.

The monotonic reference function can be obtained by equating the integrated voltage at node N with that of the required transduction function. Let us assume the required response is,

$$V_{\text{out}} = f(I_{\text{ph}}) \quad (3.2)$$

where I_{ph} is the photocurrent and V_{out} is required response. Let f' be the inverse function

for this operator [38], such that $I_{ph} = f'(V_{out})$. The integrating potential at node N can be expressed as,

$$V_N(t) = V_N(t_0) - \frac{I_{ph}}{C_{PD}}(t - t_0). \quad (3.3)$$

where C_{PD} is photodiode capacitance. Transistor $M2$ will remain on, till this potential is higher than the reference voltage V_{ref} . At the instance, we expect the reference voltage to be same as the pixel response for the given photocurrent, $V_{out} = V_{ref}(t)$. This result was published in Procedia Computer Science, vol.41 2014 [38]. Therefore,

$$f'(V_{ref}(t)) = C_{PD} \frac{V_{G,M2}(t) - V_{G,M2}(t_0)}{(t - t_0)} \quad (3.4)$$

shows the reference voltage function in terms of integration time. It should be noted that Equation 3.4 presents the general form of reference function extraction from pixel response. Different reference function will be presented in next sub-sections. The proposed new pixel can produce wide dynamic range response with the help of a suitable reference function.

3.3.2 Tone Mapping Reference Function

In order to derive the reference voltage from the tone mapping operator, one needs to translate luminance values from the mapping operator into a current voltage relationship that is suitable for a pixel. Different reference functions are derived and discussed below.

Reinhard Simple Reference Function

As discussed earlier, Reinhard mapping operator is given as [17],

$$L_d(x, y) = \frac{L(x, y)}{1 + L(x, y)} \quad (3.5)$$

where

$$L(x,y) = \frac{a}{L_{av}} L_w(x,y) \quad (3.6)$$

L_d is output display luminance, a is a user controllable value, L_w is input world luminance and $L_{x,y}$ is scaled luminance. Translating Equation 3.5 into voltage-current relationship provides a mapping equation given as,

$$v = \frac{gkI_pV_{dd}}{1 + gkI_p}, \quad (3.7)$$

where g maps $\frac{a}{L_{av}}$ into Equation 3.5. k is proportionality constant and V_{dd} is pixel operating voltage and v is pixel output voltage. The reference function can be obtained by comparing the required transduction function with that the integrated voltage at node N . Let us assume that pixel required output transduction function at the gate of transistor M_3 is,

$$V_{out} = V_N(t0) - \frac{gkI_pV_{dd}}{1 + gkI_p} \quad (3.8)$$

and the voltage at node N is given as,

$$V_N(t) = V_N(t0) - \frac{t_{int}I_p}{C_{pd}} \quad (3.9)$$

where C_{pd} is photodiode capacitance, I_{ph} is photocurrent and t_{int} is effective integration time. Transistor $M2$ will remain on, till this potential is higher than the reference voltage V_{ref} . At the instance, we expect the reference voltage to be same as the pixel response for the given photocurrent [38], $V_{out} = V_{ref}(t)$, therefore,

$$V_{ref} = V_N(t0) - \frac{gkI_pV_{dd}}{1 + gkI_p} \quad (3.10)$$

$$\frac{t_{int} I_p}{C_{pd}} = \frac{gk I_p V_{dd}}{1 + gk I_p} \quad (3.11)$$

$$V_N(t0) = V_{dd} - V_{thM1}$$

By solving Equations 3.10 and 3.11 for the value of reference function with respect to t_{int} leads to equation given as [39],

$$V_{ref} = \frac{t_{int}}{C_{pd} gk} - V_o \quad (3.12)$$

where V_o is an offset related to the threshold voltages.

Reinhard Complex Reference Function

The simple version of Reinhard function provides limited burning for bright illumination. Hence, the following modification was proposed by [17]

$$L_d(x, y) = \frac{L(x, y)}{1 + L(x, y)} \left(1 + \frac{L(x, y)}{L_{white}^2} \right) \quad (3.13)$$

where L_{white}^2 is the smallest luminance that will be mapped to white. Translating Equation 3.13 into voltage-current relationship provides an equation given as,

$$v_c = \frac{gk I_p V_{dd}}{1 + gk I_p} \left(1 + \frac{gk I_p}{I_w^2} \right) \quad (3.14)$$

where g maps $\frac{a}{L_{av}}$ into Equation 3.5. k is proportionality constant, V_{dd} is pixel operating voltage and I_w corresponds the value of L_{white} . The reference function can be obtained by comparing the required transduction output with the integrated voltage at node N .

The output transduction function at the gate of transistor M_3 is,

$$V_{out} = V_N(t0) - \frac{gkI_p V_{dd}}{1 + gkI_p} \left(1 + \frac{gkI_p}{I_w^2}\right) \quad (3.15)$$

and the voltage at node N is given as,

$$V_N(t) = V_N(t0) - \frac{t_{int} I_p}{C_{pd}} \quad (3.16)$$

where C_{pd} is photodiode capacitance, I_{ph} is photocurrent and t_{int} is effective integration time. At the instance, we expect the reference voltage to be same as the pixel response for the given photocurrent [38], $V_{out} = V_{ref}(t)$, Therefore

$$V_{ref} = V_N(t0) - \frac{gkI_p V_{dd}}{1 + gkI_p} \left(1 + \frac{gkI_p}{I_w^2}\right) \quad (3.17)$$

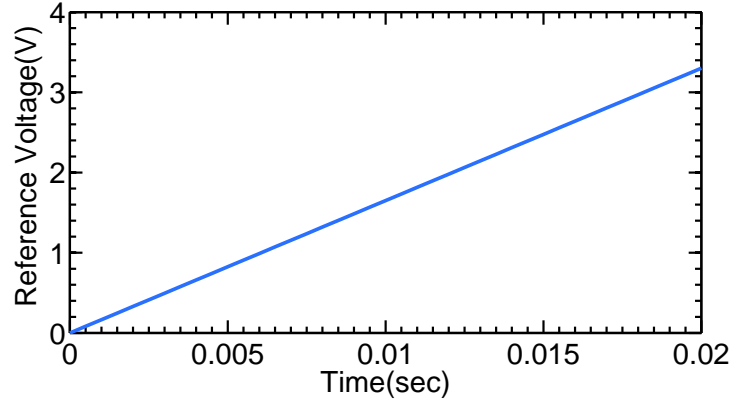
$$\frac{t_{int} I_p}{C_{pd}} = \frac{gkI_p V_{dd}}{1 + gkI_p} \left(1 + \frac{gkI_p}{I_w^2}\right) \quad (3.18)$$

$$V_N(t0) = V_{dd} - V_{thM1}$$

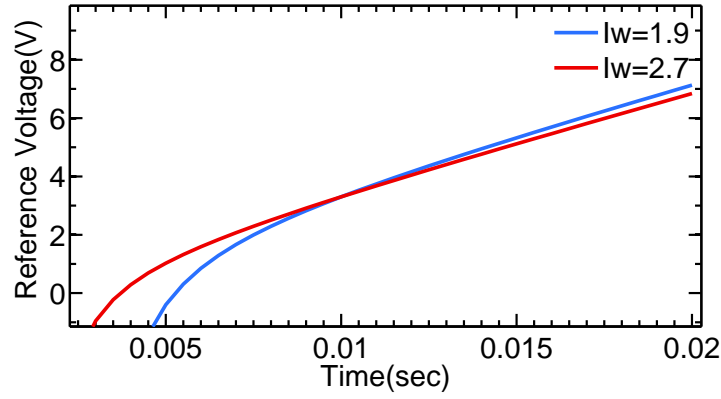
By solving Equations 3.17 and 3.18 for the value of reference function with respect to t_{int} leads to the reference function for Reinhard complex given as [39],

$$V_{ref}(t) = V_{dd} - V_o - \frac{tI_w^2(t - aV_{dd})}{a(aV_{dd} - tI_w^2)}. \quad (3.19)$$

Where V_o is an offset related the threshold voltages, a is user controllable value and I_{wh} corresponds the value of L_{white} .



(a) Reinhard simple reference function.



(b) Reinhard complex reference function.

Figure 3.3: Monotonically increasing reference function for Reinhard simple and complex mapping operator with two different values of I_w .

Figure 3.3 shows reference function for Reinhard simple and Reinhard complex mapping operators. It can be noted that both reference voltages are monotone increasing functions. Reinhard simple reference function a straight line with sufficient wide dynamic range capture, whereas Reinhard complex reference function has some negatives values that can be discarded as we are only interested in monotonically positive reference function.

Drago Reference Function

The mapping operator presented by Drago [26] discussed earlier is given as,

$$L_d(x,y) = \frac{L_{dmax} \log_{10}(1 + L_w(x,y))}{100 \log_{10}(1 + L_{wmax}) \log_{10}[2 + 8(\frac{L_w(x,y)}{L_{wmax}})^{\frac{\log_{10}(p)}{\log_{10}(0.5)}}]} \quad (3.20)$$

Transforming luminance into current voltage relationship leads to equation given as,

$$v = \frac{\log_{10}(1 + gI_p)}{\log_{10}(1 + gI_{pmax}) \log_{10}[2 + 8(\frac{gI_p}{gI_{pmax}})^{\frac{\log_{10}(p)}{\log_{10}(0.5)}}]} \quad (3.21)$$

where g is proportionality constant, I_{pmax} is maximum photocurrent and p is user controllable value. The reference function for the Drago operator can be calculated by equating two equations for WDR pixel given as

$$V_{ref} = V_N - \frac{\log_{10}(1 + gI_p)}{\log_{10}(1 + gI_{pmax}) \log_{10}[2 + 8(\frac{gI_p}{gI_{pmax}})^{\frac{\log_{10}(p)}{\log_{10}(0.5)}}]} \quad (3.22)$$

$$\frac{t_{int} I_p}{c_{pd}} = \frac{\log_{10}(1 + gI_p)}{\log_{10}(1 + gI_{pmax}) \log_{10}[2 + 8(\frac{gI_p}{gI_{pmax}})^{\frac{\log_{10}(p)}{\log_{10}(0.5)}}]} \quad (3.23)$$

A derivable reference function does not exist due to complex nature of Drago equation. However, Drago reference function can be generated using a look up table with respect to integration time t . First, values of t is assumed between $0sec$ and $0.02sec$, and inserted into Equation 3.23 that in turn provide the values of I_p . Hence, by using the values of I_p and other parameters into Equation 3.22 provide the solution of V_{ref} function that is shown in Figure 3.4.

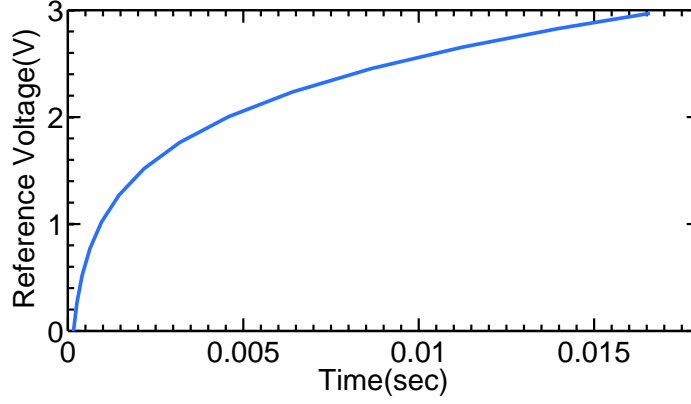


Figure 3.4: Drago reference function.

Exponential Reference Function

Exponential mapping operator is given as [25],

$$L_d(x, y) = 1 - \exp\left(\frac{-L_w(x, y)}{L_{av}}\right) \quad (3.24)$$

Transforming luminance equation into pixel voltage-current relationship leads to equation given as,

$$v = [1 - \exp(-gI_p)]V_{dd} \quad (3.25)$$

where g is a proportionality constant, V_{dd} is pixel operating voltage and I_p is photocurrent. The reference function can be extracted by comparing the output transduction function with the integrating voltage at node N . The required transduction function and the integrating voltage is given as

$$V_{out} = V_N(t0) - [1 - \exp(-gI_p)]V_{dd} \quad (3.26)$$

and the voltage at node N is given as,

$$V_N(t) = V_N(t_0) - \frac{t_{int} I_p}{C_{pd}} \quad (3.27)$$

where C_{pd} is photodiode capacitance, I_{ph} is photocurrent and t_{int} is effective integration time. It can be assumed that $V_{out} = V_{ref}$ to solve above equation for the value of V_{ref} . Hence by solving two above equation one can find the required monotone reference function and is given as [38]

$$t = \frac{v_{dd} C_{pd} g (V_{ref} + V_{off} - 1)}{\log(V_{ref} + V_{off})} \quad (3.28)$$

where where C_{pd} is photodiode capacitance, g is constant and V_{off} is the offset related to threshold voltages in pixel. The required monotonous function is shown in Figure 3.5. It can be seen that Exponential tone mapping function produce the required monotone transduction curve that will be used to capture the wide dynamic of a CMOS pixel.

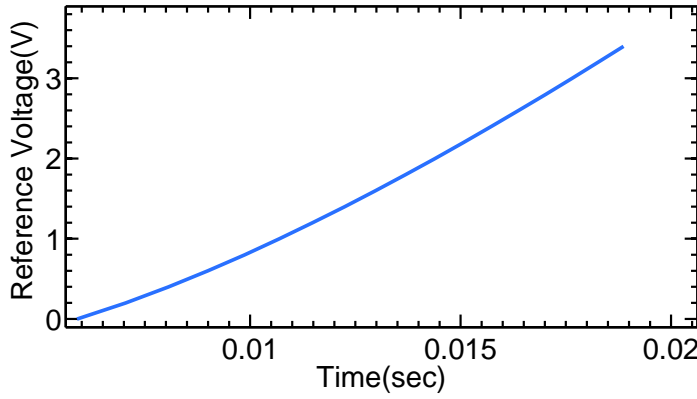


Figure 3.5: Exponential reference function.

Schlick Reference Function

Schlick tone mapping operator as discussed earlier is given as [27],

$$L_d(x, y) = \frac{p L_w(x, y)}{(p - 1)L_w(x, y) + L_{max}} \quad (3.29)$$

where p is user controllable value and L_{max} is maximum world luminance in scene.

Translation of luminance values into pixel voltages leads to equation given as,

$$v = \frac{pkI_p V_{dd}}{(p - 1)kI_p + I_{pmax}} \quad (3.30)$$

where k is constant and I_{pmax} is the maximum photocurrent. The required reference voltage can be calculated by comparing the output transduction voltage with the integrating voltage at node N and given as [38],

$$V_{ref} = V_{dd} - V_{off} - \frac{pV_{dd} - \frac{I_{pmax}t}{C_{pd}k}}{p - 1} \quad (3.31)$$

where V_{off} is the offset related to various threshold voltages in the readout chain of the pixel, C_{pd} is a photodiode capacitance, k is a constant and I_{pmax} is maximum photocurrent in the frame. Figure 3.6 shows the simple linear reference for Schlick operator. It can be seen that Schlick tone mapping function produce the required monotone transduction curve that will be used to capture the wide dynamic of a CMOS pixel.

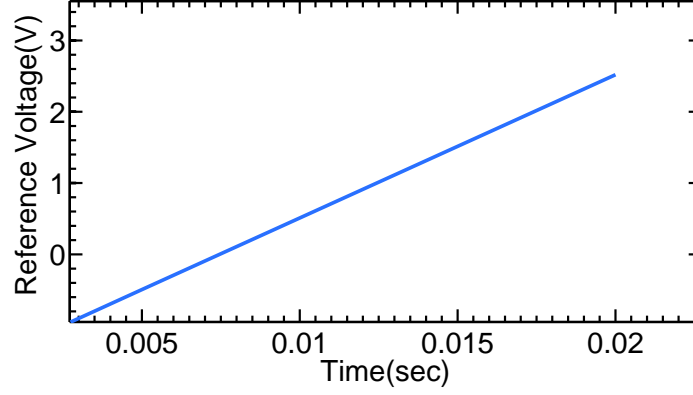


Figure 3.6: Schlick reference function.

Miller Reference Function

The mapping operator presented by Miller [30] is given as,

$$Q = k L_v^b \quad (3.32)$$

where Q is brightness and L_v is the luminance. The values of k and b is given as

$$\begin{aligned} b &= 0.338 L_v^{0.034} \\ k &= -1.5 \log_{10} L_v + 6.1 \end{aligned} \quad (3.33)$$

Transforming luminance values into pixel voltages leads to equation given as

$$v = [-1.5 \log_{10}(g I_p + 6.1)] (g I_p)^{0.338 (g I_p)^{0.034}} V_{dd} \quad (3.34)$$

/colorred where g is a constant. A derivable reference function does not exist due to complex nature of Miller function. However, the reference function can be calculated

using look up table generation by comparing the two pixel equations given as

$$\begin{aligned} V_{ref} &= V_{dd} - V_{off} - (-1.5 \log_{10}(gI_p + 6.1)) (gI_p)^{0.338} (gI_p)^{0.034} V_{dd} \\ \frac{tI_p}{c} &= (-1.5 \log_{10}(gI_p + 6.1)) (gI_p)^{0.338} (gI_p)^{0.034} V_{dd} \end{aligned} \quad (3.35)$$

The reference function using look up table is shown in Figure 3.7. It can be seen that Schlick tone mapping function does not produce the required monotone transduction curve because the reference voltage has a constant value of 2.5V that cannot be used for wide dynamic range capture.

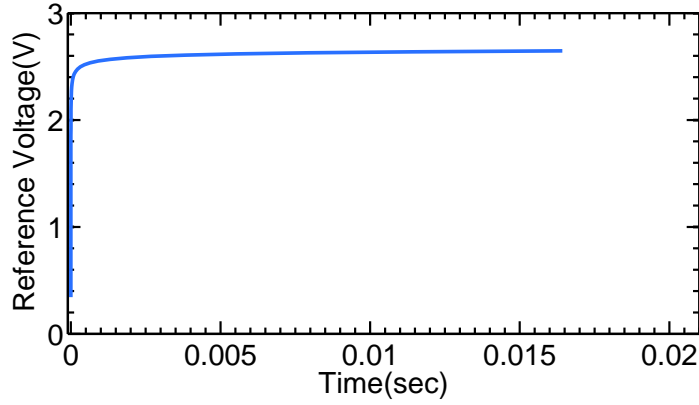


Figure 3.7: Miller reference function.

Tumblin and Rushmeier Reference Function

Tumblin and Rushmeier presented a mapping operator inspired by Stevens work on brightness [28, 29] and given as,

$$\begin{aligned} L_d(x, y) &= m L_{da} \left(\frac{L_w(x, y)}{L_{wa}} \right)^\alpha \\ \text{where } \alpha &= \frac{\gamma(L_{wa})}{\gamma(L_{da})} \end{aligned} \quad (3.36)$$

L_{da} and L_{wa} are display and image adaptation luminance values respectively. Transforming luminance into pixel voltage gives

$$V = V_{dd}(gI_p)^e \quad (3.37)$$

where g and e are user controllable values. The required reference voltage can be calculated by adapting the technique discussed earlier and given as,

$$V_{ref} = V_{dd} - V_{off} - V_{dd}g^e \frac{cgV_{dd}^f}{t} \quad (3.38)$$

where f is constant. The Figure 3.8 shows the reference function for Tumblin and Rushmeier operator. It can be seen that Tumblin and Rushmeier tone mapping function produce the required monotone transduction curve that will be used to capture the wide dynamic of a CMOS pixel.

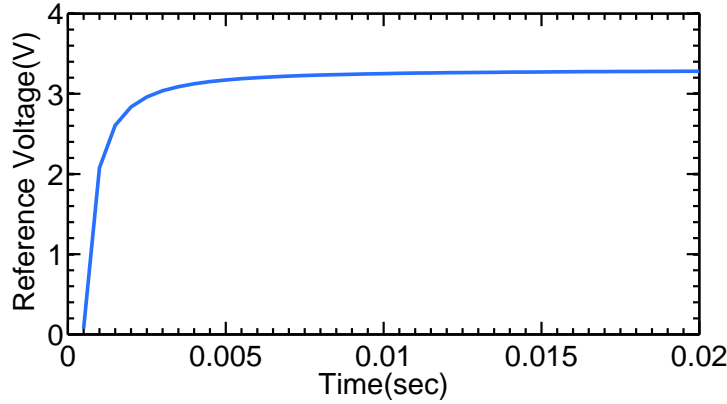


Figure 3.8: Tumblin and Rushmeier reference function.

Logarithmic Reference Function

Logarithmic mapping compress the HDR using logarithm function and given as,

$$L_d(x, y) = \frac{\log_{10}(1 + L_w(x, y))}{\log_{10}(1 + L_{max})} \quad (3.39)$$

where L_{max} is maximum world luminance. Transforming luminance values into pixel voltages and comparing the pixel equations leads to the value of V_{ref} given as,

$$\begin{aligned} V_{ref} &= V_{dd} - V_{off} - aV_{dd}\log(1 + gI_p) \\ \frac{tI_p}{c} &= aV_{dd}\log(1 + gI_p) \end{aligned} \quad (3.40)$$

where a and g is constant. The reference voltage V_{ref} can be calculated using look up table generation and shown in Figure 3.9.

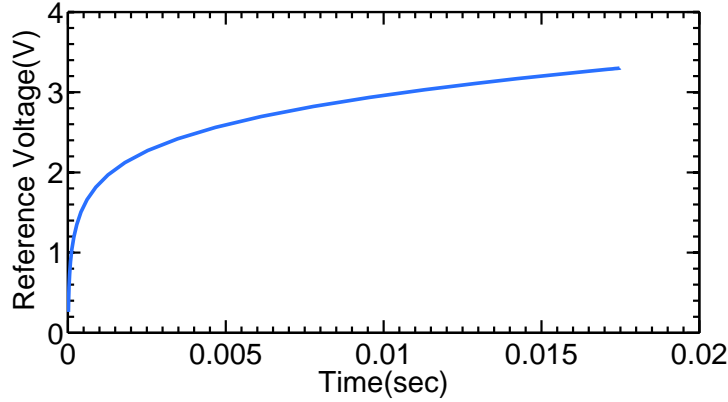


Figure 3.9: Logarithmic reference function.

Different tone mapping reference functions are discussed in this section. These monotonically increasing reference functions will be applied on the pixel to capture the wide dynamic range of intensities. The next section presents the WDR pixel simulation with different reference functions.

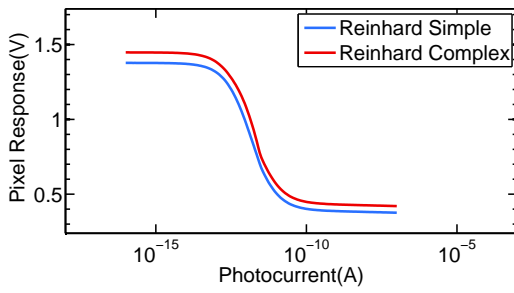
3.4 WDR Pixel Simulation

The wide dynamic range pixel was simulated in the Cadence circuit simulator using a $0.35\mu m$ CMOS process from Austria Microsystems (AMS). The pixel schematic is shown in Figure 3.2. Transistor $M1$, $M2$, $M3$ and $M4$ are reset device, reference switch, source follower and row select switch respectively. The dimension $\frac{Width}{Length}$ of the reset transistor $M1$ is $\frac{1\mu m}{0.6\mu m}$ whereas that of the source follower $M3$, reference switch $M2$ and row select switch $M4$ is $\frac{2\mu m}{0.6\mu m}$. The WDR pixel is simulated with varying reference voltages in order to find the pixel response. The monotonous reference functions used for this purpose are Reinhard simple, Reinhard complex, Schlick, Exponential, Logarithmic, Drago, Tumblin and Rushmeier, and Miller.

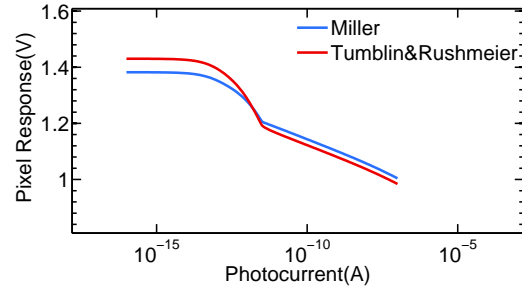
Figure 3.10 shows WDR pixel response for different tone mapping reference functions. Figure 3.10(a) shows the pixel response of Reinhard simple and complex operator. It can be seen that Reinhard pixel has sensitivity problems at very low and high photocurrent. This means Reinhard pixel is unable to read much information at these photocurrents. However, overall Reinhard pixel is able to capture over 5 – 6 decades of light. Similarly, Figure 3.10(b) shows the pixel response for Miller and Tumblin operator. These two operators produced good results and able to capture upto 6 decades of light intensity. Figure 3.10(c)(d) shows the pixel response of Schlick, Exponential and Drago operator. Unfortunately, their pixel response has low light sensitivity and able to capture 4 decades of light intensity. Figure 3.10(e) shows the Logarithmic pixel response with 6 decades of light intensity capture. Overall, It can be seen that the reported pixel with different mapping operator is able to capture over 6 decades of light intensity. Some pixel operators were performed better than others in capturing the very dark and bright intensities. By tuning the parameters, one can change the intensities which are tone-

mapped and hence enhance either the lower intensity or, the higher intensity regions of an image. Furthermore, these reference signals can be changed during the operation of the pixel. The WDR pixel can capture the dynamic range of more than 6 decades with in-pixel tone mapping operation.

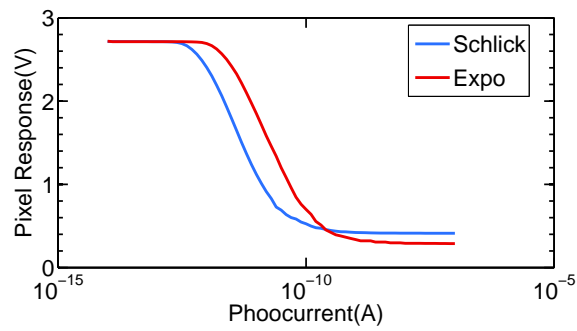
Tone mapping operation on CMOS pixel in practice performs two operations, one is to capture wide dynamic range using reference voltage and second is to enable direct display of an image on low dynamic range display devices. This reduces the two step process of typical cameras, where the image is captured in one stage and tone mapping is then applied to make this image displayable on display devices.



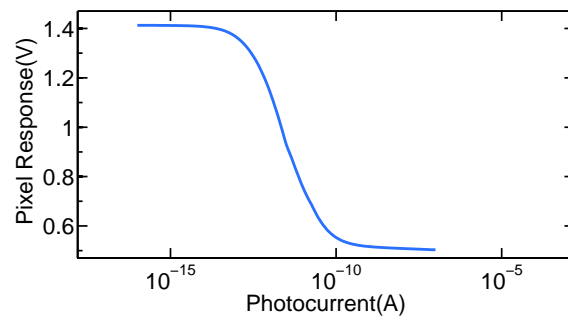
(a) Reinhard Pixel Response.



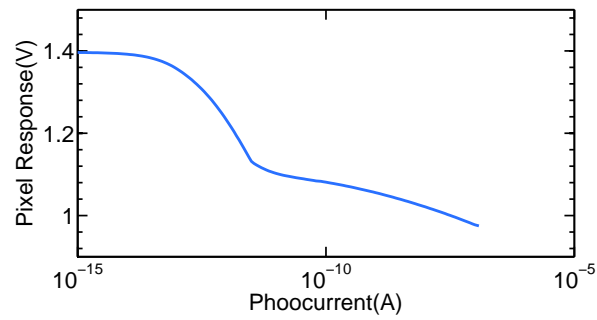
(b) Tumlin& Rushmeier and Miller Response.



(c) Exponential and Schlick Response.



(d) Drago Pixel Response.



(e) Logarithmic Pixel Response.

Figure 3.10: WDR pixel response at different monotonous reference functions.

3.5 Conclusion

In this chapter, a new CMOS pixel is presented with tone mapping technique which aims to capture wide dynamic range available in nature. Tone mapping operation on CMOS pixel in practice performs two operations; one is to capture wide dynamic range using reference voltage and second is to enable direct display of an image on low dynamic range display devices.

Different tone mapping reference curves are extracted from luminance mapping functions. First, luminance mapping curve is transformed into voltage-time relationship and this monotone voltage curve is applied on CMOS pixel in order to obtain wide dynamic range information. The monotonically increasing functions are Reinhard, Schlick, Exponential, Drago and Logarithmic. WDR pixel was simulated in cadence tools using $0.35\mu m$ CMOS process from Austria Microsystems (AMS). Pixel response was measured and presented with different reference functions applied on the pixel. Some pixel operators were performed better than others in capturing the very dark and bright intensities. Overall, pixel simulation result is presented showing the pixel ability to capture more than 6 decades of dynamic range.

Chapter 4

Pixel Modeling and Fixed Pattern Noise

4.1 Introduction

To investigate the different noise sources and errors in WDR pixel, there is a need to develop a model with different parameters that characterises the pixel response. Such a model can be developed by analysing the pixel schematic. An error between pixel's simulated and model response can be examined after developing pixel model. Pixel modeling will provide the fundamental background to the fixed pattern noise (FPN).

Fixed pattern noise (FPN) limits the performance of image sensors, and it is mainly due to the variations in the responses of individual pixels within an array of pixels. The variations between the responses of pixels are caused by the device and interconnect parameter mismatches in an individual pixel. It appears as a salt and pepper noise pattern on an image taken by the WDR image sensor. In addition, it can also be expressed

as intensity and contrast error on an image taken by WDR sensor. This chapter also presents a simple procedure to reduce FPN in which the parametric response of pixel is used, with FPN modeled as variations in the individual parameters. The parameters of each pixel are measured, recorded and then used to correct their response.

Section 4.2 presents the Reinhard pixel model using semiconductor theory for the WDR pixel. Section 4.3 discusses the parameter extraction procedure for Reinhard simple and complex operator. Section 4.4 presents the model error for Reinhard WDR pixel. Section 4.5 presents the brief overview of FPN and transistor mismatch. Section 4.6 presents the procedure used to measure FPN in WDR sensor. Section 4.7 discusses the FPN correction technique. Section 4.8 presents the impact of FPN on a test image before and after correction and section 4.9 discusses the conclusion.

4.2 Pixel Modeling

Figure 4.1 shows the WDR pixel with a typical column circuitry. x is the pixel input luminance or light and y is the pixel output response. A WDR pixel model can be developed by examining Figure 4.1. The current in the photodiode have two components. One of these is the dark or leakage current which is produced even without the presence of light. Its origins include thermal generation and recombination as well as defects at the diode junction and surface [40]. The second term is an optical term produced by the photon flux falling on diode surface. Hence the photodiode current is given as [41]

$$I_{PD} = I_{dark} + Q_{PD}G_A G_L A_{PD} L_{opto} \quad (4.1)$$

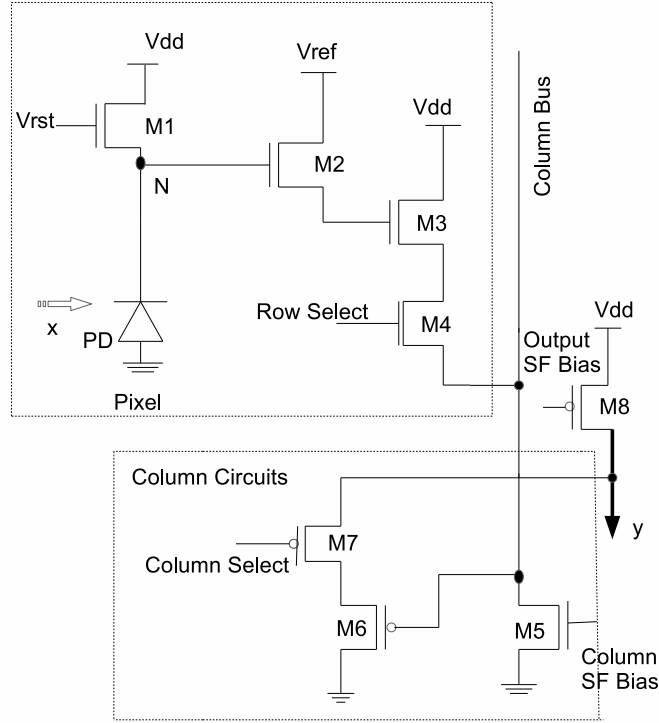


Figure 4.1: A WDR pixel with a typical column circuitry.

where Q_{PD} is the quantum efficiency of the photodiode, A_{PD} is the light sensitive area of the photodiode, G_A is the gain factor related to the photodiode area, G_L is the gain of optical assembly, and L_{opto} is the input intensity. As discussed earlier, at the start of integration time pixel operation starts by resetting the transistor M_1 , by applying the high reset signal V_{rst} at the gate of transistor M_1 . This transfer a reset signal $V_{dd} - V_t$ to device M_1 source node N . The high voltage placed on the capacitance of node N is discharged by the photo-generated charge when transistor M_1 is off, when its gate voltage is reduced. At the same time, a monotonically increasing reference function

V_{ref} is applied to transistor M_2 drain. At the start of integration, the voltage V_{ref} is lower than node voltage V_N and hence transistor M_2 is on. However, discharging V_{N1} and monotonically increasing V_{ref} leads to transistor M_2 being switched off. After some point of time, the gate voltage of M_3 is held by its gate capacitance until it's read out and pixel is reset. The output voltage of the pixel depends on the signal V_{ref} and I_{ph} . We are assuming Reinhard reference function here. Similarly, other reference functions can also be used for pixel model. The voltage at the gate of transistor M_3 by considering all threshold voltages and applying reference voltage at the drain of transistor M_2 is given as,

$$V_{GM3} = V_{dd} - V_{tM1} - V_{tM2} - \frac{gkI_{PD}V_{dd}}{1 + gkI_{PD}} \quad (4.2)$$

where V_{TM1} and V_{TM2} are threshold voltages of transistor M_1 and M_2 respectively. Transistor M_3 is a source follower and M_4 is a row select switch used to enable a particular row of pixels to place their output on the column bus. The voltage at the source of transistor M_3 is given, as [41]

$$V_{SM3} = V_{GM3} - V_{tM3} - \sqrt{\frac{2I_{DSM3}}{\beta_{M3}}} \quad (4.3)$$

where I_{DSM3} is the drain current in the transistor M_3 and β_{M3} is the transconductance parameter. It can be noted that when M_4 is "on", the gate voltage V_{GM6} of transistor M_6 is equal to the source voltage of transistor M_3 . The column bus is biased by transistor M_5 and therefore the drain-source currents in M_3 and M_5 are same when M_4 is on [42]. The voltage at the gate of transistor M_6 is given as [41],

$$V_{GM6} = V_{GM3} - V_{tM3} - \sqrt{\frac{\beta_{M5}}{\beta_{M3}}}(V_{GSM5} - V_{tM5}) \quad (4.4)$$

Transistor M_6 and M_7 makes a second stage of readout circuits need to connect a pixel to the single output of the array. When transistor M_7 is "on", the output of source follower M_6 is connected to output bus Y . Transistor M_8 is common to the whole array and provides the current bias to the column source followers. The final expression for the output is given as [41],

$$V_Y = V_{GM6} - V_{tM6} - \sqrt{\frac{\beta_{M8}}{\beta_{M6}}} (V_{GSM8} - V_{TM8}) \quad (4.5)$$

Combining all above equations leads to the output from an array of pixels as,

$$\begin{aligned} V_Y = V_{dd} - V_{tM1} - \frac{gk(I_{dark} + Q_{PD}G_A G_{LAPD}L_{opto})V_{dd}}{1 + gk(I_{dark} + Q_{PD}G_A G_{LAPD}L_{opto})} - (V_{tM2} + V_{tM3} + V_{tM6}) \\ - \sqrt{\frac{\beta_{M5}}{\beta_{M3}}} (V_{GSM5} - V_{tM5}) - \sqrt{\frac{\beta_{M8}}{\beta_{M6}}} (V_{GSM8} - V_{tM8}) \end{aligned} \quad (4.6)$$

This equation can be rewritten in the form of pixel parameters and given as,

$$y = a - \frac{b(x+d)}{1+c(x+d)} \quad (4.7)$$

with the terms given as,

$$y = V_Y$$

$$a = V_{dd} - V_{tM1} - (V_{tM2} + V_{tM3} + V_{tM6}) - \sqrt{\frac{\beta_{M5}}{\beta_{M3}}}(V_{GSM5} - V_{tM5}) - \sqrt{\frac{\beta_{M8}}{\beta_{M6}}}(V_{GSM8} - V_{tM8})$$

$$b = gkV_{dd}$$

$$c = gk$$

$$d = I_{dark}$$

$$x = Q_{PD}G_A G_L A_{PD} L_{opto}$$

(4.8)

where y is the pixel output, x is the input photocurrent, a is the pixel offset voltage, b and c represents the pixel gain and d is the dark current. Hence, Equation 4.7 shows the pixel model for Reinhard simple operator. Similarly, the pixel model for Reinhard complex can be rewritten in the form of parameters and given as,

$$y_c = a - \frac{b(x+d)(1+e(x+d))}{1+c(x+d)} \quad (4.9)$$

It should be noted that Reinhard reference function is used for a pixel model demonstration. Similarly, other operators can also be used for this purpose. The parameter terms of Reinhard complex are same as Reinhard simple operators except the parameter $e = I_w^{-2}$ which corresponds user controllable value.

Fixed pattern noise is mainly due to the variations between the responses of individual pixels within an array of pixels. In order to remove FPN, a simple procedure has been adapted to reduce FPN in which parametric response of the pixel is used, with FPN

modeled as variations in the individual parameters. The parameters of each pixel are measured, recorded and then used to correct their response. Hence, we need to measure and extract the individual parameters in each pixel to remove FPN and the next section 4.3 presents the parameter extraction routine.

4.3 Parameter Extraction

4.3.1 Reinhard Simple

In order to check the validity of the analytical pixel model, its response has to be compared with the simulated response at the same illumination. However, parameters need to be extracted before determining the model response and comparison with simulated response. Parameters can be extracted by assuming different calibration currents. The model response for Reinhard simple pixel is given as,

$$y = a - \frac{b(x+d)}{1+c(x+d)} \quad (4.10)$$

This equation can be simplified by assuming that dark or leakage current is small enough to be neglected for high photocurrents. Hence the model response equation can be simplified to,

$$y_s = a - \frac{bx}{1+cx} \quad (4.11)$$

In this equation three parameters are unknown hence three calibration currents are sufficient. The extraction procedure of parameters can be performed by assuming three different currents x_1, x_2, x_3 and their response y_1, y_2 and y_3 . The model response using

Parameter	a (V)	b (V/A)	$c(A^{-1})$	d (A)
Value	1.38	7.11×10^{11}	7.13×10^{11}	1.10×10^{-14}

Table 4.1: Extracted parameters using different calibration currents over 9 decades of photocurrent.

calibration currents are given as,

$$\begin{aligned}
 y_{s1} &= a - \frac{bx_1}{1 + cx_1} \\
 y_{s2} &= a - \frac{bx_2}{1 + cx_2} \\
 y_{s3} &= a - \frac{bx_3}{1 + cx_3}
 \end{aligned} \tag{4.12}$$

Parameters value can be extracted by solving above equations and given as,

$$\begin{aligned}
 c &= \frac{x_1y_{s2} - x_2y_{s1} - x_1y_{s3} + x_3y_{s1} + x_2y_{s3} - x_3y_{s2}}{x_1x_2y_{s1} - x_1x_2y_{s2} - x_1x_3y_{s1} + x_1x_3y_{s3}x_2x_3y_{s2} - x_2x_3y_3} \\
 b &= \frac{y_{s2} - y_{s3}}{\frac{x_3}{1+cx_3} - \frac{x_2}{1+cx_2}} \\
 a &= y_{s3} + \frac{bx_3}{1 + cx_3}
 \end{aligned} \tag{4.13}$$

The parameter d which represents the dark current can be extracted form Equation 4.10 by putting input photocurrent value $x = 0$. The value of d is given as,

$$d = \frac{a - y_s}{b - ac + cy_s} \tag{4.14}$$

Table 4.1 shows the extracted parameters by assuming three different calibration currents. Hence, by using the simulated response of the pixel at three different current, it is possible to find the parameters required to model the pixel. The calibration currents chosen to extract parameters are one dark current and three middle range photocurrents.

4.3.2 Reinhard Complex

The model response for Reinhard complex by ignoring dark current contribution is given as,

$$y_c = a - \frac{bx(1+ex)}{1+cx} \quad (4.15)$$

However, this equation is not suitable for simple parameters extraction. Hence, it needs simplification in order to get parameters extracted. A simple model response can be calculated by simplifying Equation 4.15 and is given as,

$$y_c = P + Qx - Rx^2 - Sy_cx \quad (4.16)$$

where $P = a$, $Q = ac - b$, $R = be$ and $S = c$. There are 4 unknown parameters, hence four calibration currents x_1, x_2, x_3, x_4 with the responses $y_{c1}, y_{c2}, y_{c3}, y_{c4}$ are required for parameters extraction. The model equations with calibration currents are given as,

$$\begin{aligned} y_{c1} &= P + Qx_1 - Rx_1^2 - Sy_{c1}x_1 \\ y_{c2} &= P + Qx_2 - Rx_2^2 - Sy_{c2}x_2 \\ y_{c3} &= P + Qx_3 - Rx_3^2 - Sy_{c3}x_3 \\ y_{c4} &= P + Qx_4 - Rx_4^2 - Sy_{c4}x_4 \end{aligned} \quad (4.17)$$

These equations can be solved for parameters by matrix method for simultaneous equation. Above equation can be rewritten as,

$$\begin{pmatrix} 1 & x_1 & -x_1^2 & -y_{c1}x_1 \\ 1 & x_2 & -x_2^2 & -y_{c2}x_2 \\ 1 & x_3 & -x_3^2 & -y_{c3}x_3 \\ 1 & x_4 & -x_4^2 & -y_{c4}x_4 \end{pmatrix} \cdot \begin{pmatrix} P \\ Q \\ R \\ S \end{pmatrix} = \begin{pmatrix} y_{c1} \\ y_{c2} \\ y_{c3} \\ y_{c4} \end{pmatrix}$$

Parameter	P (V)	Q (V/A)	R (V)	$S(A^{-1})$	d (A)
Value	1.44	2.53×10^{11}	1.88×10^{-4}	5.88×10^{11}	-8.80×10^{-15}

Table 4.2: Reinhard complex extracted parameters using different calibration currents over 9 decades of photocurrent.

$$A \cdot X = B$$

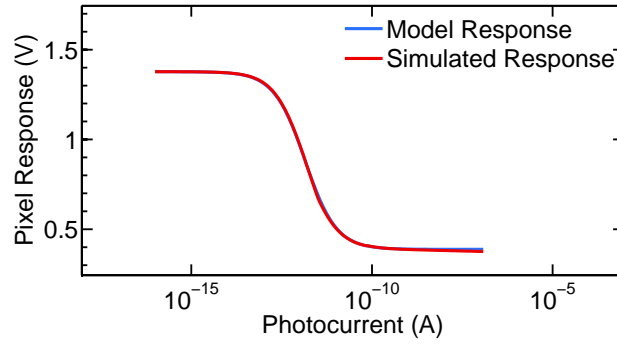
$$X = A^{-1}B$$

Hence, parameters matrix X can be calculated by multiplication of matrix A^{-1} with matrix B . The calibration current with their response chosen to extract parameters are one dark current, two mid-range photocurrents and one high photocurrent. Table 4.2 shows the extracted parameters at four different calibration photocurrent.

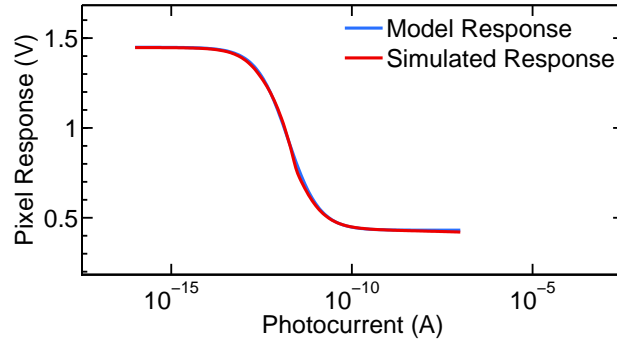
4.4 Model Error

In order to check the validity of the analytical pixel model, its response has to be compared with the simulated response at the same illumination. The pixel model response can be calculated using the model equation with parameters extracted in earlier section. Figure 4.2 shows the comparison of simulated and model response of Reinhard simple and complex mapping operator. Figure 4.3 shows the model error between pixel model and simulated response. It can be seen that the suggested model fits well with the simulated data except at some middle range photocurrents i.e., $10^{-12}A - 10^{-11}A$. Reinhard simple model fits well as compared to the Reinhard complex. The maximum model error in Reinhard simple case is around $15mV$, whereas Reinhard complex exhibits the

model error of around $40mV$ which are very promising results. The model error generates due to the arbitrary selection of calibration currents x_1, x_2, x_3, x_4 with the responses $y_{c1}, y_{c2}, y_{c3}, y_{c4}$ and can be reduced by choosing the suitable calibration currents.



(a) Reinhard simple Pixel Response.



(b) Reinhard complex Response.

Figure 4.2: Comparison of parameter model and simulated pixel response.

4.5 Fixed Pattern Noise

The variations between the responses of individual pixels and readout circuits within an array of pixels lead to differences in the response of each pixel. These variations lead to the presence of a spatial, but not temporal, noise in images acquired by these

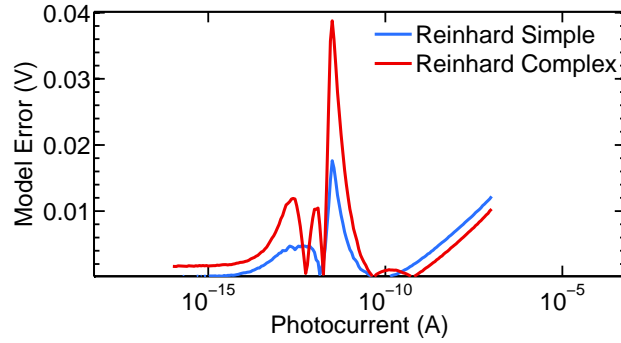


Figure 4.3: Model error between pixel simulated and model response.

pixels [42]. This kind of noise is called fixed pattern noise (FPN) and appear as a fixed pattern on an image. FPN appears as a striping noise in one-dimensional imagers, whereas in two-dimensional imagers, it appears as salt and pepper noise. Fixed pattern noise has been observed in most imaging devices, including charge coupled devices [43, 44], active pixel sensors (APSs) [7], logarithmic pixels [41, 45] infrared detectors [46] magnetic resonance imagers [47]. The main effect of fixed pattern noise on an image is the reduction in intensity and contrast of the image. In addition, FPN also affects the tone mapped image taken by WDR pixel proposed earlier. The source of FPN can be identified by analysing the signal chain in an array of a pixel. A WDR pixel circuit was analysed in the last section to obtain its model. The next subsection briefly describes the device and interconnect parameter mismatches in an individual pixel. These device mismatches generate fixed pattern noise.

4.5.1 Transistor Mismatch

Two identical transistors on the same chip have some random differences in their behavior. These variations are due to the lateral diffusion of the source and drain implants

as well as the field oxide encroachment in the MOS channel. In addition to these two, other factors including local mobility fluctuations, oxide granularity, oxide charge, and gate dielectric thickness have also been considered as sources of mismatch [48,49]. The standard models for the mismatch caused by different devices are characterized by the random variation of the differences in their threshold voltage V_T , their body factor γ and their current factor β . Experimentally verified model for these variations are given as [48,49],

$$\begin{aligned}\sigma^2(\Delta V_T) &= \frac{A_{V_T}^2}{WL} + S_{V_T}^2 D^2 \\ \sigma^2(\Delta \gamma) &= \frac{A_\gamma^2}{WL} + S_\gamma^2 D^2 \\ \frac{\sigma^2(\Delta \beta)}{\beta^2} &= \frac{A_\beta^2}{WL} + S_\beta^2 D^2\end{aligned}\tag{4.18}$$

Here, W is the effective gate width, L is the effective gate length, D is the mutual distance between devices and A_{V_T} , A_β , S_{V_T} , S_γ , S_β are process dependent constants. Despite the fact that the threshold voltage and the transconductance factor have similar origins, their variations have been found to be independent of one another. The above models shows that the smaller geometry devices will have large variations in their threshold voltage and current gain factors.

4.6 Fixed Pattern Noise Measurement

Most of the images we capture, store and manipulate are used by human viewers for decision-making, aesthetics, surveillance and control [2]. Hence, fixed pattern noise

can be quantified by making the human visual system (HVS) as a standard. It has been reported that HVS can see differences in illumination δI , against the background illumination I , to an accuracy of about 1% in high illumination and 10% in low light levels [50, 51]. In other words, the human eye has a contrast threshold of 1%, which means the human eye is unable to perceive errors in misrepresented illuminations that are less than 1% of the original illumination. Therefore, fixed pattern noise can be described as a contrast threshold error and 1% error value becomes the required standard at matching FPN error to the sensitivity of the human visual system. The fixed pattern noise expressed as contrast threshold error is given as,

$$\text{Relative Contrast Error} = \frac{\text{StandardDeviation}(I_{ext})}{\text{Mean}(I_{ext})} \quad (4.19)$$

where I_{ext} is the extracted current from pixel model response. Fixed pattern noise effects can be measured by simulating the WDR pixel multiple times with different parameter values. Using the Monte Carlo simulations in Cadence circuit simulator, the response of 1000 pixels was obtained by sweeping the photocurrent over 8 decades. In Monte Carlo simulations, process parameters like the transistor aspect ratio, gate capacitance per unit area and threshold voltages were inherently altered in a controlled manner while determining the pixel response to a range of photocurrents [2]. The Reinhard simple and complex pixel response are given as,

$$ys_{ij} = a_j - \frac{b_j(x_i + d_j)}{1 + c_j(x_i + d_j)} \quad (4.20)$$

$$yc_{ij} = P_j + Q_j x_i - R_j x_i^2 - S_j yc_{ij} x_i \quad (4.21)$$

Parameters	a (V)	b (V/A)	$c(A^{-1})$	d (A)
Mean	1.39	7.13×10^{11}	7.13×10^{11}	1.10×10^{-14}
SD	0.13	4.40×10^{10}	1.93×10^{10}	7.26×10^{-16}

Table 4.3: Mean and standard deviations of 1000 extracted parameters for Reinhard simple pixel.

Parameters	P (V)	Q (V/A)	R (V)	$S(A^{-1})$	D (A)
Mean	1.45	2.53×10^{11}	1.89×10^{-4}	5.89×10^{11}	-8.28×10^{-15}
SD	0.145	1.64×10^{10}	1.40×10^{-5}	4.68×10^{10}	2.53×10^{-15}

Table 4.4: Mean and standard deviations of 1000 extracted parameters for Reinhard complex pixel.

where ys_{ij} and yc_{ij} are the pixel responses to an illumination represented by a photocurrent x_i for Reinhard simple and complex operator respectively, j and i are pixel index and photo illumination, respectively. In order to extract different parameters from the 1000 pixel response data, calibration currents are needed. Four different calibration current were selected for this purpose, i.e. one dark current and three middle range($x_1 = 10fA$), ($x_2 = 7.08pA$), ($x_3 = 10nA$) photocurrent. The parameters extraction procedure was discussed in detail in last section. The parameters of 1000 pixels were extracted using 1000 pixel response data and a calibration current for Reinhard simple and complex operator. The mean and standard deviation of 1000 pixel parameters are given in Table 4.3 and 4.4.

Fixed pattern noise can be calculated by finding the extracted current mean and standard deviation value. By solving Equation 4.20, extracted current for Reinhard simple in terms of parameters is given as,

$$I_{s_{ext}} = \frac{ys_{ij} - a_j - a_j d_j c_j + ys_{ij} c_j d_j + b_j d_j}{a_j c_j - ys_{ij} c_j - b_j} \quad (4.22)$$

Extracted current for Reinhard complex pixel in terms of parameters is given as,

$$I_{c_{ext}} = \frac{Q_j - 2d_j R_j - S_j y c_{ij} \pm (Q_j^2 - 2Q_j S_j y c_{ij} + S_j^2 y c_{ij}^2 - 4R_j y c_{ij} + 4P_j R_j)^{1/2}}{2R_j} \quad (4.23)$$

The mean extracted current can be calculated by inserting the mean values of parameters in Equation 4.22 and 4.23. In addition, the mean value of extracted current was also used to find the fixed pattern noise before correction. Figures 4.4 and 4.5 shows the fixed pattern noise before correction for Reinhard simple and complex operators. FPN simulation result shows that both operators exhibited a high fixed pattern noise. Reinhard simple operator exhibit a contrast error in the range of 10%-200%. Whereas complex operator exhibit a contrast error in the range of 100%-400%. Hence, a simple and effective technique is needed to reduce FPN.

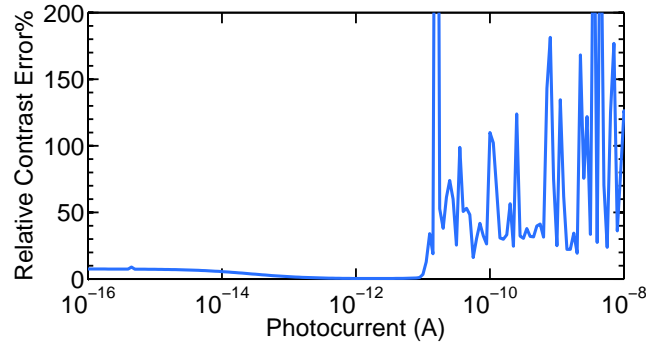


Figure 4.4: Reinhard simple FPN expressed as contrast error before correction.

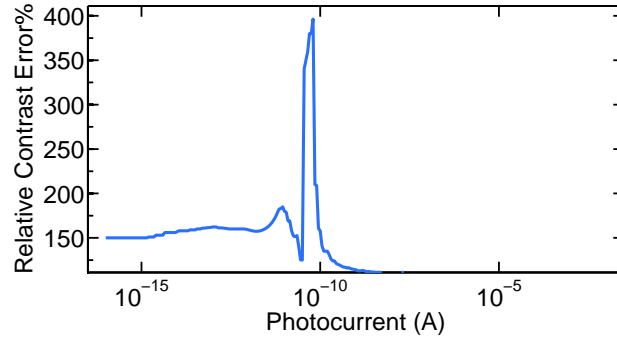


Figure 4.5: Reinhard complex FPN expressed as contrast error before correction.

4.7 FPN Correction

The last section presented the FPN noise measurement technique and contrast error before correction. The results show that FPN before correction is quite high which needs to be corrected. FPN correction can be performed by using the parameters values extracted in the last section. FPN measurement before the correction was performed using the mean values of parameters. However, FPN can be corrected by inserting the value of each parameter. Multiple parameters correction technique is used to correct FPN. Firstly, one parameter was corrected to check the quality of FPN correction technique. Secondly, the second and third parameter was corrected, if one parameter correction did not produce good results.

Reinhard Simple Correction

Firstly, the extracted current given in Equation 4.22 was calculated by inserting each parameters individual value instead of mean value. 1000 pixels individual data was used for this purpose. Secondly, this extracted current was used to calculate the FPN by

using Equation 4.19. Parameter a was corrected first, by inserting the value of a in each pixel extracted current and then this current was used to calculate FPN. One parameter a FPN correction expressed as contrast error is shown in Figure 4.6. One parameter FPN correction exhibits the high contrast error around 20% at middle range currents i.e $1\text{ pA} - 1\text{ nA}$. Hence, second b and third c parameter correction procedure was performed. Figure 4.7 shows the contrast error using two parameters a, b correction. FPN correction using two parameters also exhibits the high contrast error of 30%. The two parameter correction procedure exhibited the high contrast error as compared to one parameter correction because of the dark current and arbitrary selection of calibration currents. Figure 4.8 presents the contrast error using three parameters a, b, c correction. Three parameters correction procedure have exhibited good results, and the relative contrast error is below than 1%. Hence, three parameters FPN correction procedure is sufficient. Figure 4.9 presents the FPN using four parameters a, b, c, d correction. FPN correction using four parameters produced a high error at low photocurrent range because of dark current contribution. Overall, a simple technique in which three parameters were used to correct FPN have performed very well and exhibited some good results. After FPN correction, Reinhard simple exhibits the contrast error less than 1%, which is a very promising result.

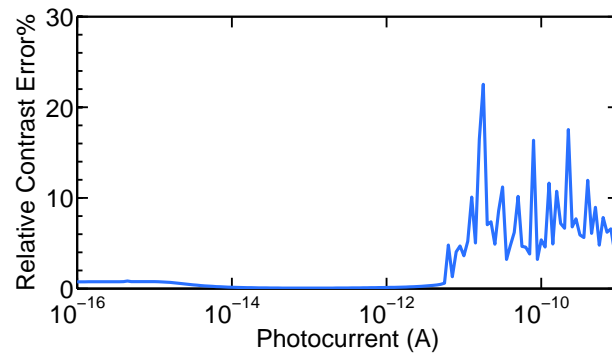


Figure 4.6: Reinhard simple FPN expressed as contrast error after one parameter a correction.

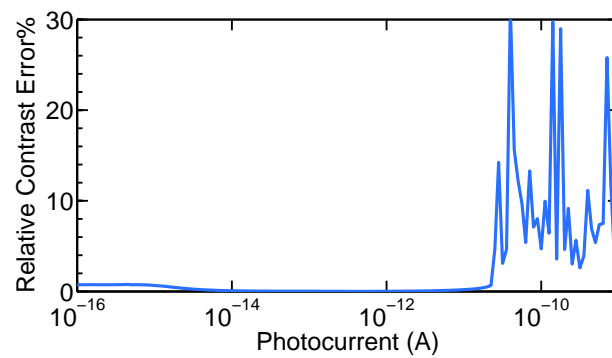


Figure 4.7: Reinhard simple FPN expressed as contrast error after two parameters a and b correction.

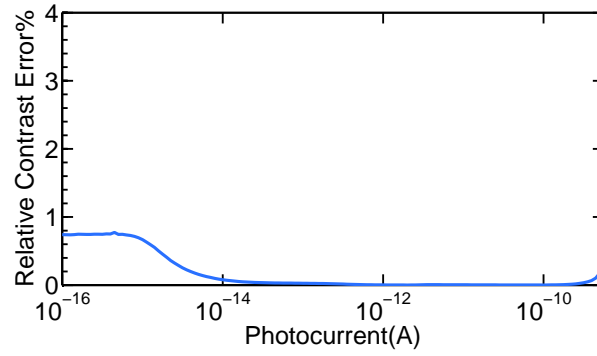


Figure 4.8: Reinhard simple FPN expressed as contrast error after three parameters a, b, c correction.

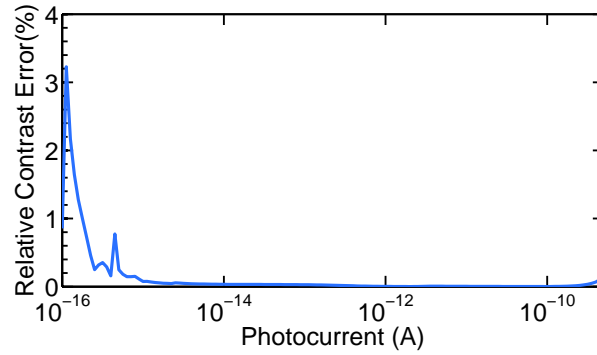


Figure 4.9: Reinhard simple FPN expressed as contrast error after all parameters correction.

Reinhard Complex Correction

A similar technique to correct FPN using multiple parameters is applied to Reinhard complex operator. Parameters P, Q, R, S, D are used for FPN correction procedure. The extracted current is calculated using Equation 4.23. First, parameter P is corrected and then followed by other parameters Q, R, S, D correction. Figure 4.10 presents the one

parameter P correction contrast error. FPN using one parameter correction procedure exhibits high contrast error at different photocurrent. Figure 4.11 and 4.12 presents the FPN expressed as contrast error using two P, Q and three P, Q, R parameters respectively. Both correction techniques still exhibit the high contrast error. Hence, four parameters P, Q, R, S correction technique is used. Figure 4.13 shows the contrast error using four parameters correction. Reinhard complex FPN correction technique using four parameters performed very well and contrast error is less than 1% over the whole range of photocurrents.

As discussed earlier, one and two parameter correction procedure produced large errors as compared to three and four parameters correction. The reason of the high error could be fact that each parameter contributes into FPN generation. One parameter correction procedure only corrects FPN of one parameter while others parameters are still uncorrected. Hence, four parameter technique is the best approach of FPN correction because each mismatch parameter is corrected in this way.

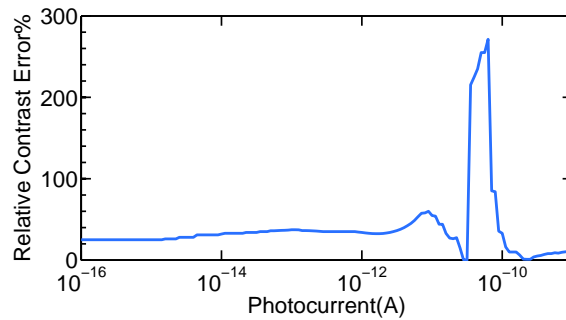


Figure 4.10: Reinhard complex FPN expressed as contrast error after one parameter P correction.

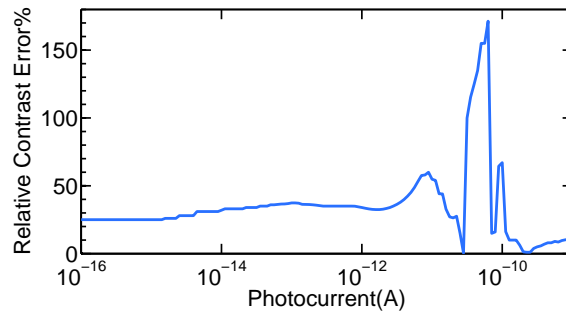


Figure 4.11: Reinhard complex FPN expressed as contrast error after two parameters P, Q correction.

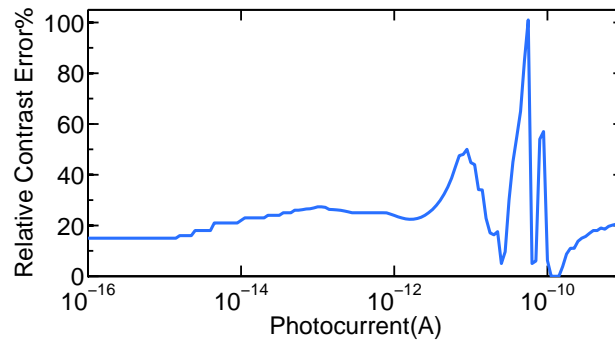


Figure 4.12: Reinhard complex FPN expressed as contrast error after three parameters P, Q, R correction.

Operator	Model Error	FPN 1 para.	FPN 2 para.	FPN 3 para.	FPN 4 para.
Reinhard Simple	15mV	20%	30%	1%	3%
Reinhard Complex	40mV	250%	150%	100%	1%

Table 4.5: Summary Table.

4.8 FPN Effects on a Test Image

The FPN correction technique was identified in the last section. This section presents the effects of FPN on a typical image. A simple test image is shown in Figure 4.14¹ was

¹image is taken from <http://www.notebookcheck.net/>

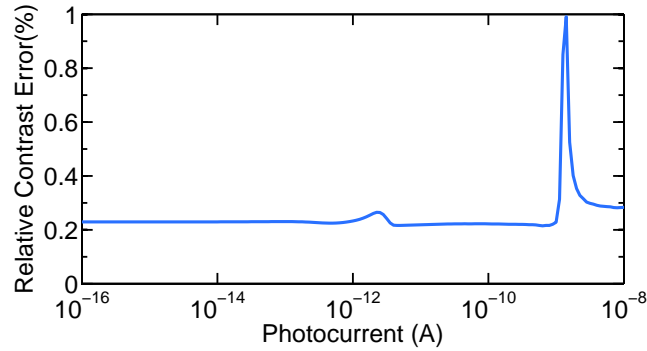


Figure 4.13: Reinhard complex FPN expressed as contrast error after four parameters correction.

used to check the effects of FPN on an image taken by CMOS sensor. In addition, how well the FPN correction technique performs on a test image is also presented. FPN is added to test image to check the image quality degradation caused by this. The FPN correction technique is later applied on a test image that already has FPN added. A test image with and without FPN is shown in Figure 4.14 and 4.15. Figure 4.16 shows the image after FPN correction for Reinhard simple and complex operator. It can be seen that FPN after correction procedure shows some artifacts in dark regions of an image. The artifacts in an image are due to an arbitrary selection of calibration currents x_1 , x_2 , x_3 and artifacts could be removed by adjusting the calibration current.



Figure 4.14: Test image.



Figure 4.15: Test image with fixed pattern noise.



(a)



(b)

Figure 4.16: (a) Test image after FPN correction of Reinhard simple. (b) Test image after FPN correction of Reinhard complex.

4.9 Conclusion

In this chapter, analytical pixel model was developed and discussed with different parameters that characterise the pixel response. Pixel modeling is the basic building block in finding fixed pattern noise. In order to check the validity of the developed pixel model, simulated response is compared with the model response. In addition, parameters extraction procedure is also discussed. FPN correction technique for Reinhard CMOS pixel is also presented in this chapter. FPN is mainly due to the variations between the responses of individual pixels within an array of pixels. We have shown that calibration technique can be used to correct the fixed pattern noise in pixels, which can produce a tone mapped response, particularly the Reinhard tone mapping. A simple procedure has been adapted to reduce FPN in which parametric response of pixel is used, with FPN modeled as variations in the individual parameters.

The parameters of 1000 individual pixels were measured, recorded and then used to correct their response. As discussed earlier, the human eye has a contrast threshold of 1% which means the human eye is unable to perceive errors in misrepresented illuminations that are less than 1% of the original illumination. Therefore, 1% error value becomes the best attempt at matching FPN error to the sensitivity of the human visual system. FPN correction results are presented with an overall relative contrast error is less than 1% for Reinhard simple and complex operator, which are very promising results. In addition, the results of FPN correction technique on a test image are also presented. FPN after correction procedure shows some artifacts in dark regions of an image. These artifacts in an image are due to an arbitrary selection of calibration currents x_1 , x_2 , x_3 and artifacts may be removed by adjusting calibration currents.

Chapter 5

Pixel Modeling for Different Mapping Operators

5.1 Introduction

The previous chapter presented the model error i.e error between the analytical and simulated results, and FPN correction technique for Reinhard tone mapping operator. This chapter deals with the pixel model and parameters extraction routine for rest of the operators i.e. Drago, Exponential, Schlick, Miller, Tumblin and Rushmier, and Logarithmic. Parameters extraction is an essential part in order to produce the FPN correction technique. The FPN correction technique for Reinhard operator presented in the last chapter can be used for other tone mapping operators. However, pixel model, a model error between pixel simulation, and the analytical model and parameters extraction technique need to be shown before FPN correction.

Section 5.2 presents the Drago pixel model with parameter extraction. Section 5.3 dis-

cusses the parameter extraction procedure for an Exponential operator. Section 5.4 presents the parameter extraction routine for Schlick tone mapping operator. Section 5.5 presents the pixel model of Miller operator. Section 5.6 presents the parameter extraction of Tumblin and Rushmeir operator. Section 5.7 discuss the pixel model of Logarithmic mapping operator.

5.2 Drago Pixel Model

A Drago pixel model can be developed using semiconductor theory and analysing the typical WDR pixel circuitry as shown in the last chapter in Figure 4.1. The pixel output for a Drago mapping operator obtained by analysing the pixel circuitry is given as,

$$V_Y = V_{dd} - V_{TM1} - \frac{V_{dd} \log_{10}(1 + g(I_{dark} + Q_{PD} G_A G_L A_{PD} L_{opto}))}{\log_{10}(1 + g I_{pmax}) \log_{10}[2 + 8(\frac{g(I_{dark} + Q_{PD} G_A G_L A_{PD} L_{opto})}{g I_{pmax}})^{\frac{\log_{10}(p)}{\log_{10}(0.5)}}]} - (V_{TM2} + V_{TM3} + V_{TM6})$$

$$- \sqrt{\frac{\beta_{M5}}{\beta_{M3}}}(V_{GSM5} - V_{TM5}) - \sqrt{\frac{\beta_{M8}}{\beta_{M6}}}(V_{GSM8} - V_{TM8}) \quad (5.1)$$

The above equation can be rewritten in the form of parameters and given as,

$$y = a - \frac{b \log_{10}(1 + c(x + d))}{\log_{10}(1 + c) \log_{10}(2 + 8(x + d)^{0.234})} \quad (5.2)$$

with terms given as,

$$y = V_Y$$

$$a = V_{dd} - V_{TM1} - (V_{TM2} + V_{TM3} + V_{TM6}) - \sqrt{\frac{\beta_{M5}}{\beta_{M3}}}(V_{GSM5} - V_{TM5}) - \sqrt{\frac{\beta_{M8}}{\beta_{M6}}}(V_{GSM8} - V_{TM8})$$

$$b = V_{dd}$$

$$c = g$$

$$d = I_{dark}$$

$$x = Q_{PD}G_A G_{LAPD} L_{opto}$$

(5.3)

Parameters extraction can be performed by assuming different calibration current x_1, x_2, x_3 with response y_1, y_2, y_3 . Model response using calibration current and assuming that the dark current d is small enough to be neglected is given as,

$$\begin{aligned} y_1 &= a - \frac{b \log_{10}(1 + cx_1)}{\log_{10}(1 + c) \log_{10}(2 + 8(x_1)^{0.234})} \\ y_2 &= a - \frac{b \log_{10}(1 + cx_2)}{\log_{10}(1 + c) \log_{10}(2 + 8(x_2)^{0.234})} \\ y_3 &= a - \frac{b \log_{10}(1 + cx_3)}{\log_{10}(1 + c) \log_{10}(2 + 8(x_3)^{0.234})} \end{aligned} \quad (5.4)$$

Unfortunately, certain parameters could not be extracted due to the complex mathematical nature of Drago model equation. We needed to use Matlab curve fitting technique to find the optimum value of each single parameter a, b, c and d and then by using the optimum value of c , the rest of the parameters a, b and d can be extracted by solving

equations given as,

$$a = y_1 + \frac{b \log_{10}(1 + cx_1)}{\log_{10}(1 + c) \log_{10}(2 + 8(x_1)^{0.234})} \quad (5.5)$$

$$b = \frac{(y_2 - y_1) \log(1 + c)}{\frac{\log(1 + cx_2)}{\log(2 + 8(x_2)^{0.234})} + \frac{\log(1 + cx_1)}{\log(2 + 8(x_1)^{0.234})}} \quad (5.6)$$

Lets choose the curve fit optimum value of $c = 10^{13}(\text{A}^{-1})$ and find the values of a and b . Three calibration currents and responses values are selected and given as $x_1 = 10^{-13}$, $x_2 = 10^{-12}$, $x_3 = 10^{-10}$, $y_1 = 1.3638$, $y_2 = 1.1442$, $y_3 = 0.5534$. The extracted values of parameters are $a = 1.4536(\text{V})$, $b = 2.7007(\text{V}/\text{A})$, $d = 10^{-15}(\text{A})$. Model response of Drago pixel can be calculated by inserting the parameters values in Equation 5.2. Figure 5.1 shows the comparison between pixel model and simulated response. It is apparent from the figure that suggested model does fit well with simulated response at middle range photocurrents, and the maximum model error between simulated and model response is around 25 mV, which is a good result. The reason of this model error is the arbitrary selection of parameter value c .

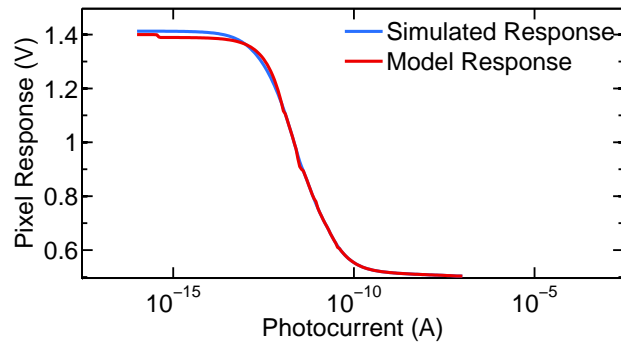


Figure 5.1: Comparison of model and simulated Drago response.

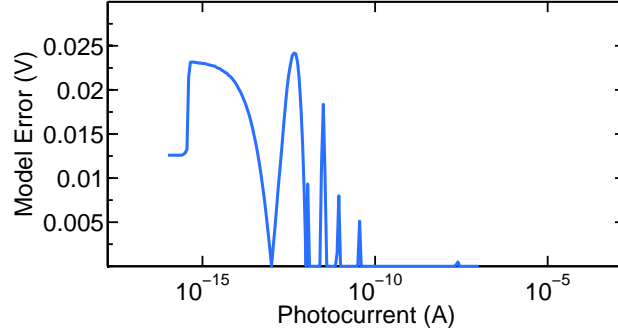


Figure 5.2: Model error between simulated and model response.

5.3 Exponential Pixel Model

The exponential model can be developed using the pixel schematic with exponential reference function and given as,

$$V_Y = V_{dd} - V_{TM1} - V_{dd}(1 - \exp(gI_p)) - (V_{TM2} + V_{TM3} + V_{TM6}) - \sqrt{\frac{\beta_{M5}}{\beta_{M3}}}(V_{GSM5} - V_{TM5}) - \sqrt{\frac{\beta_{M8}}{\beta_{M6}}}(V_{GSM8} - V_{TM8}) \quad (5.7)$$

This equation can be rewritten in the form of model parameters given as,

$$y = a + b \exp(c(x + d)) \quad (5.8)$$

with different term given as,

$$y = V_Y$$

$$a = 2V_{dd} - V_{TM1} - (V_{TM2} + V_{TM3} + V_{TM6}) - \sqrt{\frac{\beta_{M5}}{\beta_{M3}}}(V_{GSM5} - V_{TM5}) - \sqrt{\frac{\beta_{M8}}{\beta_{M6}}}(V_{GSM8} - V_{TM8}) \quad (5.9)$$

$$\begin{aligned}
b &= V_{dd} \\
c &= g \\
d &= I_{dark} \\
x &= Q_{PD}G_A G_L A_{PD} L_{opto}
\end{aligned} \tag{5.10}$$

Parameters can be extracted by assuming different calibration currents x_1, x_2, x_3 and respective responses y_1, y_2, y_3 . Parametric equations with calibration currents are given as,

$$\begin{aligned}
y_1 &= a + b \exp(cx_1) \\
y_2 &= a + b \exp(cx_2) \\
y_3 &= a + b \exp(cx_3)
\end{aligned} \tag{5.11}$$

A mathematical solution for the parameters does not exist due to the complex nature of the equation. However, certain parameter values can be assumed using Matlab curve fit technique in order to find the solution of exponential pixel model equation. Assuming the optimum value of parameter $c = 10^{10} (A^{-1})$ from curve fit technique, and use this value to find the rest of parameters a, b and d . The parameter a and b can be calculated using the equations given as,

$$a = y_1 - b \exp(cx_1) \tag{5.12}$$

$$b = \frac{y_2 - y_1}{\exp(cx_2) - \exp(cx_1)} \tag{5.13}$$

By assuming different calibration currents x_1, x_2, x_3 and response y_1, y_2, y_3 leads to the extraction of parameters a, b and d . The extracted parameters values are $a = 2.71(V)$, $b = 5.5 \times 10^8(V/A)$, $c = 10^{10}(A^{-1})$ and $d = 1.42 \times 10^{-16}(A)$. Equation 5.8 is used for the exponential model response and Figure 5.3 shows the comparison between model and simulated exponential response. It can be seen that suggested model fits well with simulated response except at middle range currents between $10^{-12}A$ - $10^{-11}A$. The maximum model error between two responses is around 300 mV . The reason of high model error at middle range current is the arbitrary selection of parameter value c and calibration currents.

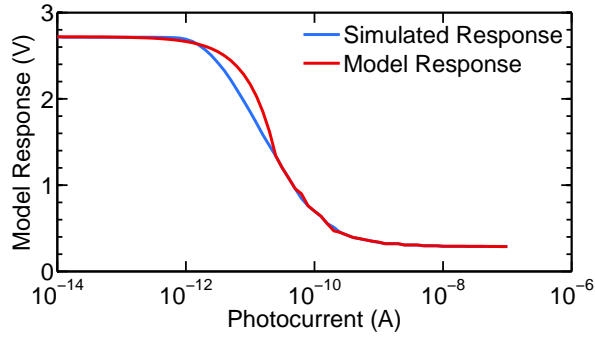


Figure 5.3: Comparison of model and simulated exponential response.

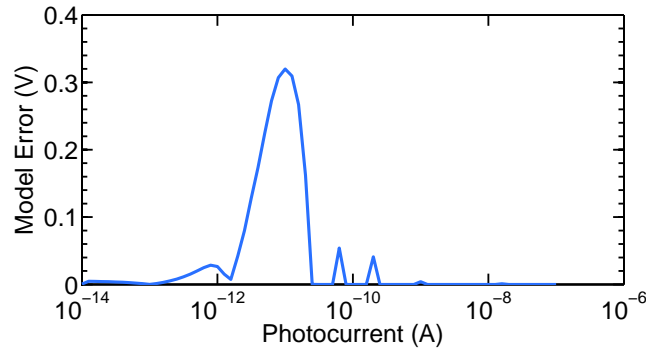


Figure 5.4: Error between simulated and model response.

5.4 Schlick Pixel Model

The Schlick pixel model using the same semiconductor technique as mentioned in earlier sections is given as,

$$y = a - \frac{b(x+d)}{c(x+d) + 10^{-6}} \quad (5.14)$$

One can extract parameters from the model equation by assuming three different calibration currents x_1 , x_2 and x_3 with response y_1 , y_2 and y_3 . In addition, the dark current d can be neglected. The model equation with different calibration currents are given as,

$$\begin{aligned} y_1 &= a - \frac{bx_1}{cx_1 + 10^{-6}} \\ y_2 &= a - \frac{bx_2}{cx_2 + 10^{-6}} \\ y_3 &= a - \frac{bx_3}{cx_3 + 10^{-6}} \end{aligned} \quad (5.15)$$

These equations can be solved for the values of parameters a, b, c , and d that is given as,

$$a = y_1 + \frac{bx_1}{cx_1 + 10^{-6}} \quad (5.16)$$

$$b = \frac{10^6(y_1 - y_2)(cx_2 + 10^{-6})(cx_1 + 10^{-6})}{x_2 - x_1} \quad (5.17)$$

$$c = \frac{10^{-6}(x_3y_2 + y_3x_1 + y_1x_2 - x_1y_2 - x_3y_1 - y_3x_2)}{x_2x_3y_3 + x_1x_3y_1 + x_1x_2y_2 - x_1x_3y_3 - x_1x_2y_1 - x_2x_3y_2} \quad (5.18)$$

$$d = \frac{(a - y)10^{-6}}{b + yc - ac} \quad (5.19)$$

A mathematical solution for parameters exist for Schlick mapping operator. Hence, Schlick model response can be calculated by inserting the values of parameters in Equation 5.14. Different calibration currents and response were chosen from pixel simulated

Parameter	a (V)	b (V/A)	$c(A^{-1})$	d (A)
Value	2.77	6.13×10^5	2.59×10^5	9.87×10^{-14}

Table 5.1: Schlick extracted parameters using different calibration current.

data to extract parameters and given as $x_1 = 10^{-13}$, $x_2 = 2.51 \times 10^{-11}$, $x_3 = 10^{-9}$, $y_1 = 2.7146$, $y_2 = 0.7270$ and $y_3 = 0.4220$.

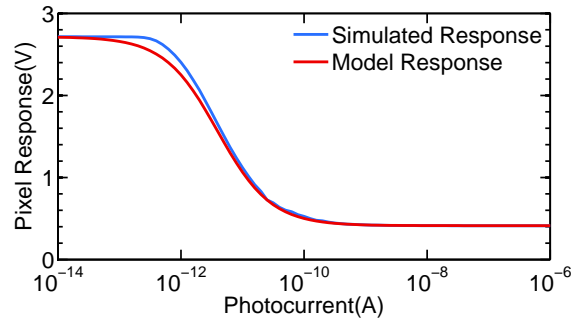


Figure 5.5: Comparison between Schlick pixel simulated and model response.

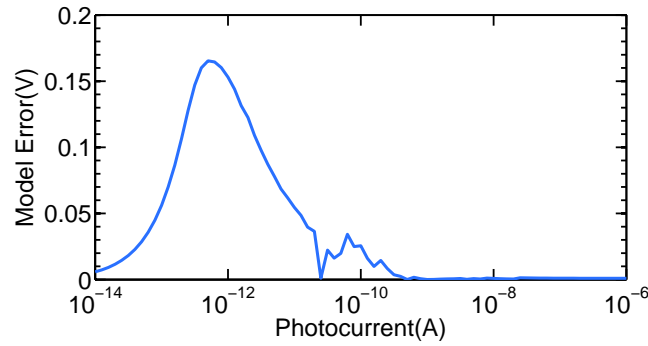


Figure 5.6: Model error between Schlick pixel simulated and model response.

The analytical and simulated responses have to be compared to check the effectiveness of a developed model. Figure 5.5 presents the comparison between pixel simulated and

model response. Also, Figure 5.6 shows the model error between model and simulated response. It can be seen that model response exhibits some model error at middle range current i.e. $I = 10^{-12}A$. The maximum model error Schlick pixel exhibits are 140 mV . The cause of model error is the arbitrary selection of calibration current. The model error of Schlick operator is high, and it needs to be corrected before the FPN correction procedure.

5.5 Miller Pixel Model

The model equation for Miller tone mapping operator can be developed using the semiconductor theory as discussed earlier and given as,

$$y = a - b(-1.5\log(c(x+d)) + 6.1)(c(x+d))^{0.338(c(x+d))^{0.0334}} \quad (5.20)$$

Model parameters can be extracted by assuming different calibration currents x_1 , x_2 and x_3 with the response y_1 , y_2 and y_3 . The dark current d is assumed small enough to be neglected. Different calibration current model equations are given as,

$$\begin{aligned} y_1 &= a - b(-1.5\log(cx_1 + 6.1)(cx_1)^{0.338(cx_1)^{0.0334}} \\ y_2 &= a - b(-1.5\log(cx_2 + 6.1)(cx_2)^{0.338(cx_2)^{0.0334}} \\ y_3 &= a - b(-1.5\log(cx_3 + 6.1)(cx_3)^{0.338(cx_3)^{0.0334}} \end{aligned} \quad (5.21)$$

A mathematical solution of different parameters a , b , c and d does not exists due to complex nature of equations. However, we can find the optimum value of parameter c using Matlab curve fit technique. This value of c and calibration currents x_1 , x_2 ,

x_3 leads to the extraction of other parameters a , b and d . Parameter $c = 10^5(A^{-1})$ and calibration currents $x_1 = 10^{-14}$, $x_2 = 10^{-12}$ and $x_3 = 10^{-10}$ with responses $y_1 = 1.3784$, $y_2 = 1.1871$ and $y_3 = 1.1007$ are chosen. Parameter value b and a can be extracted using the equations given as,

$$a = y_1 + b(-1.5\log(cx_1 + 6.1))(cx_1)^{0.338(cx_1)^{0.0334}} \quad (5.22)$$

$$b = \frac{y_1 - y_2}{(-1.5\log(cx_2) + 6.1)(cx_2)^{0.338(cx_2)^{0.0334}} - (-1.5\log(cx_1) + 6.1)(cx_1)^{0.338(cx_1)^{0.0334}}} \quad (5.23)$$

The extracted value of parameters are $a = 1.45(V)$, $b = 1.6 \times 10^{-4}(V/A)$ and $d = 10^{-14}(A)$. Figure 5.7 shows the comparison between model and simulated response of Miller operator. It is apparent from the figure that suggested model does fit well with simulated data in this case too. Figure 5.8 shows the model error between two responses, that is around 15 mV. This model error is due to the selection of calibration currents and parameter c .

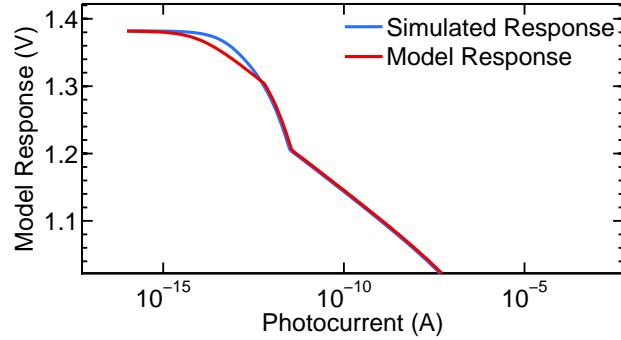


Figure 5.7: Comparison between Miller pixel simulated and model response.

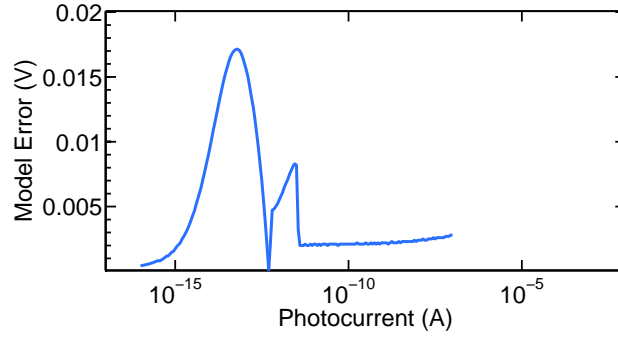


Figure 5.8: Model error between Miller pixel simulated and model response.

5.6 Tumblin and Rush Pixel Model

Like other operators, the model equation for Tumblin and Rush mapping operator can be developed using semiconductor theory discussed in last chapter and given as,

$$y = a - b(x + d)^c \quad (5.24)$$

The parameters can be extracted using the calibration currents and different current model equations are given as,

$$\begin{aligned} y_1 &= a - bx_1^c \\ y_2 &= a - bx_2^c \\ y_3 &= a - bx_3^c \end{aligned} \quad (5.25)$$

A mathematical solution of different parameters a , b , c and d does not exist due to the complex nature of the equations. Using Matlab curve fit technique gives the optimum value of $c = 10^{-10} \text{ (A}^{-1}\text{)}$. By using the value of c and different calibration currents $x_1 = 10^{-14}$, $x_2 = 10^{-12}$, $x_3 = 10^{-10}$ with responses $y_1 = 1.4261$, $y_2 = 1.1669$ and $y_3 =$

1.0799 provides the parameter a and b given as,

$$a = y_1 + bx_1^c \quad (5.26)$$

$$b = \frac{y_1 - y_2}{x_2^c - x_1^c} \quad (5.27)$$

Figure 5.9 shows the comparison between model and simulated response of Miller operator. It is apparent from the figure that suggested model fits well with simulated data. Figure 5.10 shows the model error between two responses, that is around 150 mV. The high model error is due to the selection of parameter c .

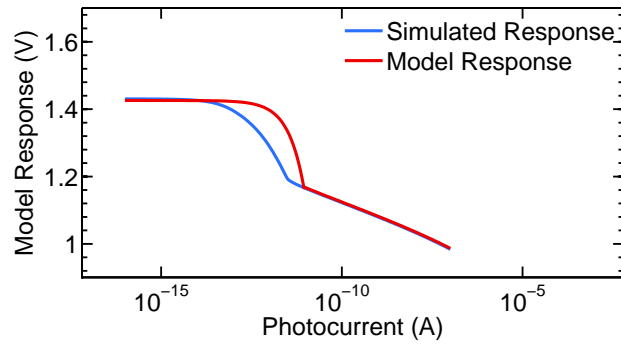


Figure 5.9: Comparison between Tumblin pixel simulated and model response.

5.7 Log Pixel Model

The pixel model equation for logarithmic mapping operator is given as,

$$y = a - b \log(1 + c(x + d)) \quad (5.28)$$

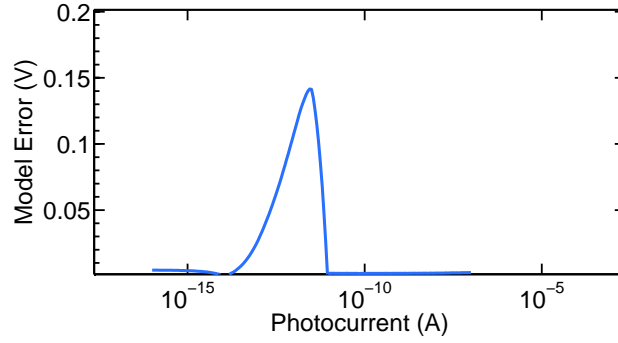


Figure 5.10: Model error between Tumblin pixel simulated and model response.

Operators	Drago	Exponential	Schlick	Miller	Log
Model Error	25 mV	300 mV	140 mV	15 mV	150 mV

Table 5.2: Summary Table.

Model parameters can be extracted by assuming different calibration currents x_1 , x_2 and x_3 with the response y_1 , y_2 and y_3 . The dark current d is assumed small enough to be neglected. Let's assume the value of $c = 10^{10} \text{ (A}^{-1}\text{)}$ using curve fit technique and find the mathematical solution of logarithmic model equation. Parameter a and b can be calculated using equation given as,

$$a = y_1 + b \log(1 + cx_1) \quad (5.29)$$

$$b = \frac{y_1 - y_2}{\log(1 + cx_2) - \log(1 + cx_1)} \quad (5.30)$$

Figure 5.11 shows the comparison between model and simulated response of logarithmic operator. It is apparent from the figure that suggested model does fit well with simulated data. Figure 5.12 shows the model error between two responses, that is around 150 mV. The high model error is due to the selection of parameter c .

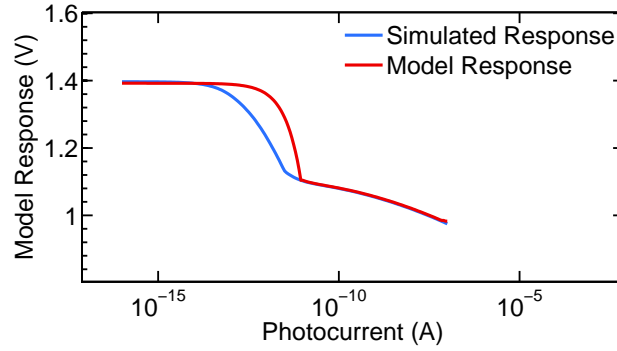


Figure 5.11: Comparison between logarithmic pixel simulated and model response.

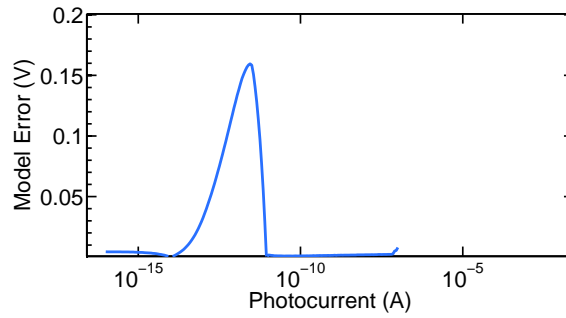


Figure 5.12: Model error between logarithmic pixel simulated and model response.

5.8 Conclusion

Pixel modeling for different tone mapping operators was discussed in this chapter. The mapping operators are Drago, Exponential, Schlick, Miller, Tumblin and Rushmier, and logarithmic. An analytical pixel model was developed using semiconductor theory by analysing the pixel schematic presented in this chapter. It is noted that the solution of a model equation that characterise the pixel response does not exist due to the complex nature of mathematical equations. Hence, we assumed the value of parameter c using the Matlab curve fit technique and find the values of rest of the parameters a , b and

d. Drago operator exhibits the model error of $25mV$, Exponential produces the model error of $300mV$, Schlick exhibits the model error of $140mV$, Miller produces the error of $15mV$ and Logarithmic operator exhibits the model error of $150mV$.

Chapter 6

Conclusion and Future Work

This chapter is devoted to summarising this thesis, and provide ideas for possible future work. The first section presents the overall summary of the thesis and results already presented. Section 1 is further divided into 3 broad subsections. The first subsection discusses the tone mapping technique and summarising the comparison results of different tone mapping algorithms. The second subsection presents the design and operation of proposed wide dynamic range pixel. Also, tone mapping operation on wide dynamic range pixel is presented. Simulation results show that WDR pixel can capture a dynamic range of more than 6 decades with in-pixel tone mapping operation. The third subsection summarises the Reinhard tone mapping operator model error and fixed pattern noise correction technique and results. The fourth subsection presents the model error of other tone mapping operators.

The rest of this chapter discusses some ideas for the future work. These includes the possible CMOS chip design of wide dynamic range sensor, local tone mapping, video tone mapping and 3D stacked CMOS image sensor chip.

6.1 Summary

Electronic imaging devices are very popular nowadays and these devices have replaced film-based cameras. Electronic imaging devices are mainly used in mobile phones, automobiles, security, biometrics and professional cameras. These devices can be divided into two categories: charge coupled device (CCD) sensor and complimentary metal-oxide semiconductor (CMOS) sensor. CCD sensor technology was a major market player in the field of digital cameras and main advantages of CCD are superior quality color images, higher signal to noise ratios, high photosensitive area, and low readout noise [2]. However, the drawbacks of CCD sensor are production costs and high power consumption. CMOS sensors have replaced CCD in the most low end as well as professional cameras. CMOS sensors were first used in low-end applications like toys and mobile phones. However, improvement in CMOS image sensors technology outperforms CCD in many applications. The ability to integrate with other circuit blocks make CMOS sensors ideal to be embedded in mobile phones, auto-mobiles, security, and biometrics.

The human eye can capture images over a wide dynamic range of illuminations available in nature, from as low as 10^{-4} lux in a starlit night to high as 10^5 lux in bright sunlight. However, typical CMOS camera has limited ability to capture the light available in nature and dynamic range of typical CMOS sensor is limited to 2-3 decades. Several approaches and CMOS circuits have been proposed to extend the dynamic range of CMOS pixels. These includes logarithmic sensors using the weak inversion region of operation of a MOS transistor [6], well capacity adjustment [7], threshold comparison, integration time control [8], neuromorphic approaches [9] and linear-logarithmic pixel [10].

In this thesis, the image has been algorithmically transformed by mathematical operators called tone mapping operators to fit the limited dynamic range. In addition, a pixel which captures a scene with inbuilt tone mapping operator, particularly, the Reinhard photographic mapping operator, was reported.

6.1.1 Tone Mapping

The dynamic range of a scene in a real world can be of the order of 10^{-3} to 10^2 from light to dark areas. Many industries like defence and night vision are looking for more realistic images that match the real scene as seen by the human visual system (HVS). However, display devices available in the market are unable to produce the image detail as seen by human eye. Typical display devices can only produce an image of a dynamic range of less than 10^2 to 10^0 [18]. This leads to an incomplete representation of captured scene. Hence, it is a problem to reproduce high dynamic range scenes using media with very limited dynamic range like CRT/LCD displays, hard-copy prints, and projectors. In order to solve the problem of displaying HDR images on LDR displays, computational algorithms known as tone mapping operators have been proposed.

Tone mapping is the operation by which one can display HDR content on LDR display device. When the dynamic range of the captured scene is smaller or larger than that of the display device, tone mapping expands or compresses the luminance respectively [19]. After tone mapping operation, the image should be a faithful representation of the real image with improved contrast and details. on the display. The purpose of applying tone mapping on an image can be different and depends on the particular application. In some cases producing just 'nice looking' image is the main goal, while other applications might emphasize reproducing as many details as possible, or might

maximize the image contrast [23]. However, the ultimate goal of tone mapping is to match the perception of tone mapped image with the real world perception seen by the human visual system.

The detailed literature review of each global tone mapping operator was presented in chapter 2. Global operators were selected because they are computationally efficient and can be executed in real time, faster than other operators. Different tone mapping operators were simulated in Matlab, in order to check the quality and faithfulness of the image after tone mapping operation. Qualitative criteria were adopted in order to assess the quality of images after tone mapping operation. Two operators, Reinhard, and Exponential performed better than others on two different dynamic range images.

6.1.2 A Wide Dynamic Range Pixel

Nature have a dynamic range of more than 6 decades of light intensity, whereas CMOS active pixel sensor dynamic range is limited from 2 to 4 decades. Hence, in order to capture and display of wide range of intensities available in nature, a new CMOS WDR pixel with tone mapping technique was presented in chapter 3. The main goal of WDR pixel with tone mapping is to capture a wide dynamic range using reference voltage and to enable direct display of image on low dynamic range display devices at image acquisition stage.

The new WDR pixel consists of four transistors, reset device, reference voltage switch, source follower and row select switch. In a typical linear pixel, high photocurrent saturates the pixel and so it cannot capture the wide dynamic range information. In our pixel approach, wide dynamic range information can be captured by introducing reference voltage switch. A monotonically increasing reference voltage is applied to a

reference switch to capture wide dynamic range information. The pixel output follows a reference signal, which is sampled and held at value when the photo generated signal on the diode becomes lower than the reference voltage. The potential at which these two signals are equal is recorded and is used as the pixel's response. A detailed discussion about WDR pixel was presented in chapter 3.

Different reference voltages were extracted from global tone mapping operators like Reinhard, Drago, Schlick, Miller, Tumblin and Rushmeier. In addition, these reference voltages were applied on a CMOS pixel to obtain wide dynamic range information. The wide dynamic range pixel was simulated in Cadence circuit simulator using a $0.35\mu M$ CMOS process from Austria Microsystems. The simulation results showed that WDR pixel can capture the dynamic range of more than 6 decades with in-pixel tone mapping operation.

6.1.3 Pixel Modeling and Fixed Pattern Noise Correction

Pixel modeling is the basic building block to investigate the noise and errors in WDR pixel. A pixel model was developed by analysing the pixel schematic using semiconductor theory. Reinhard simple and complex operator pixel model with different parameters was developed. Reinhard simple model parameters were a which is pixel offset voltage, b and c represents the pixel gain and d is the dark current. The parameter terms of Reinhard complex are same as Reinhard simple operators except for the additional parameter e that is user controllable value. Parameters values need to be extracted to find the required model response. By using the simulated response of the pixel at three different currents, it is possible to find the parameters required to model the pixel.

Pixel model response is compared with the simulated response to check the validity of

pixel model. The results showed that the proposed model fitted well with the simulated data except at some middle range photocurrents i.e $10^{12}A$ $10^{11}A$. Reinhard simple model fits well as compared to the Reinhard complex. The maximum model error in Reinhard simple case is around 15 mV whereas Reinhard complex exhibits the model error of around 40mV .

FPN originates from the variations between the characteristics of individual pixels within an array of a pixel. In order to limit the effects of FPN, a simple FPN removal procedure was adopted. This technique used the parametric response of pixel with FPN modeled as variations in the individual parameters. It is known that the human eye has a contrast threshold of 1% [52]. Hence, it is important that the fixed pattern noise in images should be reduced below this level.

The parameters of 1000 individual pixels were measured, recorded and then used to correct their response. The data of 1000 pixels were extracted using Monte Carlo simulations. Multiple parameters correction technique was used to reduce FPN. The FPN correction result was presented with an overall relative contrast error is less than 1% for Reinhard simple and complex operator, which are very promising results. In addition, the results of FPN correction technique on a test image was also presented. FPN after correction procedure showed some artifacts in dark regions of an image. These artifacts in an image were due to an arbitrary selection of calibration currents x_1 , x_2 and x_3 which can be removed by adjusting calibration currents.

6.1.4 Pixel Modeling of Different Mapping Operators

Pixel modeling of different mapping operators like Drago, Exponential, Schlick, Miller, Tumblin and Rushmier, and Logarithmic were discussed. Pixel model was developed

using semiconductor theory similar to Reinhard operator. It is noted that the solution of a model equation that characterises the pixel response does not exist due to the complex nature of mathematical equations. Hence, parameter c value have been assumed using curve fit technique in order to solve the model equation.

6.2 Future Work

6.2.1 Image Sensor Chip Design

Future work would include the image sensor chip design and calibration. The proposed image sensor IC block diagram is shown in Figure 6.1. Sensor test chip would consist of 200×100 pixel array, with a dimension of $10\mu m \times 10\mu m$. The simulations and design would be performed by Cadence tools. Also, the test chip would be manufactured using a $0.18\mu m$ CMOS process from Austria Microsystems. The pixel output data from simulation and the experimental chip would be compared. In addition, the difference between two data sets would also be analysed. The results of FPN correction procedure from chip would also be discussed.

6.2.2 Local Tone Mapping

In global operators, world luminances are mapped to display luminances using a single tone mapping curve that is same for all pixels of the image. This operation makes global operators more efficient and easy to implement, however there is a limit to the dynamic range of the input image beyond which successful compression becomes difficult [17]. Global operators are monotonically increasing functions with an aim to mimic

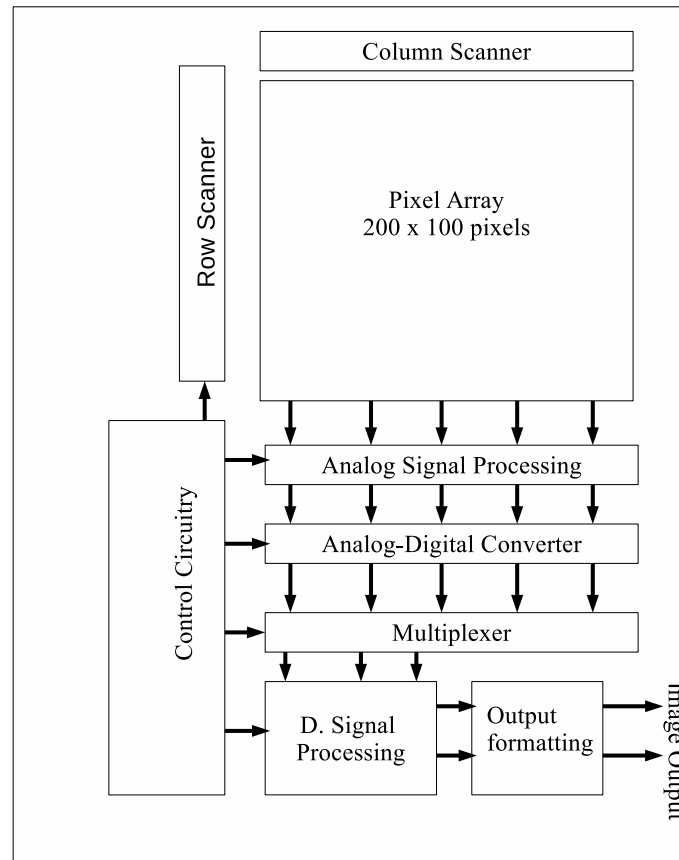


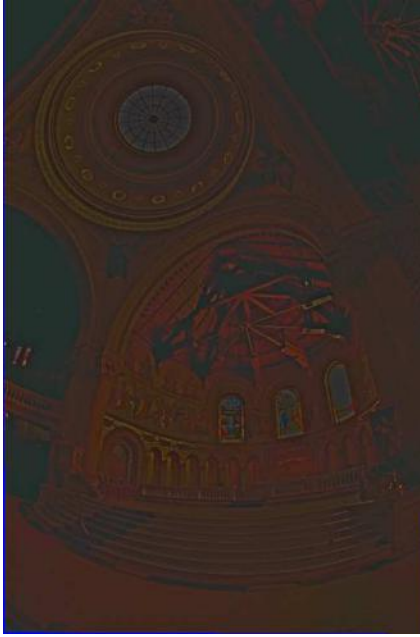
Figure 6.1: Block diagram of image sensor chip.

the performance of HVS non-linearity in order to get a visually more appealing image. Display devices available in the market are able to accommodate 256 levels, all world luminance must be mapped to that range and quantized to unit increments [17]. The higher the dynamic range of an image, the more values must be mapped to 256 different numbers by monotonically increasing functions. For extreme HDR images, this will lead to lose of visibility and contrast. Hence, global operators are more suitable for mid

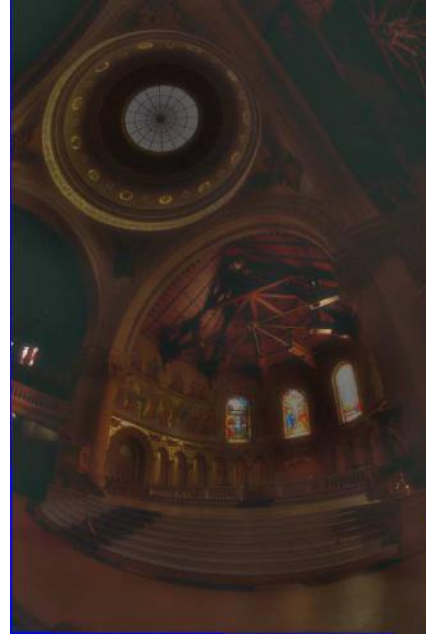
dynamic range images. For very high dynamic range images, global operators compress the illumination too much, which results in a perceived loss of local contrast and detail visibility.

This limitation may be lifted by local operators by compressing each pixel value according to its luminance values and set of neighboring pixels luminance values. Hence, for each pixel the computation is adjusted according to an average over a local neighborhood of pixels [18]. Local operators usually do not mimic the features of the human visual system. A reasonable assumption is that a viewer does not adapt to the scene as a whole, but to smaller regions instead. An active observer's eyes tend to wander across the scene, focusing on different regions. For each focus point, there is a surrounding region that helps determine the state of adaptation of the viewer [18]. There are a number of local tone mapping operators presented in literature includes Chiu variant operator [53], Duan and Quis algorithm [54], Rahman retinex [55], iCAM [53] and Ashikhmin operator [56]. Each operator uses a different technique e.g. Duan and Quis algorithm compresses the HDR image to enhance the local contrast [54]. iCAM algorithm, a new image appearance model, incorporates edge preserving spatial filtering with human vision photoreceptor response functions in a dual-processing framework [53]. Figure 6.2 presents the Chiu operator results with and without global contrast. It can be seen that halos effects are extensive in the images. Halos effects can be reduced by using the glare mask simulations.

Future work can include the Matlab simulations of different local tone mapping operators using the HDR images. In addition, halos reduction techniques can also be analysed. CMOS image sensor using local tone mapping operator can also be presented in the future work.



(a) Chiu oprator with no global contrast.



(b) Chiu operator with both local and global contrast.

Figure 6.2: Chiu local tone mapping operator.

6.2.3 Video Tone Mapping

Video tone mapping is the process to display high dynamic range video on low dynamic range display device. It is similar to static tone mapping except that to take care of temporal domain in video tone mapping. Static tone mapping algorithms can be applied to videos by a frame by frame methods but they often exhibit haloing artifacts and do not guarantee temporal coherence, resulting in flickering [57]. It was reported that video tone mapping has been less active than still image tone mapping. The main hindrance for video tone mapping research has been the lack of good quality HDR content available to the research community, which has been partially addressed by the recent developments in high-end cameras (such as the Red Epic Dragon, Sony *F55* and *F65*, and ARRI

Alexa XT) and other experimental systems now can natively capture High Dynamic Range (HDR) video up to 14 f -stops [57,58] . Despite the recent development in high-end HDR video cameras, the other end of HDR video pipeline i.e HDR video display technology is not yet in the market.

There are a number of video TMO in the literature. Among them, the global operators [59–64] including the S-shaped camera response curve generally produce results with good temporal coherency but poor spatial contrast. On the other hand, the local operators [65–68] often maintain high contrast at the cost of more temporal artifacts. The pros and cons of these operators have been discussed and subjectively evaluated by [35].

Future work would include the evaluation of different tone mapping operators for video purposes. Qualitative criteria could be used for the quality assessment of tone mapping operators. In addition, the feasibility of implication of video tone mapping on a HDR CMOS video camera could also be discussed.

6.2.4 3D Stacked CMOS Image Sensor

In recent years, CMOS image sensor camera requires much more functionalities and compactness due to the strong demand of smart phone camera. In addition to the image quality, speed, and pixel counts that conventional image sensors require, there is high demand for new functions that can respond to various photo-taking scenes [69]. In conventional CMOS image sensors, pixels and circuits are made on the same silicon substrate. Due to the constraints of pixels and circuits on the same substrate, a new CMOS 3D stacked CMOS image sensor was developed. Two different layers of pixels and circuits are proposed in 3D stacked CMOS image sensors. Stacking the pixel

section and the circuit section enables compact size, high image quality, faster speeds and flexible integration of versatile functions [69]. Figure 6.3¹ shows the structure of conventional and stacked CMOS image sensor.

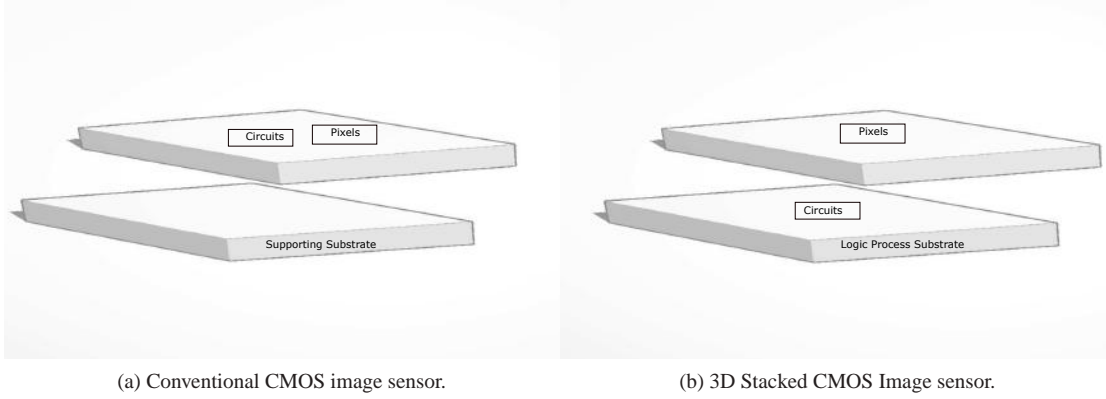


Figure 6.3: Structure of conventional and 3D stacked CMOS image sensor.

A 3D stacked image sensor consists of two substrate layers bonded by micro bumps. The top substrate usually comprises a photo diode array, vertical scanning circuit and readout circuit for readout signals from the photodiode array. The bottom substrate usually comprises a storage node array, vertical scanning circuit and readout circuit for readout signals from the storage node array [70].

Future work can include the design of 3D stacked CMOS image sensors using local tone mapping operators. As discussed earlier, each pixel has a separate tone map curve in local tone mapping. Hence, a frame buffer is needed to store each curve. Therefore, 3D stacked CIS would be the ideal choice to place all extra circuitry like frame buffer on the same chip.

¹image is taken from [69]

6.3 Conclusion

This thesis was divided broadly into two main topics, Tone mapping and Wide dynamic range CMOS image sensor. A detailed discussion about tone mapping was presented in earlier chapters. Also, different tone mapping algorithms were also discussed. It should be noted that only global operators were presented in this thesis and other tone mapping operators were out of the scope. The comparison results of different global tone mapping operators were also discussed. Qualitative criteria were used to assess the quality of images after tone mapping operation. It means that we assessed the image quality visually. The quantitative measure of image quality was not taken into consideration. The qualitative criteria used to assess the image quality is simple and straightforward to implement. On the other hand, the quantitative technique is time consuming and need number of resources. Hence, qualitative criteria were chosen to evaluate different tone mapping operators.

The operation of tone mapping was mimicked and applied on CMOS image sensor with an aim to capture wide dynamic range. Different reference functions were extracted with the aim to capture and display the wide dynamic range simultaneously. A new wide dynamic range pixel was proposed that is capable of in-pixel tone mapping operation. A pixel model was developed and discussed with different parameters that characterise the pixel response. FPN correction technique for Reinhard CMOS pixel was also presented in this thesis.

The work presented in this thesis can be extended to further topics like local tone mapping and video tone mapping operators. Future work can also include the design and manufacturing of standard and 3D stacked CMOS image sensor. 3D stack will improve the overall efficiency, speed and fill factor of the image sensor.

Chapter 7

A Appendix

This appendix presents the different Matlab codes used in this research. These codes presents the operation of different tone mapping techniques on HDR and standard dynamic range images. In addition, the Matlab extraction routine is also presented. Model error and fix pattern noise codes are also discussed.

7.1 Tone Mapping Operators

This section summarises the different tone mapping operator Matlab code. This code simply takes the input high dynamic range or standard dynamic range image. Later, tone mapping algorithm is applied on an input image. Different tone mapping operators have several parameters that controls the intensity or contrast. Due to tone mapping operation, dynamic range of an image is enhanced or compressed that depends on particular application. Finally, tone mapped output image is displayed with a better contrast and details than input image.

Logarithmic Matlab code

```

function imgOut = LogarithmicTMO(img,qlogarithmic,klogarithmic)

img = hdrimread('image.jpg');    %input image read
check3Color(img);    %3 color check
L = lum(img);    %Luminance extraction from image
if( exist('qlogarithmic')|| exist('klogarithmic'))
qlogarithmic = 20;
klogarithmic = 15;
end
if(qlogarithmic < 1)    %check for qlogarithmic >= 1
qlogarithmic = 1;
endif(klogarithmic < 1)    %check for klogarithmic >= 1
klogarithmic = 1;end
LMax = max(max(L));    %computing maximum luminance value
Ld = log10(1+L*qlogarithmic)/log10(1+LMax*klogarithmic); %dynamic Range Reduction
imgOut = zeros(size(img));
fori = 1 : 3
imgOut(:, :, i) = img(:, :, i) .* Ld ./ L;
end
imgOut = RemoveSpecials(imgOut);
figure();
imshow(imgOut);    %out put image display
end

```



(a) Image before tone mapping operation.



(b) Image after logarithmic tone mapping operation.

Figure 7.1: Input and output image after logarithmic tone mapping operation.

Exponential Mapping Operator

```

function imgOut = ExponentialTMO(img, qexponential, kexponential)
img = hdrimread('image.jpg');    %input image read
check3Color(img);    %3 color check
L = lum(img);    %Luminance extraction from image
if( exist('qexponential') || exist('kexponential'))
    qexponential = 1;
    kexponential = 1;
end
if(qexponential < 1)    %check for qexponential >= 1

```

```
qexponential = 1;  
end  
if(kexponential < 1)    %check for kexponential >= 1  
kexponential = 1;  
end  
Lwa = logMean(L);    %computing log luminance value  
Ld = 1 - exp(-(L*qexponential)/(Lwa*kexponential)); %dynamic Range Reduction  
imgOut = zeros(size(img));  
for i = 1 : 3  
    imgOut(:, :, i) = img(:, :, i). * Ld ./ L;  
end  
imgOut = RemoveSpecials(imgOut);  
figure();  
imshow(imgOut);    %out put image display  
end
```



Figure 7.2: Image before tone mapping operation.



Figure 7.3: Image after Exponential tone mapping operation.

Drago Mapping Operator

```

function[imgOut,DragoLMax] = DragoTMO(img,DragoLdMax,Dragob,DragoLMax)
img = hdrimread('image.jpg');    %input image read
check3Color(img);    %3 color check
L = lum(img);    %Luminance extraction from image
if( exist('DragoLdMax'))
DragoLdMax = 100;
if( exist('Dragob'))    %Dragob constatnt check
Dragob = 0.3;
end
if( exist('DragoLMax'))
DragoLMax = max(max(L));
LMax = DragoLMax*0.5 + 0.5 * max(max(L));
DragoLMax = LMax;
constant = log(Dragob)/log(0.5);
costant2 = (DragoLdMax/100)/(log10(1 + LMax));
Ld = costant2 * log(1 + L)./log(2 + 8 * ((L/LMax).^constant)); %dynamic Range Reduction
imgOut = zeros(size(img));

```

```
for i = 1 : 3  
    imgOut(:,:,i) = img(:,:,i) .* Ld ./ L;  
end  
imgOut = RemoveSpecials(imgOut);  
imshow(imgOut);    %out put image display  
end
```



(a) Image before tone mapping operation.



(b) Image after Drago tone mapping operation.

Figure 7.4: Input and output image after Drago tone mapping operation.

Reinhard Mapping Operator

```

function[imgOut,pAlpha,pWhite] = ReinhardTMO(img,pAlpha,pWhite,pLocal,phi)
img = hdrimread('image.jpg');    %input image read
check3Color(img);    %3 color check
L = lum(img);    %Luminance extraction from image
if( exist('pWhite')|| exist('pAlpha')|| exist('pLocal')|| exist('phi'))
pWhite = 2 * max(max(L));
pAlpha = 0.85;
pLocal = 0;
phi = 8;
end
Lwa = logMean(L);    %Log mean calculation
L = (pAlpha * L)/Lwa;
pWhite2 = pWhite * pWhite;
if(pLocal)
Ld = (L./(1 + Ladapt));    %Simple mapping operation
else
Ld = (L.* (1 + L/pWhite2))./(1 + L);    %Mapping operation with burning effect
end
imgOut = zeros(size(img));
fori = 1 : 3
imgOut(:, :, i) = img(:, :, i) ./ lum(img) .* Ld;
end
imgOut = RemoveSpecials(imgOut);
figure();
imshow(imgOut);    %output image display
end

```

Schlick Mapping Operator

```

function imgOut = SchlickTMO(img, schlickmode, schlickp, schlickbit, schlickdL0, schlickk)
img = hdrimread('image.jpg');    %input image read
check3Color(img);    %3 color check
if( exist('schlickmode')| exist('schlickp')| exist('schlickbit')
| exist('schlickdL0')| exist('schlickk'))
schlickmode = 'standard';
schlickp = 1/0.1;
end
L = lum(img);    %Luminance extraction from image
LMax = max(max(L));    %Maximum Luminance
LMin = min(min(L));    %MinumumLuminance
if(LMin <= 0.0)
ind = find(LMin > 0.0);
LMin = min(min(L(ind)));
switchschlickmode    %Different mode selection
case 'standard'
p = schlickp;
if(p < 1)
p = 1;
Ld = p.*L./((p-1).*L+LMax); %dynamic Range Reduction
imgOut = zeros(size(img));
for i = 1 : 3
imgOut(:, :, i) = (img(:, :, i).*Ld)./L;
end
imgOut = RemoveSpecials(imgOut);
imshow(imgOut);    %output image display

```




(a) Image before tone mapping operation.



(b) Image after Reinhard tone mapping operation.

Figure 7.5: Input and output image after Reinhard tone mapping operation.

Tumblin&Rushmeier Mapping Operator

```

function imgOut = TumblinRushmeierTMO(img, Lda, CMax, Lwa)
img = hdrimread('image.jpg');    %input image read
check3Color(img);                %3 color check
L = lum(img);                    %Luminance extraction from image
if(
    exist('Lda')| exist('CMax'))  %parameter check
    Lda = 200;
    CMax = 100;
end

```

```

if( exist('Lwa'))
    Lwa = exp(mean(mean((log(L + 2.3 * 1e - 5)))));    %Log luminance
end

gammaw = gammaTumRushTMO(Lwa);
gammad = gammaTumRushTMO(Lda);
gammawd = gammaw./(1.855 + 0.4 * log(Lda));
mLwa = (sqrt(CMax)).^(gammawd - 1);
Ld = Lda * mLwa * (L./Lwa).^(gammaw./gammad); %dynamic Range Reduction
imgOut = zeros(size(img));
for i = 1 : 3
    imgOut(:, :, i) = img(:, :, i) * Ld./L;
end
imgOut = imgOut / 100;
figure();
imshow(imgOut);    %out put image display
end

```



(a) Image before tone mapping operation.



(b) Image after Schlick tone mapping operation.



(c) Image after Tumblin & Rushmeier tone mapping operation.

Figure 7.6: Input images used for Matlab simulation.

7.2 Reference Function Extraction

This section presents the reference function extraction of different tone mapping operators. Matlab code analyses the behavior of reference function. As discussed earlier, monotonically reference function is used to capture the wide dynamic range of a CMOS pixel.

Exponential Reference Function

```

 $I_{pm} = 10^6;$ 
 $v_{th} = 0.4;$ 
 $v_{dd} = 3.3;$ 
 $c = 6.06 * 10^{-10};$  %Different parameter values
 $k = 1 * 10^6;$ 
 $g = 4.5;$ 
 $vc = (-0.001 : 0.2 : 3.5);$ 
 $t = c * g * k * v_{dd} * (vc + v_{th} - 1) ./ \log(vc + v_{th});$  %Reference Function
plot(t,vc);

```

Schlick Reference Function

```

 $p = 4;$   $I_{pm} = 10^6;$   $c = 6.6 * 10^{-10};$   $v_{th} = 0.4;$   $v_{dd} = 3.3;$ 
 $k = 3.98 * 10^{-13};$  %Different parameter values
 $t = (0 : 0.005 : 0.02);$ 
 $vc = v_{dd} - v_{th} - (p * v_{dd} - I_{pm} * t ./ c * k) ./ (p - 1);$  %Reference Function
plot(t,vc);

```

Reinhard Simple Reference Function

```

vdd = 3.3;
Iw = 1.9;
c = 6.06 * 10-9;
g = 1;
k = 10-6;
ka = 1;  %Different parameter values
vth = 0;
z = 106;
t = (0.00 : 0.0005 : 0.02);
vc = (t/c * g * k - (vth));  %Reference Function
plot(t,vc);

```

Miller Reference Function

```

g = 3.16 * 106;
c = 10-16;
vdd = 3.3; vth = 0;  %Different parameter values
Ip = logspace(-8, -14.4, 40);
a1 = (0.338) .* (g * Ip).(0.034);
a = (g * Ip).a1;
t = c * (-1.5 * log10(g * Ip) + 6.1) .* a ./ Ip;
vc = vdd - vth - (-1.5 * log10(g * Ip) + 6.1) .* a;  %Reference Function
plot(t,vc);

```

Reinhard complex Reference Function

```

vdd = 3.3;
Iw = 1.9;
c = 6.06 * 10-9;
g = 0.5; %Different parameter values
k = 106;
ka = 1;
vth = 0;
z = 106;
t = (0.0035 : 0.0005 : 0.02);
Vc = -(t.* (t - c * g * k * vdd). * Iw2)./((c * g * k * vdd - t.* Iw2). * c * g * k) +
3.3; %Reference Function
plot(t,Vc);

```

Tumblin & Rushmeier reference Function

```

vth = 0;vdd = 3.3;c = 4 * 10-16;k = 10-2;g = 106;e = 2.65;f =
1.4; %Different parameter values
t = (0.00 : 0.0005 : 0.02);
vc = vdd - vth - vdd * ((g * k)e). * (c * vdd * g * k./t)f; %Reference Function
plot(t,vc);

```

Logarithmic Reference Function

```

vdd = 3.3; c = 5.3 * 10-14; a = 10-1; g = 1012; vth = 0; %Different parameter values
Ip = logspace(-8, -16, 40);
t = a * c * vdd * log(1 + g * Ip) ./ Ip;
vc = vdd - vth - a * vdd * log(1 + g * Ip); %Reference Function
plot(t, vc);

```

Ward histogram Reference Function

```

vdd = 3.3; c = 5.3 * 10-13; p = 10-1; k = 1012; vth = 0; %Different parameter values
Ip = logspace(-8, -12, 40);
t = c * exp((-1 + 1.518 * p * log(k * Ip)) * vdd) ./ Ip;
vc = vdd - vth - exp((-1 + 1.518 * p * log(k * Ip)) * vdd); %Reference Function
plot(t, vc, 'r');

```

Drago Reference Function

```

vdd = 3.3; vth = 0; g = 1016; g1 = 1017; c = 1.59 * 10-19.5; %Different parameter values
Ip = logspace(-7, -16, 40);
t1 = log10(1 + g * Ip) ./ (log10(2 + 8 * (g * Ip ./ g1 * 10-7)).0.234);
t = c * vdd * t1 ./ Ip * log10(1 + g1 * 10-7);
vc = vdd - vth - vdd * t1 ./ log10(1 + g1 * 10-7); %Reference Function
plot(t, vc);

```

7.3 Model Error

This section discusses the model error between pixel model and simulated response for Reinhard simple, complex and Schlick operator. Firstly, parameters are extracted using calibration currents. Secondly, these parameters are used to measure the pixel model and model error.

Reinhard Simple

```

z1 = load('Reinhardsimple12.7.txt'); %simulation data load
x1 = 10^-14;x2 = 7.08 * 10^-12;x3 = 10^-10;x4 = 10^-8;y1 = 1.3710;y2 =
0.5459 %calibration currents;y3 = 0.4021;y4 = 0.3814;y = 1.3773;
c1 = x1 * y4 - x2 * y4 - x1 * y2 + x4 * y2 + x2 * y1 - x4 * y1;
c2 = x1 * x2 * y2 - x1 * x2 * y1 + x1 * x4 * y1 - x1 * x4 * y4 + x2 * x4 * y4 - x2 * x4 * y2;
c = c1/c2;
b1 = (x1/(1 + c * x1)) - (x2/(1 + c * x2)); %Parameter Extraction
b = (y2 - y1)/b1;
a = y3 + b * x3/(1 + c * x3);
d = (a - y)/(b - a * c + c * y);
v = a - b * (Ip1 + d)./(1 + c * (Ip1 + d)); %Model Response
semilogx(Ip1,v,'k',Ip1,z1,'k');
v1 = abs(v - z1); %Model Error
semilogx(Ip1,v1,'k');

```


Reinhard Complex

```

z2 = load('Reinhardcomplex12.7.txt'); %simulation data load
A = [1x1 - x12 - y1 * x1; 1x2 - x22 - y2 * x2; 1x3 - x32 - y3 * x3; 1x4 - x42 - y4 *
x4]; %Parameter Extraction
B1 = [y1y2y3y4];
B = reshape(B1,4,1);
X = inv(A) * B;
P = X(1); Q = X(2); R = X(3); S = X(4); d = (P - y) / S * y; %Parameter Extraction
v = (P + Q * (Ip1 + d) - R * (Ip1 + d).2) ./ (1 + S * (Ip1 + d)); %Model Response
semilogx(Ip1, v, Ip1, z2, 'r');

```

Schlick Model Error

```

a2 = load('schlick.txt');
x1 = 10-13; x2 = 2.51 * 10-11; x3 = 10-9; y1 = 2.7146; y2 = 0.7270; y3 =
0.4220; %Calibration Currents
c = (10-6) * (x3 * y2 + y3 * x1 + y1 * x2 - x1 * y2 - x3 * y1 - y3 * x2) / (x2 * x3 * y3 + x1 * x3 *
y1 + x1 * x2 * y2 - x1 * x3 * y3 - x1 * x2 * y1 - x2 * x3 * y2);
b = (106) * (y1 - y2) * (c * x2 + 10-6) * (c * x1 + 10-6) / (x2 - x1); %Parameter Extraction
a = y1 + b * x1 / (10-6 + c * x1); d = (10-6) * (a - y) / (b + y * c - a * c);
y = a - b * (Ip1 + d) ./ (c * (Ip1 + d) + 10-6); %Model Response
v1 = abs(y - a1); %Model Error
semilogx(Ip1, v1);

```

7.4 Fixed Pattern Noise

This section summarises the FPN Matlab code. FPN arises due to the variations of parameters. Matlab code calculates the mean and standard deviation of parameters and measures the FPN.

Reinhard Simple

```

z = mcddata(); %Montecarlo simulation data
fori = 1 : 1 : 1000
x1 = 10-14; x2 = 7.08 * 10-12; x3 = 10-10; x4 = 10-8; y1(i) = z(i,41); y2(i) = z(i,98)
y4(i) = z(i,161); y(i) = z(i,1); %1000 parameter values
c1(i) = x1 * y4(i) - x2 * y4(i) - x1 * y2(i) + x4 * y2(i) + x2 * y1(i) - x4 * y1(i);
c2(i) = x1 * x2 * y2(i) - x1 * x2 * y1(i) + x1 * x4 * y1(i) - x1 * x4 * y4(i) + x2 * x4 * y4(i);
c(i) = c1(i) ./ c2(i);
b1(i) = (x1 / (1 + c(i) * x1)) - (x2 / (1 + c(i) * x2));
b(i) = (y2(i) - y1(i)) / b1(i); %1000 parameter values
a(i) = y3(i) + b(i) * x3 / (1 + c(i) * x3);
d(i) = (a(i) - y(i)) / (b(i) - a(i) * c(i) + c(i) * y(i));
c = 7.1330 * 101; d = 1.1017 * 10-14;
Iext(i,:) = (z(i,:) - a(i) - a(i) * d * c + d * z(i,:) * c + b(i) * d) ./ (a(i) * c - z(i,:) * c - b(i)); %Current Extraction
e = num2cell(Iext,1);
forn = 1 : 1 : 181
error(n) = std(abs(en)) ./ mean(abs(en)); %FPN error calculation

```

Reinhard Complex FPN

$z1 = mcdataRC();$ %Montecarlo simulation data

$fori = 1 : 1 : 1000$

$x1 = 5.01 * 10^{-14}; x2 = 5.01 * 10^{-13}; x3 = 1 * 10^{-11}; x4 = 10^{-9}; y1(i) = z1(i, 55);$

$y2(i) = z1(i, 75); y3(i) = z1(i, 101); y4(i) = z1(i, 141); y(i) = z1(i, 1);$ %Parameters Extraction

$s1(i) = x1 * y3(i) - x2 * y3(i) - x1 * y4(i) + x2 * y4(i) - x3 * y1(i) + x4 * y1(i) + x3 * y2(i) - x4 * y2(i) - (y3(i) * x2$

$- x3 * y3(i) - x2 * y4(i) + x3 * y4(i) - x3 * y2(i) + x4 * y2(i) + x3 * y3(i) - x4 * y3(i)) * (x1 + x2 - x3 - x4);$

$s2(i) = x1 * y1(i) * x3 - x1 * y1(i) * x4 - x2 * y2(i) * x3 + x2 * y2(i) * x4 - x1 * x3 * y2(i) + x1 * x4 * y4(i) + x2 * x3 * y3(i)$

$- x2 * x4 * y4(i) + (x2 * y2(i) * x3 - x2 * y2(i) * x4 + x3 * x4 * y3(i) - x3 * x2 * y3(i)$

$+ x2 * y4(i) * x4 - x3 * x4 * y4(i)) * (x1 + x2 - x3 - x4);$

$S(i) = s1(i) ./ s2(i);$

$r1(i) = (y3(i) - y4(i)) * (x1 - x2) - (y1(i) - y2(i)) * (x3 - x4) - S(i) * (x1 * y1(i) * x3 - x1 * y1(i) * x4$

$- x2 * y2(i) * x3 + x2 * y2(i) * x4 - x1 * x3 * y3(i) + x1 * x4 * y4(i) + x2 * x3 * y3(i) - x2 * x4 * y4(i));$

$r2 = x1 + x2 - x3 - x4;$

$R(i) = r1(i) ./ r2;$

$Q(i) = R(i) * (x1 + x2) + ((y1(i) - y2(i)) / (x1 - x2)) + S(i) * (x1 * y1(i) - x2 * y2(i)) / (x1 - x2);$

$P(i) = y1(i) - Q(i) * x1 + R(i) * x1^2 + S(i) * y1(i) * x1;$

$D(i) = (P(i) - y(i)) ./ S(i) * y(i);$

$Iext(i, :) = (Q(i) - 2 * D(i) * R(i) - S(i) * z1(i, :) - (Q(i).^2 - 2 * Q(i) * S(i) * z1(i, :) + S(i).^2 * z1(i, :)).^2 - 4 * R(i) * z1(i, :) + 4 * P(i) * R(i)).^1 / 2) ./ 2 * R(i);$ %Current extraction

$e1 = num2cell(Iext, 1);$

$fori = 1 : 1 : 181$

$error(i) = abs(std(e1i) ./ mean(e1i));$ %FPN calculation

$semilogx(Ip1, error);$

Bibliography

- [1] D. Joseph, “Modelling and calibration of logarithmic cmos image sensors,” tech. rep., University of Oxford, 2002.
- [2] S. O. Otim, *Simplified fixed pattern noise correction and image display for high dynamic range CMOS logarithmic imagers*. PhD thesis, University of Oxford, 2007.
- [3] P. D. E. Mounier and J. Jaffard, “Status of the cmos image sensor industry,” tech. rep., Yole Developement, 2014.
- [4] A. E. Gamal and H. Eltoukhy, “Cmos image sensors,” *Circuits and Devices Magazine, IEEE*, vol. 21, no. 3, pp. 6–20, 2005.
- [5] B. Choubey, W. Mughal, and L. Gouviea, “Circuits for high performance complementary metal-oxide-semiconductor (cmos) image sensors,” *High Performance Silicon Imaging: Fundamentals and Applications of CMOS and CCD sensors*, pp. 124–164, 2014.
- [6] H. Y. Cheng, B. Choubey, and S. Collins, “A high-dynamic-range integrating pixel with an adaptive logarithmic response,” *IEEE Photonics Technology Letters*, vol. 19, pp. 1169–1171, Aug 2007.

- [7] S. Decker, R. McGrath, K. Brehmer, and C. Sodini, "A 256x256 cmos imaging array with wide dynamic range pixels and column-parallel digital output," *IEEE Journal of Solid-State Circuits*, vol. 33, pp. 2081–2091, Dec 1998.
- [8] O. Yadid-Pecht, R. Ginosar, and Y. Shacham-Dimand, "A random access photodiode array for intelligent image capture," in *17th Convention of Electrical and Electronics Engineers in Israel*, pp. 301–304, Mar 1991.
- [9] T. Kinugasa, M. Noda, T. Imaide, I. Aizawa, Y. Todaka, and M. Ozawa, "An electronic variable-shutter system in video camera use," *IEEE Transactions on Consumer Electronics*, vol. CE-33, pp. 249–255, Aug 1987.
- [10] H.-Y. Cheng, B. Choubey, and S. Collins, "An Integrating Wide Dynamic-Range Image Sensor With a Logarithmic Response," *IEEE Transactions on Electron Devices*, vol. 56, pp. 2423–2428, Nov. 2009.
- [11] R. Guidash, "Variable collection of blooming charge to extend dynamic range," Oct. 23 2001. US Patent 6,307,195.
- [12] J. Hyneczek, "High dynamic range active pixel cmos image sensor and data processing system incorporating adaptive pixel reset," July 18 2006. US Patent 7,079,178.
- [13] T. Anaxagoras, P. Kent, N. Allinson, R. Turchetta, T. Pickering, D. Maneuski, A. Blue, and V. O'Shea, "A parametric cmos active-pixel sensor for the evaluation of reset noise reduction architectures," *IEEE Transactions on Electron Devices*, vol. 57, no. 9, pp. 2163–2175, 2010.

- [14] M. Schanz, C. Nitta, A. Bussmann, B. J. Hosticka, and R. Wertheimer, “A high-dynamic-range cmos image sensor for automotive applications,” *IEEE Journal of Solid-State Circuits*, vol. 35, pp. 932–938, July 2000.
- [15] T. Yasuda, T. Hamamoto, and K. Aizawa, “Adaptive-integration-time image sensor with real-time reconstruction function,” *IEEE Transactions on Electron Devices*, vol. 50, pp. 111–120, Jan 2003.
- [16] W. Mughal and B. Choubey, “Fixed pattern noise correction for wide dynamic range cmos image sensor with reinhard tone mapping operator,” in *Nordic Circuits and Systems Conference (NORCAS): NORCHIP & International Symposium on System-on-Chip (SoC), 2015*, pp. 1–4, IEEE, 2015.
- [17] E. Reinhard, M. Stark, P. Shirley, and J. Ferwerda, “Photographic tone reproduction for digital images,” *ACM Trans. Graph.*, vol. 21, pp. 267–276, July 2002.
- [18] E. Reinhard, G. Ward, S. Pattanaik, and P. Debevec, *High Dynamic Range Imaging: Acquisition, Display, and Image-Based Lighting (The Morgan Kaufmann Series in Computer Graphics)*. San Francisco, CA, USA: Morgan Kaufmann Publishers Inc., 2005.
- [19] L. Meylan, *Tone mapping for high dynamic range images*. PhD thesis, IC, Lausanne, 2006.
- [20] F. Banterle, A. Artusi, K. Debattista, and A. Chalmers, *Advanced high dynamic range imaging : theory and practice*. Natick, MA: A K Peters, 2011.
- [21] G. Mather, *Foundations of Perception*. Psychology/Neuroscience, Psychology Press, 2006.

- [22] H. Seetzen, W. Heidrich, W. Stuerzlinger, G. Ward, L. Whitehead, M. Trentacoste, A. Ghosh, and A. Vorozcovs, “High dynamic range display systems,” in *ACM Transactions on Graphics (TOG)*, vol. 23, pp. 760–768, ACM, 2004.
- [23] B. H. (ed.), *High-dynamic-range (HDR) vision: microelectronics, image processing, computer graphics*. Berlin New York: Springer, 2007.
- [24] J. Stockham, T.G., “Image processing in the context of a visual model,” *Proceedings of the IEEE*, vol. 60, pp. 828–842, July 1972.
- [25] P. Ferschin, I. Tastl, and W. Purgathofer, “A comparison of techniques for the transformation of radiosity values to monitor colors,” in *IEEE International Conference on Image Processing*, vol. 3, pp. 992–996, Nov 1994.
- [26] F. Drago, K. Myszkowski, T. Annen, and N. Chiba, “Adaptive Logarithmic Mapping For Displaying High Contrast Scenes,” *Computer Graphics Forum*, vol. 22, pp. 419–426, 2003.
- [27] C. Schlick, “Quantization Techniques for Visualization of High Dynamic Range Pictures,” pp. 7–20, Springer-Verlag, 1994.
- [28] S. S. Stevens and J. Stevens, “Brightness function-parametric effects of adaptation and contrast,” in *Journal of the Optical Society of America*, vol. 50, pp. 1139–1139, 1960.
- [29] J. Stevens and S. S. Stevens, “Brightness function: Effects of adaptation,” *JOSA*, vol. 53, no. 3, pp. 375–385, 1963.
- [30] G. S. Miller and C. R. Hoffman, “Illumination and reflection maps: Simulated objects in simulated and real environments, 1984,” *Cited on*, pp. 19–23.

- [31] A. Adams and R. Baker, *The print*. Little, Brown, 1983.
- [32] G. W. Larson, H. Rushmeier, and C. Piatko, “A visibility matching tone reproduction operator for high dynamic range scenes,” *IEEE Transactions on Visualization and Computer Graphics*, vol. 3, no. 4, pp. 291–306, 1997.
- [33] M. Čadík, M. Wimmer, L. Neumann, and A. Artusi, “Image attributes and quality for evaluation of tone mapping operators,” 2006.
- [34] A. Yoshida, V. Blanz, K. Myszkowski, and H.-P. Seidel, “Perceptual evaluation of tone mapping operators with real-world scenes,” pp. 192–203, 2005.
- [35] G. Eilertsen, R. Wanat, R. K. Mantiuk, and J. Unger, “Evaluation of tone mapping operators for hdr-video,” vol. 32, no. 7, pp. 275–284, 2013.
- [36] P. Ledda, A. Chalmers, T. Troscianko, and H. Seetzen, “Evaluation of tone mapping operators using a high dynamic range display,” *ACM Transactions on Graphics (TOG)*, vol. 24, no. 3, pp. 640–648, 2005.
- [37] G. Holst and T. Lomheim, *CMOS/CCD Sensors and Camera Systems*. SPIE Press monograph, J C D Publishing, 2011.
- [38] W. Mughal, L. C. Gouveia, and B. Choubey, “On Threshold Comparing Biomorphic Image Sensors,” *Procedia Computer Science*, vol. 41, pp. 140–145, 2014.
- [39] L. C. Gouveia, W. Mughal, and B. Choubey, “A reconfigurable cmos pixel for applying tone mapping on high dynamic range images,” in *IEEE International Instrumentation and Measurement Technology Conference (I2MTC) Proceedings, 2014*, pp. 1098–1101, IEEE, 2014.

- [40] B. Choubey and S. Collins, "Wide dynamic range cmos pixels with reduced dark current," *Analog Integrated Circuits and Signal Processing*, vol. 56, no. 1-2, pp. 53–60, 2008.
- [41] D. Joseph and S. Collins, "Modeling, calibration, and correction of nonlinear illumination-dependent fixed pattern noise in logarithmic cmos image sensors," *IEEE Transactions on Instrumentation and Measurement*, vol. 51, pp. 996–1001, Oct 2002.
- [42] B. Choubey, *Fixed Pattern Noise*, ch. 54, pp. 1–10.
- [43] J. R. Janesick, *Scientific charge-coupled devices*, vol. 117. SPIE press Bellingham, 2001.
- [44] Y. Ohkubo, "An analysis of fixed pattern noise for mos-ccd type image sensors under quasi-stationary conditions," *IEEE Journal of Solid-State Circuits*, vol. 21, no. 4, pp. 555–560, 1986.
- [45] S. Kavadias, B. Dierickx, D. Scheffer, A. Alaerts, D. Uwaerts, and J. Bogaerts, "A logarithmic response cmos image sensor with on-chip calibration," *IEEE Journal of Solid-State Circuits*, vol. 35, no. 8, pp. 1146–1152, 2000.
- [46] A. Milton, F. Barone, and M. Kruer, "Influence of nonuniformity on infrared focal plane array performance," *Optical Engineering*, vol. 24, no. 5, pp. 245855–245855, 1985.
- [47] B. Belaroussi, J. Milles, S. Carne, Y. M. Zhu, and H. Benoit-Cattin, "Intensity non-uniformity correction in mri: existing methods and their validation," *Medical Image Analysis*, vol. 10, no. 2, pp. 234–246, 2006.

- [48] M. J. Pelgrom, A. C. Duinmaijer, A. P. Welbers, *et al.*, “Matching properties of mos transistors,” *IEEE Journal of solid-state circuits*, vol. 24, no. 5, pp. 1433–1439, 1989.
- [49] P. R. Kinget, “Device mismatch and tradeoffs in the design of analog circuits,” *IEEE Journal of Solid-State Circuits*, vol. 40, no. 6, pp. 1212–1224, 2005.
- [50] F. W. Billmeyer, “Color science: Concepts and methods, quantitative data and formulae,” pp. 950–955, 1983.
- [51] B. WANDEL, “Foundation of vision sinauer associates,” *Inc. Sunderland MA*, 1995.
- [52] H. Blackwell, “Contrast thresholds of the human eye,” *SPIE MILESTONE SERIES MS*, vol. 169, pp. 33–52, 2001.
- [53] J. Kuang, G. M. Johnson, and M. D. Fairchild, “icam06: A refined image appearance model for hdr image rendering,” *Journal of Visual Communication and Image Representation*, vol. 18, no. 5, pp. 406–414, 2007.
- [54] J. Duan and G. Qiu, “Fast tone mapping for high dynamic range images,” in *Proceedings of the 17th International Conference on Pattern Recognition, 2004. ICPR 2004.*, vol. 2, pp. 847–850, IEEE, 2004.
- [55] D. J. Jobson, Z.-u. Rahman, and G. A. Woodell, “A multiscale retinex for bridging the gap between color images and the human observation of scenes,” *IEEE Transactions on Image Processing*, vol. 6, no. 7, pp. 965–976, 1997.

- [56] M. Ashikhmin, “A tone mapping algorithm for high contrast images,” in *Proceedings of the 13th Eurographics workshop on Rendering*, pp. 145–156, Eurographics Association, 2002.
- [57] T. O. Aydin, N. Stefanoski, S. Croci, M. Gross, and A. Smolic, “Temporally coherent local tone mapping of hdr video,” *ACM Transactions on Graphics (TOG)*, vol. 33, no. 6, pp. 196–210, 2014.
- [58] M. D. Tocci, C. Kiser, N. Tocci, and P. Sen, “A versatile hdr video production system,” *ACM Transactions on Graphics (TOG)*, vol. 30, no. 4, pp. 41–50, 2011.
- [59] J. A. Ferwerda, S. N. Pattanaik, P. Shirley, and D. P. Greenberg, “A model of visual adaptation for realistic image synthesis,” in *Proceedings of the 23rd annual conference on Computer graphics and interactive techniques*, pp. 249–258, ACM, 1996.
- [60] S. N. Pattanaik, J. Tumblin, H. Yee, and D. P. Greenberg, “Time-dependent visual adaptation for fast realistic image display,” in *Proceedings of the 27th annual conference on Computer graphics and interactive techniques*, pp. 47–54, ACM Press/Addison-Wesley Publishing Co., 2000.
- [61] P. Irawan, J. A. Ferwerda, and S. R. Marschner, “Perceptually based tone mapping of high dynamic range image streams,” in *Rendering Techniques*, pp. 231–242, 2005.
- [62] J. Van Hateren, “Encoding of high dynamic range video with a model of human cones,” *ACM Transactions on Graphics (TOG)*, vol. 25, no. 4, pp. 1380–1399, 2006.

- [63] R. Mantiuk, S. Daly, and L. Kerofsky, "Display adaptive tone mapping," *ACM Transactions on Graphics (TOG)*, vol. 27, no. 3, pp. 68–78, 2008.
- [64] R. Boitard, R. Cozot, D. Thoreau, and K. Bouatouch, "Zonal brightness coherency for video tone mapping," *Signal Processing: Image Communication*, vol. 29, no. 2, pp. 229–246, 2014.
- [65] P. Ledda, L. P. Santos, and A. Chalmers, "A local model of eye adaptation for high dynamic range images," in *Proceedings of the 3rd international conference on Computer graphics, virtual reality, visualisation and interaction in Africa*, pp. 151–160, ACM, 2004.
- [66] E. P. Bennett and L. McMillan, "Video enhancement using per-pixel virtual exposures," *ACM Transactions on Graphics (TOG)*, vol. 24, no. 3, pp. 845–852, 2005.
- [67] A. Benoit, D. Alleysson, J. Herault, and P. Le Callet, "Spatio-temporal tone mapping operator based on a retina model," 2009.
- [68] E. Reinhard, T. Pouli, T. Kunkel, B. Long, A. Ballestad, and G. Damberg, "Calibrated image appearance reproduction," *ACM Transactions on Graphics (TOG)*, vol. 31, no. 6, pp. 201–220, 2012.
- [69] S. Sukegawa, T. Umebayashi, T. Nakajima, H. Kawanobe, K. Koseki, I. Hirota, T. Haruta, M. Kasai, K. Fukumoto, T. Wakano, K. Inoue, H. Takahashi, T. Nagano, Y. Nitta, T. Hirayama, and N. Fukushima, "A 1/4-inch 8mpixel back-illuminated stacked cmos image sensor," in *2013 IEEE International Solid-State Circuits Conference Digest of Technical Papers*, pp. 484–485, Feb 2013.

-
- [70] T. Kondo, Y. Takemoto, K. Kobayashi, M. Tsukimura, N. Takazawa, H. Kato, S. Suzuki, J. Aoki, H. Saito, and Gomi, “A 3d stacked 16m pixel global-shutter cmos image sensor using 4 million interconnections,” *ITE Transactions on Media Technology and Applications*, vol. 4, no. 2, pp. 129–135, 2016.